Title
Quantum Amplification of Triplet Sensitized Dewar Benzenes in the Crystalline Solid State

Author
Rivera, Edris

Publication Date
2021

Peer reviewed|Thesis/dissertation

UNIVERSITY OF CALIFORNIA

Los Angeles

Quantum Amplification of Triplet Sensitized Dewar Benzenes in the Crystalline Solid State

A dissertation submitted in partial satisfaction of the requirements for the degree Doctor of Philosophy in Chemistry

by

Edris Andrew Rivera

2021

ABSTRACT OF THE DISSERTATION

Quantum Amplification of Triplet Sensitized Dewar Benzenes in the Crystalline Solid State

by

Edris Andrew Rivera

Doctor of Philosophy in Chemistry

University of California, Los Angeles, 2021

Professor Miguel A. Garcia-Garibay, Chair

This dissertation describes the development of triplet Dewar benzenes for photonic amplification in the crystalline solid, verification of the quantum chain process in solution and the solid state, and further potential for the quantum chain process by addressing limitations in crystal packing and electronics. This work relied heavily upon understanding how each component of the quantum chain reaction effects its reactivity, including transient absorption spectroscopy to determine triplet lifetimes and quenching rates in solution, concentration dependence through quantum yield calculations, and computational studies to gain insight on the mechanistic photochemical isomerization of Dewar benzene. Solid state irradiation

experiments were performed in nanocrystalline suspensions via reprecipitation method in surfactant to stabilize particles.

Chapter One is an overview of quantum chain reactions as part of a class of nonlinear photochemical processes. This chapter outlines known quantum chain reactions, the complexity of this process as it requires several steps to occur, and seminal work that inspired exploration in expanding this reaction in crystalline Dewar benzenes.

Chapter Two describes the development and study of crystalline benzophenone-linked Dewar benzene. This work demonstrates the ability to access triplet excitation and photochemical isomerization of Dewar benzene in the solid state. Lifetimes and triplet energy of the photoproduct (responsible for the energy transfer event) were determined using transient absorption spectroscopy and fluorimetry. The crystalline Dewar benzene proved to undergo quantum amplification in the solid state environment, possessing quantum yields greater in solid state than in solution.

Chapter Three establishes similar reactivity in the solid state within other Dewar benzene derivatives and showcases enhanced reactivity of derivatives over the example from Chapter Two. This work demonstrated the significance of the solid state packing influence on the extent of the quantum chain process. Confirmation of suspension crystallinity was performed using pXRD. Comparisons between bulk powder and suspension packing revealed polymorphism crystalline Dewar benzenes. This work also established that the solid state reaction from Dewar benzene to Hückel benzene proceeds via solid-to-solid transformation, starting from a polycrystalline powder reactant to give an amorphous resulting photoproduct

upon irradiation. It was demonstrated that electronics play a significant role upon comparison of quantum yields between di- and mono-sensitizer linked Dewar benzenes, revealing the potential for benzophenone surface quenching.

Chapter Four focuses on exploring unique reactivity of Dewar benzenes and proposing promising new derivatives that have the potential to extend the quantum chain to 10^6. This work addresses the bulk properties and irradiation of a Dewar benzene-sensitizer salt pair, a non-sensitizer linked Dewar benzene and a mono-sensitizer linked Dewar benzene. Further exploration into the exceptional reactivity of the mono-sensitizer linked Dewar benzene was carried out via transient absorption analysis, revealing longer-lived intermediates than that of the di-sensitizer linked Dewar benzene. To further validate the presence of benzophenone self-quenching in the solid state and extending the quantum chain, four Dewar benzenes and their synthesis were proposed.

The dissertation of Edris Andrew Rivera is approved.

Ellen Sletten

Margot Quinlan

Hosea Nelson

Miguel A. Garcia-Garibay, Committee Chair

University of California, Los Angeles

2021

For my family Roslyn Leon (Mother), Ross Rivera (Father), Ross Rivera Jr. (Brother), Essie Mae Rivera (Grandmother) who would have loved to see me achieve my doctorate, and Rachael Day who believed in me every step of the way

TABLE OF CONTENTS

LIST OF FIGURES

CHAPTER ONE

CHAPTER TWO

LIST OF SCHEMES

CHAPTER ONE

CHAPTER TWO

CHAPTER THREE

CHAPTER FOUR

LIST OF TABLES

CHAPTER TWO

CHAPTER THREE

LIST OF ABBREVIATIONS

°C	degrees Celsius
$^{13}C\{^{1}H\}$ NMR	proton-decoupled carbon-13 nuclear magnetic resonance
^{1}H NMR	proton nuclear magnetic resonance
μL	microliter
Ad	adamantyl
DB-OBPh	Dewar benzene coupled to benzophenone via ester linkage
HB-OBPh	Huckel benzene couples to benzophenone via ester linkage
BPh	benzophenone
t-butyl	*tert*-butyl
DCK	dicumyl ketone
DC	dicumene
CD_3CN	deuterated acetonitrile
$CDCl_3$	deuterated chloroform
cm^{-1}	inverse centimeter
ca.	approximately
TTA	triplet-triplet annihilation

DI	deionized
equiv	equivalents
eq.	equation
DMF	N,N-dimethylformamide
DCM	dichloromethane
g	gram
mg	milligram
mM	millimolar
M	Molarity
hr	hour
min.	minute
sec	seconds
Hz	hertz
FTIR	Fourier Transform Infrared
m.p.	melting point
MeCN	acetonitrile
mHz	megahertz

kcal/mol	kilocalories/mole
$MgSO_4$	magnesium sulfate
ISC	intersystem crossing
ET	energy transfer
Nd-YAG	neodymium-doped yttrium aluminum garnet
nm	nanometer
ns	nanosecond
ppm	parts per million
pXRD	powder X ray diffraction
SEM	Scanning electron microscopy
EDC	1-ethl-3-(3-dimethylaminopropyl)carbodiimide
rt	room temperature
adiab rxn	adiabatic reaction
THF	tetrahydrofuran
TLC	thin layer chromatography
UV-vis	ultraviolet-visible
w/v	weight per volume

4-AcOBPh	4-acetoxybenzophenone
Ar	Argon
A	preexponential factor
τ	lifetime
η_{MeCN}	refractive index of acetonitrile
$\eta_{Benzene}$	refractive index of benzene
SI	Supplemental Information
CTAB	Cetrimonium bromide
SDS	sodium dodecyl sulfate
$AlCl_3$	aluminum chloride
KOH	potassium hydroxide
DMAP	4-dimethylaminopyridine
OD	optical density
DLS	dynamic light scatter
DSC	differential scanning calorimetry
Tg	glass transition temperature
NC	nanocrystalline

E	energy
T_1	triplet excited state
T_2	second triplet excited state
S_0	ground state
S_1	singlet excited state
R	reactant
k_a	rate of adiabatic reaction
$k_{P\text{-}decay}$	rate of product decay
$k_{relaxation}$	rate of relaxation
μm	micrometer
LFP	laser flash photolysis
R*	excited reactant
P	product
P*	excited product
DPCP	diphenylcyclopropenone
DPA	diphenylacetylene
S_2	second excited singlet state

ACKNOWLEDGEMENTS

I'd like to dedicate the majority of my acknowledgements to all the amazing women in my life who made it possible for me to be where I am today. It was through their maturity, patience, and strength that I learned to grow into who I am today. Mom, without all of your sacrifice throughout my life I'm not sure what life would hold for me at this moment. You have always made the importance of my education apparent. Back in Queens, after I graduated from New World, you were heavily invested on getting me into a school district that had more rigorous coursework and opportunity. Although I may have been a bit hesitant to leave my friends, I quickly noticed how well that investment paid off. I was accepted to District 26 in Bayside/Flushing, Queens, where all the schools were massive in size compared to the schools located in my neighborhood. As part of my acceptance into the school district we had to provide our own transportation to and from school. As much as I may have disliked getting to school an hour earlier than most of the students, I truly believe our commute allowed us to build our bond. I remember those cold mornings waiting in the car and listening to music (most of which I still listen to today) while you'd sit with me for a 10-15 minutes before dropping off at school. I couldn't see it then but now I can truly see how much you sacrificed for me to go P.S. 31; because as my commute ended with you dropping me off, yours was just beginning. It was only a few years of this commute until you taught me how to take the city bus on my own. I vividly remember that trip, how nervous I was and yet eager to reach this level of autonomy in my life. Along with challenging coursework and an abundance of opportunity for after school activities, District 26 possessed an amazing attribute that was not as readily accessible to the schools in my neighborhood: diversity (this is an important one). At a very early age I learned to interact with

students from different ethnicities/cultures, which allowed me to become more adaptable (If anyone reading this is at all interested in gaining more perspective of the New York City district school system, it's all nicely detailed in the New York Times: Nice White Parents podcast). While we hadn't ever discussed college before my senior year of high school, I appreciate how extremely supportive you were of me attending, both emotionally and financially.

Another important figure who was instrumental to my growth is my former high school partner, Yon-Soo Lee. This goes without saying, but if it were not for you I probably would have never pursued going through higher education to achieve my PhD. As a high school student I often took on the identity of the class clown or someone who always had to be the center of attention, but you saw more in me than that. You really made me believe I was intelligent. When I needed to figure out a summer internship before my senior year, you encouraged me to reach out to Mia's father who actually got me started working in lab under a graduate student (shout out to that poor graduate student who had to deal with an immature high schooler). This really paved the way for me becoming interested in research based science. You will always have my support in life.

Rachael, I honestly can't believe how things have turned out for us since we first met five years ago. Your patience and love has been superior and has really helped me mature throughout my time in graduate school. The most powerful quality I learned in our time together is compromise; I can't say that I had ever done so properly before meeting you. Having come from such different upbringing and experiences, we were two totally different people who found a way to make things work (key word here is compromise). You truly made me want to be a better person and with you the change felt so natural (although it took years of smoothing out to get

there). Whenever I was faced with a challenge, whether in lab or personal life, I always knew that I would overcome because you believed in me. Now I know that seems like a given with any partner, but you definitely made it clear when I was in way over my head on certain things, so to have your validation felt especially genuine. As we move on to our own worlds, I am so excited to see how far life takes you and know that you have my support every step of the way.

Dad, thank you for always being my emotional support system. I might not have always been the most kind or sensitive but I have always loved you despite having only told you a handful of times. Although there may have been some strain on our relationship after I graduated high school, I was never ashamed to call you my father. You were always very proud of me and I could see it in your eyes even as I've grown older. I only hope to continue to make you proud. I also want you to know that I am very proud of you! I remember the last time I saw you we were attending grandma's (your mother's) funeral and how much I learned about your job at the phone company and being close to the World Trade Center on 9/11 and feeling like I was really learning about you for the first time. Ross (my brother), we spent such a short time together and yet many of my memories of you are so clearly burned into my brain. Although we haven't seen each other in years, when we speak it feels like no time has passed at all. I think about you a lot and hope that you're safe, healthy, but most of all happy. We missed out on a lot of each other's lives but I still believe we can make up for lost time. I'll never forget when we spoke a few months ago about how we never seen a movie or even had a drink with each other! I really want to change that. We are so different but when I hear your voice or see you on FaceTime I'm always taken back to those times in St. Albans when my goal was to impress you. You were (and still are)

so funny, handsome, and so damn kind to me; I only wish I made more of an effort to see you then.

Dan and Sydnee, thank you for being awesome roommates. I will miss our alcohol fueled debates which seemingly became worse during the pandemic (I won't put that on Dan though that was mostly on me and Sydnee). I'll also miss those days of playing Call of Duty online, screaming at the TV screen while Sydnee and Rachael "cheered" us on. I always felt like I could rely on you two to give sound advice and put me in my place when needed. I could not have asked for better friends and roommates in the department. I'd also like to apologize to Dan again for taking off the bumper to his car, I could only imagine the anger swirling through your head at 6 AM when I told you. Also a special shout out to Milauni, Cesar, and Anthony for being a great source of diversity in the department and bringing more color into my life.

Miguel, you have been an amazing advisor. I am so grateful to you for allowing me to explore my interests and getting me excited about our work through your love of obtaining knowledge. You have been extremely supportive of me these past five years (even more so than my parents) and have always made yourself available even with a very busy schedule. I will truly miss you, your wisdom, and all the advice. You are the smartest person I've ever met and I have always felt fortunate to have you on my side. You taught me to always keep obtaining knowledge and understanding concepts to the fullest.

Chapter One is an unpublished review of literature precedents for nonlinear photochemical processes to establish seminal work for this thesis. Rivera was responsible for this writing.

Chapter Two is a manuscript currently in revision for the Journal of Physical Chemistry. Rivera was responsible for the experimental work. Rivera and Garcia-Garibay were responsible for writing.

Chapter Three describes unpublishes studies. Rivera and Ruesch were responsible for experimental work. Liepuoniute and Friedl were responsible for computational studies. Rivera and Garcia-Garibay were responsible for writing.

Chapter Four describes unpublishes studies. Rivera was responsible for experimental work. Liepuoniute was responsible for computational studies. Rivera and Garcia-Garibay were responsible for writing.

These studies were supported by Eugene V. Cota-Robles Fellowship

BIOGRAPHICAL SKETCH

Edris A. Rivera

EDUCATION

University of California, Los Angeles — 2021
Doctoral student in Organic Chemistry

Virginia Commonwealth University — 2016
B.S. in Chemistry

RESEARCH EXPERIENCE

Solid State Photochemistry

Garcia-Garibay Research Group, UCLA — August 2016 – Current

- Studied chemical and physical properties of crystalline, photochemically reactive small molecules utilizing solid-state characterization techniques
- Developed methods for analytical instrumentation to study stability, reactivity, and size distribution of small molecules in solution and solid state (including aqueous nanocrystalline suspension)
- Multi-step synthesis of highly-strained, photochemically responsive organic small molecules on small and large scale
- Skills: FTIR, DLS, SEM, HPLC, LC/GC-MS, AFM, pXRD, zeta potential, DSC, TGA, UV-vis, NMR, Polarized Light Microscopy, Transient Absorption Spectroscopy

Synthetic Inorganic Chemistry

Farrell Research Group, Virginia Commonwealth University — November 2012 – May 2016

- Synthesized platinum-based inorganic small molecule drugs for selective targeting of HIV-1 nucleocapsid protein, NCp7 to displace/disrupt C-terminal zinc finger, NCp7, responsible for viral replication
- Measured binding affinities of synthesized platinum-based small molecules and nucleocapsid protein binding site via fluorescence spectroscopy
- Skills: NMR, Synthetic Inorganic Chemistry, Fluorescence Spectroscopy

PUBLICATIONS

- **Rivera, E. A**; Garcia-Garibay, M. A. "Quantum Amplification of Triplet Sensitizer-linked Dewar Benzenes Within a Crystalline Environment," **Submitted**

- **Rivera, E. A.**; Garcia-Garibay, M. A. "The Effects of unique Crystal Packing and Structural Electronics on the Quantum Chain Reaction of Benzophenone-linked Crystalline Dewar benzenes," **In Preparation**
- Park, J. H.; Chung, T. S.; Hipwell, V. M.; **Rivera, E. A.**; Garcia-Garibay, M. A. "Transient Kinetics and Quantum Yield Studies of Nanocrystalline a-Phenyl-Substituted Ketones: Sorting Out Reactions from Singlet and Triplet Excited States," *J. Am. Chem. Soc.* **2018**, *140*, 8192–8197; **Published**
- Tsotsoros, S. D.; Lutz, P. B.; Daniel, A. G.; Peterson, E. J.; Paiva, R. E. F. D.; **Rivera, E. A**.; Qu, Y.; Bayse, C. A.; Farrell, N. P. "Enhancement of the physicochemical properties of [Pt(dien)(nucleobase)]$^{2+}$ for HIVNCp7 targeting." *Chem. Sci.* **2017**, *8*, 1269-1281; **Published**
- Egodawatte, S.; Greenstein, K. E.; Vance, I.; **Rivera, E.A.**; Myung, N. V.; Parkin, G. F.; Cwiertny, D. M.; Larsen, S. C. "Electrospun hematite nanofiber/mesoporous silica core/shell nanomaterials as an efficient adsorbent for heavy metals." *RSC Advances*, **2016**, *6*, 90516-90525; **Published**

PRESENTATIONS

NSF-AGEP California Alliance Retreat 2019

- Poster presentation: Quantum Chain Reactions of Triplet Sensitized Dewar Benzenes Within a Crystalline Environment

PhotoIUPAC Dublin 2018 Conference

- Poster presentation: Quantum Chain Reactions of Dewar Benzene in Crystalline Media

University of Iowa REU Conference 2013

- Poster presentation: Electrospun Iron (III) oxide Nanofibers for Application to Arsenic Removal in Wastewater

AWARDS AND HONORS

Graduate

UCLA Eugene V. Cota-Robles Fellowship (2016), UCLA Competitive Edge Program (2016)

Undergraduate

Howard Hughes Medical Institute: Exceptional Research Opportunities Program (HHMI EXROP) (2015), Maximizing Access to Research Careers (MARC) (2014), Summer Research Opportunities Program (SROP) (2013)

CHAPTER ONE

Introduction: Exploring Dewar Benzene Quantum Chain Reactions in the Crystalline Solid State

1.1 Nonlinear Photochemical Processes

Nonlinear photochemical processes introduce alternative electronic pathways that enhance the breadth of photochemical outcomes compared to canonical photochemical process. Over the past few years these processes have gained attention and have made significant contributions in physical organic chemistry and catalysis. One example of this involves photonic upconversion known as triplet-triplet annihilation, in which two low-energy triplets generate a single excited singlet of equal or greater energy than the two triplets (**Figure 1.1**).[1-2] This type of upconversion was first introduced by Parker and Hatchard in 1962 involving donor/acceptor interactions between phenanthrene and naphthalene in solution.[3,4]

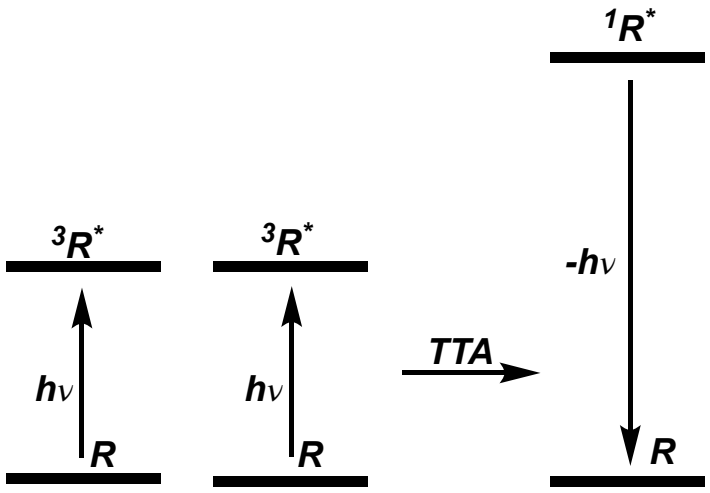

Figure 1.1 Triplet-triplet annihilation

There are three requirements for triplet-triplet annihilation: 1) the triplet energy of an acceptor, R, is less than or equal to the triplet energy of the sensitizer (if a sensitizer is involved) ($^3R^* \leq {}^3Sens^*$), 2) the singlet energy of an acceptor is greater than or equal to twice its triplet energy ($^1R^* \geq 2\ ^3R^*$), 3) acceptors exist as long lived triplets (τ_{3Sens*}, $\tau_{3A*} \approx 10^{-6}$-$10^{-3}$ s), and 4) the quantum yields of intersystem crossing and fluorescence of the sensitizer and acceptor, respectively, are near unity (Sens-Φ_{ISC}, R-$\Phi_F \sim 1$).[5,6] The maximum possible quantum yield for a triplet-triplet annihilation system is 50% to date, and the highest quantum yield under coherent laser excitation reported since 2018 was 16%.[7-9] Since its initial discovery, early work has focused on observing similar photochemical behavior in aromatic hydrocarbons and organometallic species, many of which occur in crystalline materials.[10]

In another example of a nonlinear photochemical reaction, singlet fission involves the interaction of a high-energy singlet excited state with a ground state singlet, resulting in the formation of two low-energy triplets (**Figure 1.2**).[11-13] Initial observations of this process, by the Singh and Swenberg groups in the 1960s, were explained by delayed fluorescence of crystalline acenes.[14,15] Renewed interest in this work during the early 2000s was sparked due to its potential to increase efficiency of organic photovoltaic devices (OPV) from 33 to 47%.[16]

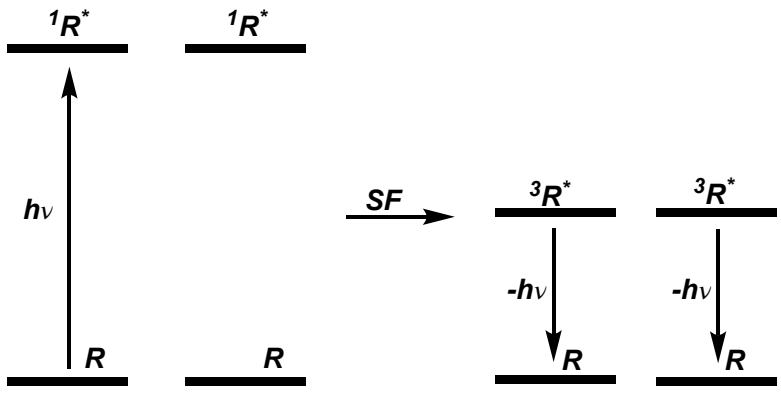

Figure 1.2 Singlet Fission

In depth computational studies were used to assess physical, chemical, and structural properties in order to determine aromatic organic compounds that will undergo singlet fission. Some key characteristics that were studied included systems that were exergonic, ultrafast, and highly efficient but show charge transfer properties. Structural and electronic requirements for optimal singlet fission include 1) adiabatic reaction conditions in which the energy of the second triplet excited state was greater than the excited singlet state and the energy of the singlet excited state is greater than or equal to the first triplet excited state ($E(T_2) - E(S_0) > E(S_1)$ and $E(S_1) - E(S_0) \geq 2(E(T_1) - E(S_0))$, 2) suitable molecular packing for intermolecular electronic coupling that avoids competitive singlet deactivation and 3) separation of triplet states into free charges.[17] Anthracene (**1.1**), perylene (**1.2**), and 1,2-diphenylisobenzofuran (**1.3**) are all classic examples of molecules that undergo singlet fission (**Figure 1.3**).[17-19] Many of these compounds undergo singlet fission as organic crystals. Previous work by the Johnson group describes the reactivity of **1.3** within polycrystalline thin films and the influence of polymorphism on its singlet fission efficiency.[20-30] Several publications detail extensive studies of singlet fission and its applications.[31-36]

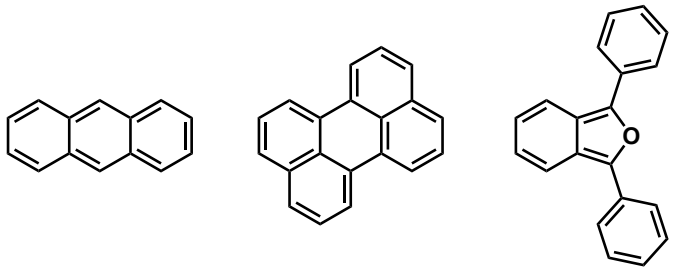

1.1 **1.2** **1.3**

Figure 1.3 Examples of conjugated molecules known to undergo singlet fission. Anthracene (**1.1**); perylene (**1.2**); and 1,2-diphenylisobenzofuran (**1.3**)

1.2 Quantum Chain Reaction

A more interesting, but less explored nonlinear photochemical process, is known as a quantum chain reaction. A quantum chain reaction occurs when a single photon leads to the formation of several photoproducts based on energy transfer mechanisms, resulting in quantum yields that exceed unity. The first known quantum chain was reported by Hammond in 1969 based on his irradiation studies of 2,4-hexadiene in solution.[37] This initial discovery reported quantum yield measurements that exceeded theoretical values for a linear photochemical system, suggesting unprecedented photochemical reactivity. Through this work several key components for a quantum chain reaction were established, including the presence of an excited intermediate engaging in an energy transfer process, concentration dependent efficiency, and the significance of impurities in early chain termination. While this work marked the first investigation into this unprecedented chain process, it was later determined that Crandall's investigation into the photochemical isomerization of 1,5,9-cyclodecatriene can be explained as a quantum chain process.[38]

Since its initial discovery, further investigation into the requirements, identification, and expansion of the quantum chain reaction continued into the late 70s. In 1977, Turro reported this observation in the triplet sensitized photochemical isomerization of highly-strained Dewar benzenes to Hückel benzene.[39-40] Dewar benzenes are one of three benzene valence isomers that are known to strictly undergo this process upon triplet activation, as Turro determined that direct irradiation (λ=254nm) gave the Hückel benzene as the major product and prismane at low concentrations ($<10^{-2}$ M). This work detailed the necessity for high energy triplet sensitizers to activate the triplet Dewar benzene and described the electronics involved in its triplet sensitized transformation to Hückel benzene (**Figure 1.4**).

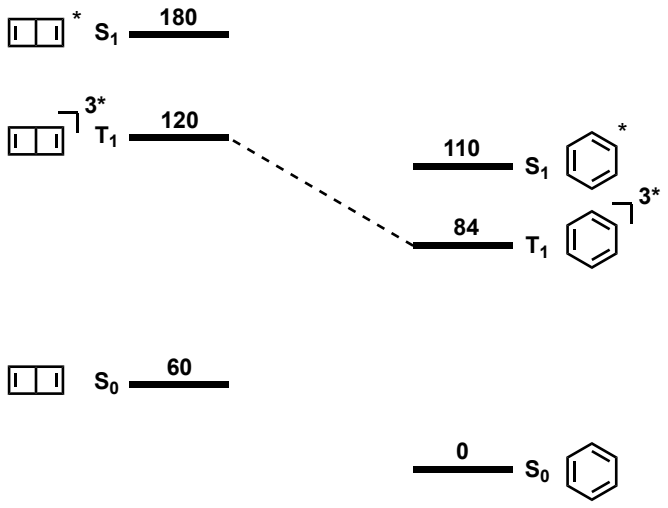

Figure 1.4 Electronic transition states of Dewar to Hückel benzene transformation with energies in kcal/mol.

Further evidence supports that a quantum chain reaction does not occur upon direct irradiation due to the absence of the singlet excited benzene intermediate. Based on this work it was concluded that a quantum chain reaction must involve activation of a high energy molecule, a transformation from excited reactant to excited photoproduct in a process known as an adiabatic reaction, and an energy transfer process from the excited photoproduct to a ground state reactant under the condition that the excited energy of the photoproduct is greater than that of the reactant. This reactivity can be visualized on an energy surface diagram, particularly for the adiabatic process that suggests the transformation is energetically favorable due to the barrierless transition and the large energy gap between excited and ground transition states (**Figure 1.4**).[40] Several of the organic small molecules that have been reported to undergo quantum chain reactions can be seen in **Figure 1.5**.

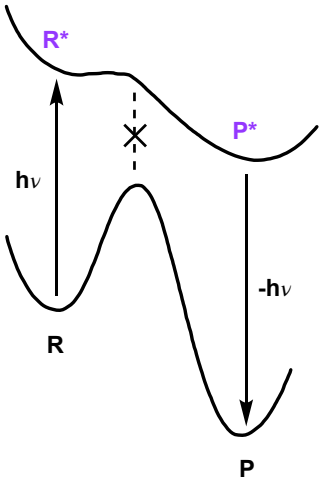

Figure 1.5 Surface energy diagram for a quantum chain reaction

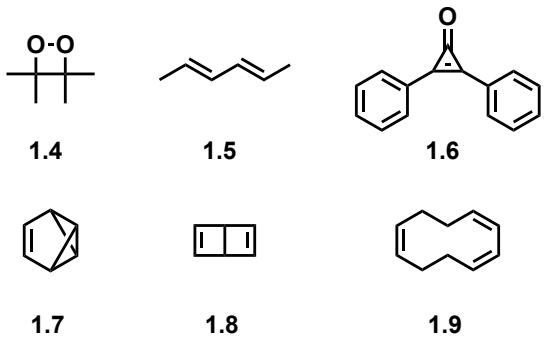

Figure 1.6 Examples of compounds that undergo a quantum chain reaction dioxetane (**1.4**), 2,4-hexadiene (**1.5**), diphenylcyclopropenone (**1.6**), benzvalene (**1.7**), Dewar benzene (**1,8**), 1,5,9-cyclododecatriene (**1.9**)

1.3 Adiabatic Reaction

The extent of the quantum chain reaction relies on two key components: the efficiency of the adiabatic process and the number of energy transfer steps that can occur. The rate and efficiency of the

adiabatic process relies on available mechanisms throughout the molecule's motion along the excited energy surface ($k_a >> k_{relaxation}$). In 1970, Forster initially described adiabatic photochemical processes in acid-base reactions and excimer/exciplexes and outlined three categories of photoreactions.[41,42] These three photoreactions can be visualized by energy surfaces in **Figure 1.7**, where class a and b reactions are adiabatic and class c are diabatic. This work highlights the electronic differences that make interconversion from excited to ground state surface unfavorable for an adiabatic process. Turro and coworkers later documented several carbon-carbon bond breaking and making transformations that involve an adiabatic pathway including electrocyclic, cycloeliminations, and isomerizations.[40,43-47]

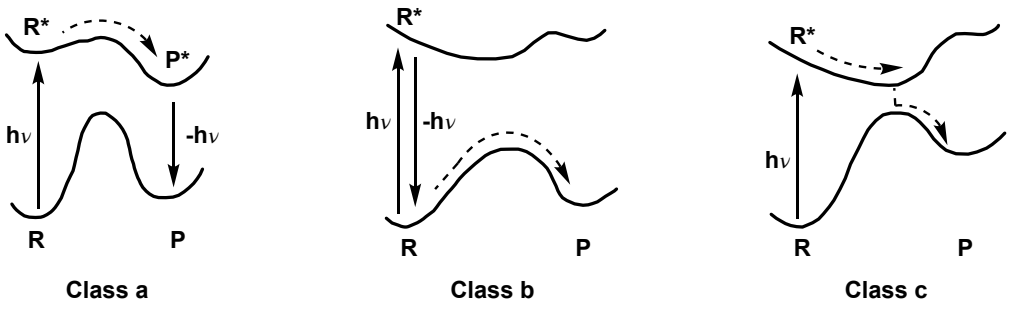

Figure 1.7 Types of photochemical reactions where class is a) an adiabatic photochemical reaction, b) a hot ground state reaction, and c) a common non-adiabatic photochemical transformation

1.4 Energy Transfer

The second component of an efficient quantum chain reaction relies on the energy transfer mechanism. The extent of the energy transfer process depends on the rate of energy transfer and the extent of the excited intermediate lifetime.[48-50] To achieve high efficiency quantum yields the excited photoproduct, often referred to as the chain carrying species, must exist long enough for the energy transfer process to occur. Thus the energy transfer process is largely limited by reactant concentration and diffusional rates of energy within media. Other factors involve proximity of photoproduct to

reactants and relaxation rates. Dinnocenzo and coworkers demonstrated the importance of these factors in controlling the extent of the Dewar benzene quantum chain reaction using co-sensitizers to expand the number of available molecules engaging in energy transfer and studying rates of energy transfer in various media.[51] Quantum yields in solution were reported at ca. 120 in ethyl acetate and ca. 4 when doped in PMMA.[52] Limitations to the extent of the energy transfer process was attributed to back energy transfer between sensitizer and reactant/photoproduct of optimal distance. The group reasoned that energy transfer occurred within a defined radius or "action sphere", which played a role in early chain termination. To further expand on this concept, they integrated Dewar benzene, co-sensitizers, and sensitizer into a polymer scaffold, which was reported to have quantum yields values of ca. 7-8 based on energy hopping between monomeric components.

Previous work from our lab revealed that the photodecarbonylation of diphenylcyclopropenones (DCPC) to give diphenylacetylene (DPA) can be achieved in quantum yields above unity in the crystalline solid state.[48-49] This work demonstrated the crystalline solid state promotes an environment that enables a quantum chain reaction, while the quantum yields of unity were achieved in solution. This reactivity was supported by the energetics of DPCP showing that the excitation of DPCP was accessed through the second singlet excited state S_2, resulting in a short-lived excited diphenylacetylene (DPA) photoproduct with an 8 ps lifetime. This allowed a maximum quantum yield potential of about 4-6 photoproducts per photon absorbed. Quantum yield experiments of DPCP in nanocrystalline suspensions determined a quantum chain in the crystalline solid state of ca. 3.3.

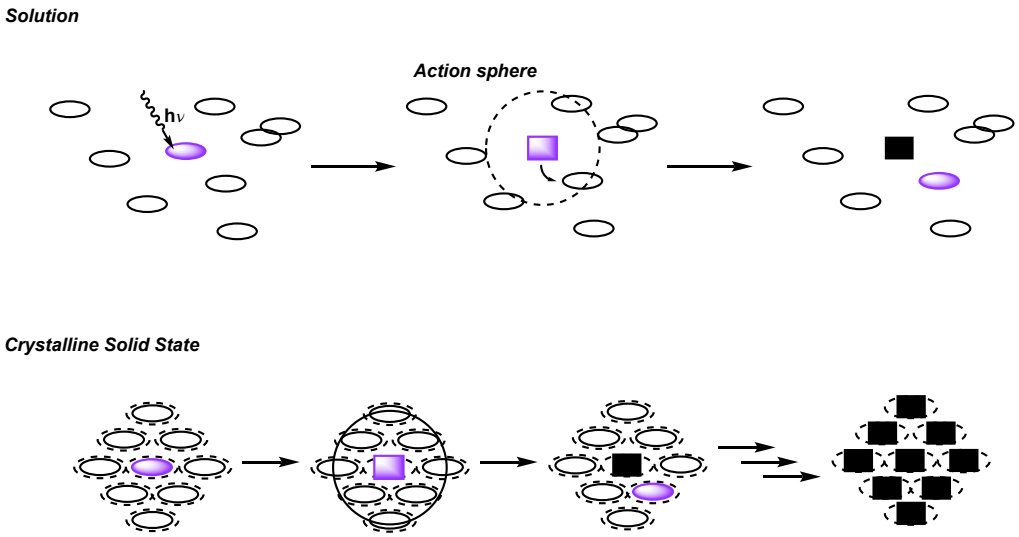

Figure 1.8 Schematic of energy transfer mechanism in solution and crystalline solid state

From this work we were interested in exploring the potential of the crystalline solid state environment in expanding the quantum chain reaction of Dewar benzenes due to excitonic energy transfer rates (10^{12} s^{-1}), long lived triplet excited photoproduct (10^{-6}-10^{-3}), homogeneity, and reduced quenching mechanisms related to solvent (**Figure 1.8**).

1.5 Sensitizer-linked Dewar benzenes

We were interested in exploring quantum chain reactions of Dewar benzenes in the crystalline solid state in order to access long-lived triplet intermediates that can engage in ultrafast energy transfer processes. In order to activate the Dewar benzene as an excited triplet in the crystalline solid state we utilized benzophenone as a triplet sensitizer to covalently attach to Dewar benzene via ester linkage.

Scheme 1.1 Proposed mechanism for photochemical isomerization of **DB-OBPh**

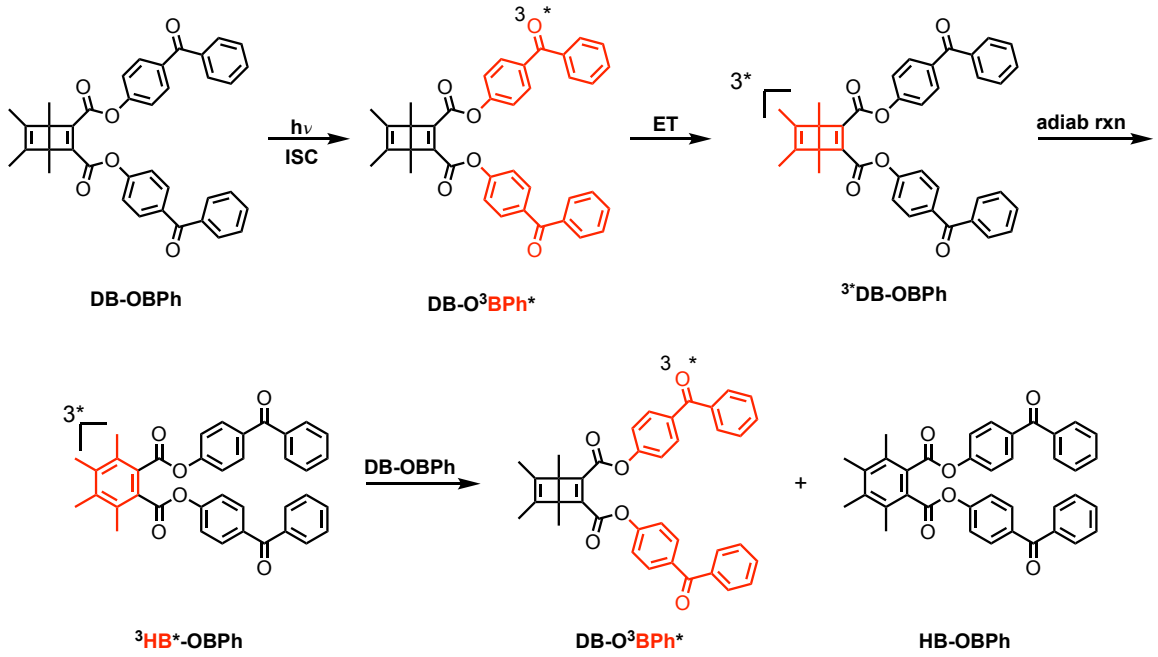

We envisioned that this Dewar benzene can undergo a quantum chain reaction that would proceed based on the mechanism provided in **Scheme 1.1**, where upon absorption of a photon would result in the excitation of the benzophenone moiety. This would be followed by rapid intersystem crossing to access the triplet excited benzophenone, which would then undergo an intramolecular energy transfer to the Dewar benzene moiety. With the triplet excited Dewar benzene generated the adiabatic transformation from Dewar to Hückel benzene photoproduct should occur with high efficiency. The excited photoproduct would then transfer its energy to a ground state Dewar benzene, resulting in a ground state photoproduct and a newly excited Dewar benzene. This dissertation explores the reactivity in solution and in the solid state through transient absorption analysis, timed irradiation experiments, and solid state analysis of **DB-OBPh** and other Dewar benzene derivatives.

1.6 References

1. Gertsen, A. S.; Koerstz, M.; Mikkelsen, K. V. Benchmarking triplet-triplet annihilation photon upconversion schemes *Phys. Chem. Chem. Phys.*, **2018**, *20*, 12182-12192.
2. Ye, C.; Gray, V.; Martensson, J.; Borjesson, K. Annihilation Versus Excimer Formation by the Triplet Pair in Triplet-Triplet Annihilation Photon Upconversion *J. Am. Chem. Soc.* **2019**, *24*, 9578-9584.
3. Rachford-Singh; T. N.; Castellano, F. N. Photon upconversion based on sensitized triplet-triplet annihilation *Coordination Chemistry Reviews*, **2010**, *254*, 2560-2573.
4. Parker, C. A.; Hatchard, C. G. Sensitized P-type delayed fluorescence *Proc. Chem. Soc.: Lond.* **1962**, 386.
5. Baldo, M. A.; Adachi, C.; Forrest, S. R. Transient analysis of organic electrophosphorescence. II. Transient analysis of triplet-triplet annihilation *Phys. Rev. B* **2000**, *62*, 10967-10977.
6. Zhao, J.; Ji, S.; Guo, H. Triplet-triplet annihilation based upconversion: from triplet sensitizers and triplet acceptors to upconversion quantum yields *RSC Adv.*; **2011**, *1*, 937-950.
7. Parker, C. A. Phosphorescence and delayed fluorescence from solutions *Adv. Photochem. 2.* **1964**, 305.
8. Monguzzi, A.; Mezyk, J.; Scotognella, F.; Tubino, R.; Meinardi, F. Upconversion-induced fluorescence in multicomponent systems: Steady-state excitation power threshold *Phys. Rev. B: Condens. Matter Mater. Phys.*, **2008**, *78*, 195112.
9. Monguzzi, A.; Tubino, R., Hoseinkhani, S., Campione, M; Meinardi, F. Low power, non-coherent sensitized photon up-conversion: modelling and perspectives *Phys. Chem. Chem. Phys.*, **2012**, *14*, 4322–4332.

10. Khnayzer, R. S.; Blumhoff, J.; Harrington, J. A.; Haefele, A.; Deng, F.; Castellano, F. N. Upconversion-powered photoelectrochemistry *Chem. Commun*., **2012**, *48*, 209–211.
11. Cao, B. Hu and P. Zhang. High upconversion efficiency from hetero triplet-triplet annihilation in multiacceptor systems *J. Phys. Chem. Lett.,* **2013**, *14*, 2334–2338.
12. Chen, J. Zhao, L. Xie, H. Guo and Q. Li. Thienyl-substituted BODIPYs with strong visible light-absorption and long-lived triplet excited states as organic triplet sensitizers for triplet-triplet annihilation upconversion *RSC Adv.*, **2012**, *2*, 3942–3953.
13. Haase, M.; Schafer, H. Upconverting Nanoparticles *Angew. Chem., Int. Ed.* **2011**, *50*, 5808-5829.
14. Wang, F.; Banerjee D.; Liu, X.; Chen, X.; Liu, X. Upconversion nanoparticles in biological labeling, imaging, and therapy *Analyst,* **2010**, *135*, 1839-1854.
15. Shalav, A.; Richards, B.; Green, M. Luminescent layers for enhanced silicon solar cell performance: Upconversion *Sol. Energy Mater. Sol. Cells*, **2007**, *91*, 829-842.
16. Van der Ende, B. M.; Aarts, L.; Meijerink, A. Lanthanide ions as spectral converters for solar cells *Phys. Chem. Chem. Phys.*, **2009**, *11*, 11081-11095.
17. Baluschev, S.; Yakutkin, V.; Wegner, G.; Miteva, T.; Nelles, G.; Yasuda, A.; Chernov, S.; Aleshchenkov, S.; Cheprakov, A. Upconversion with ultrabroad excitation band: simultaneous use of two sensitizers *Appl. Phys. Lett*., **2007**, *90*, 181103.
18. Wilke, B. M.; Castellano, F. N. Photochemical upconversion: a physical or inorganic chemistry experiment for undergraduates using a conventional fluorimeter *J. Chem. Educ*., **2013**, *90*, 786–789.
19. Ekins-Daukes, N. J.; Schmidt, T. W. Amolecular approach to the intermediate band solar cell: The symmetric case *Appl. Phys. Lett.*, **2008**, *93*, 063507.

20. Nattestad, A.; Cheng, Y. Y.; MacQueen, R. W.; Schulze, T. F.; Thompson, F. W.; Mozer, A. J.; Burkhard, F.; Khoury, T.; Crossley, M. J.; Lips, K.; Wallace, G. G; Schmidt, T. W. Dye-sensitized solar cell with integrated triplet-triplet annihilation upconversion system *J. Phys. Chem. Lett*., **2013**, *4*, 2073–2078.
21. Gray, V.; Dzebo, D.; Abrahamsson, M.; Albinsson, B.; Moth-Poulsen, K. Triplet-triplet annihilation photon-upconversion: towards solar energy applications *Phys. Chem. Chem. Phys*. **2014**, *16*, 10345-10352.
22. Huang, L.; Wu, W.; Li, Y.; Zeng, K.; Lin, W.; Han, G. Selenium Heterocyclic Electron Acceptor with Small Urbach Energy for As-Cast High-Performance Organic Solar Celles *J. Am. Chem. Soc.* **2020,** *142*, 18469-18470.
23. Swenberg, C. E.; Geacintov, N. E. Exciton interactions in organic solids *Org. Mol. Photophysics* **1973**, *18*, 489.
24. Pope, M.; Swenberg, C. E. *Elecronic Processes in Organic Crystals and Polymers*, 2nd ed.; Oxford University Press: Oxford, U.K.K, 1999; pp 134-191.
25. Singh, S.; Jones, W.; Siebrand, W.; Stoicheff, B.; Schneider, W. Laser generation of excitons and fluorescence in anthracene crystals *J. Chem. Phys.* **1965**, *42*, 330-342.
26. Swenberg, C.; Stacy, W. Bimolecular radiationless transistions in crystalline tetracene *Chem. Phys. Lett.* **1968**, *2*, 237-328.
27. Hanna, M.; Nozik, A. Solar conversion efficiency of photovoltaic and photoelectrolysis cells with carrier multiplication absorbers *J. Appl. Phys*. **2006**, *100*, No. 074510
28. Felter, K. M.; Grozema, F. C. Singlet fission in crystalline organic materials: Recent insights and future directions *J. Phys. Chem. Lett.* **2019**, *10*, 7208-7214.

29. Pun, A. B.; Asadpoordarvish, A.; Kumarasamy, E.; Tayebjee, M. J. Y.; Niesner, D.; McCamey, D. R.; Sanders, S. N.; Campos, L. M.; Sfeir, M. Y. Ultra-fast intramolecular singlet fission to persistent multiexcitons by molecular design *Nat. Chem.* **2019**, *11*, 821-828.
30. Schnedermann, C.; Alvertis, A. M.; Wende, T.; Lukman, S.; Feng, J.; Schroder, F. A.Y.N.; Turban, D. H.P.; Wu, J.; Hine, N. D. M.; Greenham, N. C.; Chin, A. W.; Rao, Akshay, R.; Kukura, P.; Musser, A. J. A molecular movie of ultrafast singlet fission *Nat. Commun.* **2019**, *10*, 4207.
31. Johnson, J. C.; Nozik, A.; Michl, J. High triplet yield from singlet fission in a thin film of 1,3-diphenylisobenzofuran *J. Am. Chem. Soc.* **2010**, *132*, 16302-16303.
32. Michl, J. Model calculations of photochemical reactivity *Pure. Appl. Chem.* **1975**, *41*, 507.
33. Michl, J. Excited potential energy hypersurfaces for hydrogen (H4) at trapezoidal geometries. Relation to photochemical 2s+ 2s processes *J. Am. Chem. Soc.* **1976**, *98*, 6427.
34. Arias, D. H.; Ryerson, J. L.; Cook, J. D.; Damrauer, N. H.; Johnson, J. C. Polymorphism influences singlet fission rates in tetracene thin films *Chem. Sci.*, **2016**, *7*, 1185-1190.
35. Smith, M. B.; Michl, J. Singlet Fission *Chem. Rev.* **2010**, *110*, 6891-6936.
36. Johnson, J. C.; Nozik, A. J.; Michl, J. The role of chromophore coupling in singlet fission *Acc. Chem. Res.* **2013**, *46*, 1290-1299.
37. Hyndman, H. L.; Monroe, B. M.; Hammond, G. S. Mechanisms of photochemical reactions in solution. LX. Photocheimcal isomerization of 2,4-hexadiene via a quantum-chain mechanism *J. Am. Chem. Soc.* **1969**, *91*, 2852-2859.
38. Crandall, J. K.; Mayer, C. F. Benzene-photosensitized transformations of the four geometrical isomers of 1,5,9-cyclododecatriene *J. Am. Chem. Soc.* **1967**, *89*, 4374-4380.
39. Turro, N. J.; Ramamurthy, V.; Katz, T. J. Energy Storage and Release. Direct and sensitized photoreactions of dewar benzene and prismane. *Nouveau Journal de Chimie* **1978**, *1*, 363–365.

40. Turro, N. J.; McVey, j.; Ramamurthy, V.; Lechtken, P. Adiabatic photoreactions of organic molecules *Angew. Chem. Int. Ed. Eng.* **1979**, *18*, 572-586.

41. Th. Forster. Diabatic and adiabatic processes in photochemistry *Pure Appl. Chem.* **1970**, *24*, 443-449.

42. Th. Forster. Excimers *Angew. Chem. Int. Ed.* **1969**, *8*, 333.

43. Skourtis, S. S.; Liu, C.; Antoniou, P.; Virshup, A. M.; Beratan, D. N. Dexter energy transfer pathways *Proc. Natl. Acad. Sci.* **2016**, *113*, 8115-8120.

44. Turro, N. J.; Ramamurthy, V.; Scaiano, J. C. *Principles of Molecular Photochemistry: An Introduction*; Viva Book: New Delhi, 2015.

45. Carr, R. V.; Kim, B.; McVey, J. K.; Yang, N. C.; Gerhartz, W.; Michl, J. *Chem. Phys. Lett*. **1974**, 39, 57-60.

46. Yang, N. C.; Carr, R. V.; Li, E.; McVey, J. K.; Rice, S. A. Photochemistry and photophysics of 1,4-dewarnaphthalene *J. Am. Chem. Soc.* **1974**. *96*, 2297-2298.

47. Linschitz, H.; Greilmann, K. H. Reaction Pathways in the Photochemical conversion of Diphenylamines to Carbazoles *J. Am. Chem. Soc*. **1964**, *86,* 303.

48. Kuzmanich, G.; Natarajan, A.; Chin, K. K.; Veerman, M.; Mortko, C. J.; Garcia-Garibay, M. A. Solid-state photodecarbonylation of diphenylcyclopropenone: a quantum chain process made possible by ultrafast energy transfer *J. Am. Chem. Soc*. **2008**, *130*, 1140-1141.

49. Kuzmanich, G.; Gard, M. N.; Garcia-Garibay, M. A. Photonic amplification by a singlet-state quantum chain reaction in the photodecarbonylation of crystalline diarylcyclopropenones. *J. Am. Chem. Soc.* **2009**, *131*, 11606–11614.

50. Wakasa, M.; Yago, T.; Sonoda; Y.; Katoh, R. Structure and dynamics of triplet-exciton pairs generated from singlet fission studied via magnetic field effects *Communications Chemistry*, **2018**, *1*, 1-6.

51. Kiau, S.; Liu, G.; Shukla, D.; Dinnocenzo, J. P.; Young, R. H.; Farid, S. Kinetics of Isomerization via Photoinduced Electron Transfer. I. Spectral Analysis and Structural Reorganization of Hexamethyl Dewar Benzene Exciplexes *J. Phys. Chem. A* **2003**, *107*, 3625-3632.

52. Ferrar, L.; Mis, M.; Dinnocenzo, J. P.; Farid, S.; Merkel, P. B.; Robello, D. R. Quantum Amplified Isomerization in Polymers Based on Triplet Chain Reactions *J. Org. Chem.* **2008**, *73*, 5683-5692.

CHAPTER TWO

Triplet State Quantum Chain Amplification in Crystalline Dewar Benzenes by Intramolecular Sensitization

Adapted from: Edris Rivera and Miguel A. Garcia-Garibay *In Revision*

2.1 ABSTRACT

The triplet-sensitized isomerization of Dewar benzene is known to undergo quantum chain reaction characterized by an adiabatic valence-bond isomerization to the excited state of Hückel benzene, which transfers its triplet energy to a new ground state Dewar benzene that reacts to continue the chain (**Scheme 2.1**). Quantum chain reactions are characterized by the formation of several photoproducts per photon absorbed ($\Phi > 1$) and constitute a promising signal amplification mechanism. Given that diffusion-mediated energy transfer is the chain-limiting event in solution, we demonstrate here that reactions in crystals are significantly more efficient by taking advantage of energy transfer by a presume exciton delocalization mechanism. Using Dewar benzenes with covalently-attached, high energy triplet sensitizer we have demonstrated the efficiency of the solid state through the amplification of a quantum yield of ca. 3 in acetonitrile solution to as much as ca. 100-120 in submicron size specimens prepared by the solvent shift or re-precipitation method, and up to ca. $\Phi_{QC} \approx 300$ with microcrystalline powders suspended in water.

Scheme 2.1 Schematic of proposed Dewar benzene quantum chain reaction

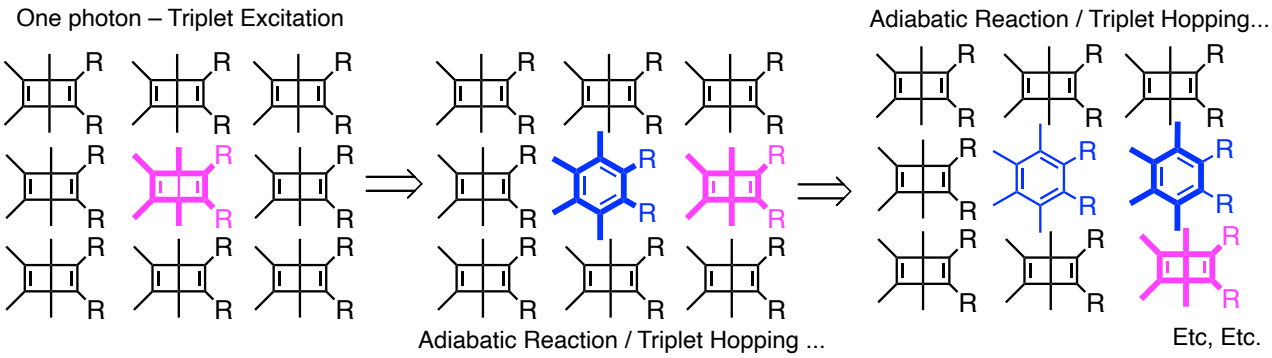

2.2 Introduction

Most organic photochemical processes involve the excitation of a single molecule followed by return to the ground state by releasing heat, emitting a single photon, transferring its energy to another molecule, or undergoing a reaction to give a primary photoproduct.[1] Exceptions from this norm include nonlinear photochemical processes involving a non-identical number of photochemical events and photons absorbed. Such systems can be utilized for signal amplification devices, catalysis, and solar cells.[2-5] Examples include coherent and stepwise[6,7] two photon absorption, fusion of two or more low energy photons to generate one high-energy excited state by triplet-triplet annihilation,[8] and the fission of a single excitation generated with a high-energy photon that result in two excited states, each with half the energy of the original.[9,10] An equally interesting, but significantly less explored process occurs when a single photon can lead to many chemical events in what is known as a "quantum chain reaction".[11] Quantum chain reactions start by formation of an excited state (Step 1, **Scheme 2.2**) and are followed by a relatively uncommon propagation step (Step 2, **Scheme 2.2**) involving an adiabatic photochemical reaction that gives rise to the photoproduct in the excited state.[12-15] This is followed by energy transfer to a new ground state reactant that prolongs the chain (Step 3, **Scheme 2.2**). Chain

termination occurs when either the excited state product (P*) or reactant (R*) undergo thermal or radiative decay (Step 4 and/or Step 5, **Scheme 2.2**).[16-32]

Despite the promise offered by chemical systems leading to multiple events per photon absorbed, the number of adiabatic reactions known at this time is relatively small, and proper strategies must be developed in order to optimize the energy transfer step. For example, singlet state quantum chains are severely limited by

Scheme 2.2 Required steps for a quantum chain reaction

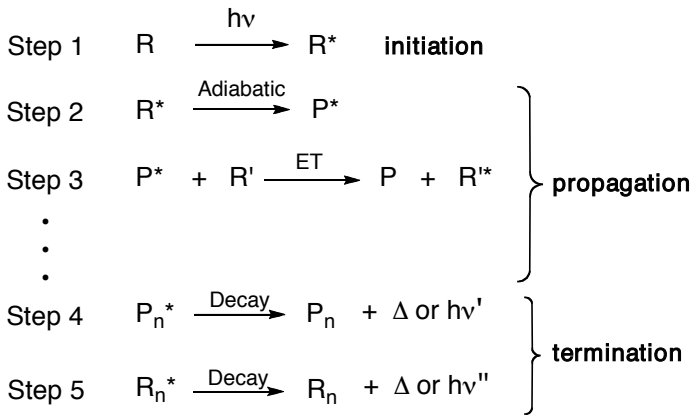

the short lifetimes of the excited state photoproducts, which make energy transfer by diffusion-mediated mechanisms unfavorable. Adiabatic reactions that take place in the singlet state are commonly established by detecting the fluorescence[33,34] or transient absorption of the excited photoproduct, rather than by observation of a quantum yield of product formation that is greater than one, which is the key signature of a quantum chain. We recently proposed that an effective way to circumvent this limitation is by carrying quantum chain reactions in crystalline solids, where energy transfer can occur by an ultrafast exciton delocalization mechanism.[35-39] We showed that the adiabatic

decarbonylation of diphenylcyclopropenone to diphenyl acetylene could not enter a quantum chain process in solution despite having an adiabatic quantum yield Φ=1, because there is no time for diffusion-mediated energy transfer within the ca. 8 ps of the excited photoproduct.[40] By contrast, quantum chain reactions with quantum yields up to Φ=3.3 could be measured in aqueous nanocrystalline suspensions of diphenylcyclopropane, where energy transfer is mediated by a rapid exciton delocalization mechanism.[40,41]

Efficient quantum chains ($\Phi_{Chain} >> 1$), require adiabatic reactions with high quantum efficiencies ($\Phi_{AR} \approx 1$), and are limited by the number of energy transfer steps, n, as shown in Equations 1 – 3.[41]

$$\Phi_{Chain} = (\Phi_{AR})^1 + (\Phi_{AR})^2 + (\Phi_{AR})^3 + ... \ (\Phi_{AR})^n \quad \text{Eq. 1}$$

$$\Phi_{AR} = k_{AR} / [k_{AR} + k_{R\text{-}dec}] \quad \text{Eq. 2}$$

$$n = k_{ET} / k_{P\text{-}dec} \quad \text{Eq. 3}$$

It should be noted that efficient adiabatic reactions ($\Phi_{AR} \approx 1$) require reaction rates that are much greater than then that of the decay of the excited reactant by all other pathways ($k_{AR} >> k_{\text{-}Rdec}$). The maximum value n in equation 1 is determined by the relative rates of energy transfer from the excited photoproduct (k_{ET}) in relation to its rate of decay ($k_{P\text{-}dec}$).[41]

Based on the above analysis, one may expect that triplet quantum chain reactions carried out in crystalline solids have the potential to reach extremely high Φ_{Chain} values by taking advantage of energy transfer by triplet exciton hopping,[42,43] which is known to approach the picosecond time scale. Assuming ideal adiabatic reactions with $\Phi_{AR} \approx 1$, the theoretical limit for a triplet quantum chain is given by the value of n in Eq. 1, as defined in Eq. 3. Based on a general approximation, one may expect n= $k_{ET}/k_{P\text{-}dec}$ to take values as large as 10^9 if triplet excitons have jumping rates of ca. $k_{ET} \approx 10^{12}$ s^{-1} and triplet lifetimes (τ_T) that extend into the millisecond time scales: $\tau_T = 1/k_{dec} \approx 10^{-3}$ s.

In order to test this hypothesis we explore here the quantum chain reaction of crystalline Dewar benzene to Hückel benzene. Early studies by Turro *et al*., demonstrated that Dewar benzene undergoes an adiabatic triplet state valence-bond isomerization in solution to give triplet (Hückel) benzene with a concentration-dependent quantum chain reaction that reaches a limiting value of ca. Φ=10. It was shown that triplet energy sensitizers with E_T > 63 kcal/mol are required for efficient energy transfer, indicating an experimental upper limit for triplet Dewar benzene.[44] More recently, using a Dewar benzene 3,4,5,6-tetramethyl-1,2-diester derivative (**DB-OMe**), Farid and coworkers reported quantum yields as high Φ=120 in ethyl acetate,[45] and showed the feasibility of quantum chain reactions in polymer matrices upon the addition of external sensitizers and co-sensitizers.[46]

A key requirement to carry out a triplet state quantum chain reaction in the crystalline state is to have an efficient access to the triplet excited state of the Dewar benzene reactant (^{3}**DB-R***). As indicated **in Scheme 2.3**, a simple solution to this problem is to substitute the two dicarboxymethyl groups for 4-hydroxy-benzophenones (**DB-OBPh**), so that triplet sensitization can occur intramolecularly. It is well known that electronic excitation of the benzophenone chromophore leads to intersystem crossing and efficient formation of the triplet ^{3}n,π* excited state within a few picoseconds. Subsequent intramolecular energy transfer to the covalently attached Dewar benzene moiety (Step 1, **Scheme 2.3**) is expected to initiate the quantum chain by forming **^{3}DB-OBPh***. An adiabatic triplet state reaction is known to form the triplet excited state of the Hückel benzene photoproduct, ^{3}**HB-OBPh** (Step 2, **Scheme 2.3**), which acts as the quantum chain carrier. In Step 3 (**Scheme 2.3**), the triplet photo product ^{3}**HB-OBPh*** should be ideally suited in crystals to transfer energy to a neighboring ground state Dewar benzene **DB-OBPh** to propagate the chain. While chain termination is expected to occur via Steps 4 or 5 when either excited state decays back to the ground state manifold, step 5 is accounted for in the quantum

Scheme 2.3 Proposed quantum chain reaction of DB-OBPh

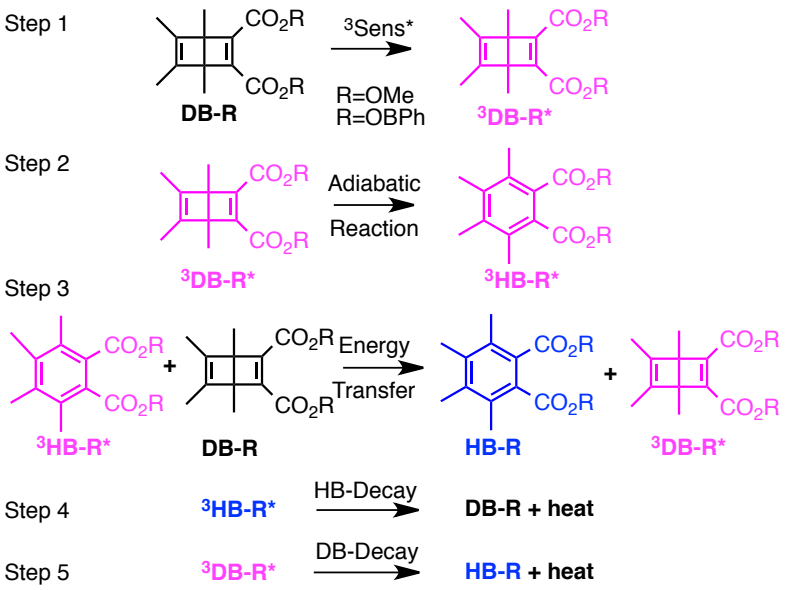

yield of the adiabatic reaction, so that the chain length given by the value of n depends on the relative rates of step 3 and 4. As described below, we were able to demonstrate a concentration dependent quantum chain in solution with modest values ranging from ca. Φ=1.9 to Φ =2.8 for reactant concentrations ranging from 3-15 mM. By contrast, quantum chain reactions carried out with samples prepared by the reprecipitation method led to average quantum chain values of ca. Φ =100, even though the samples were shown to be semi-crystalline. Notably, a qualitative comparison of the latter with microcrystalline powders suspended in water showed an increase in quantum chain values up to ca. $\Phi\approx300$. Evidence for a fast adiabatic reaction was obtained by nanosecond laser flash photolysis experiments showing that the transient generated from the starting Dewar benzene **DB-OBPh** is identical to the one generated from the Hückel benzene photoproduct (^{3}**HB-BPh***).

Scheme 2.4 Synthesis of **DB-OBPh**

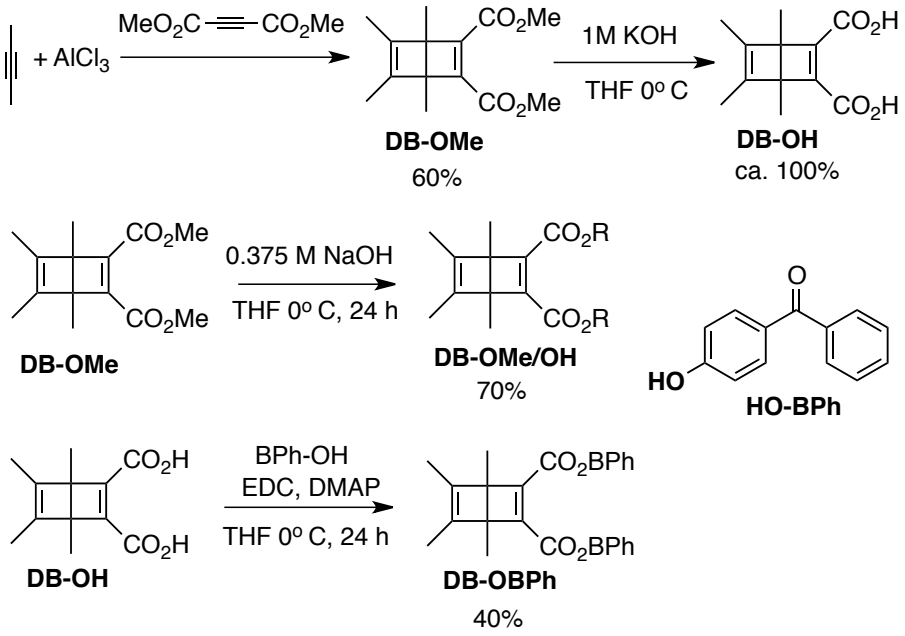

2.3 Results and Discussion

2.3.1 Synthesis and Characterization

Samples of tetramethyl-dewar benzene dicarboxylate derivatives with methoxy (**DB-OMe**), one (**DB-OMe/OH**) or two free carboxylic acids (**DB-OH**), and 4-hydroxy benzophenone (**DB-OBPh**) esters were prepared as indicated in **Scheme 2.4** from the previously reported **DB-OMe**. Full and partial hydrolysis of the **DB-OMe** yielded diacid **DB-OH** and acid/ester **DB-OMe/OH** as a white powder. The desired sensitizer-linked Dewar benzene **DB-OBPh** was obtained by EDC-mediated coupling of 4-hyrdoxybenzophenone with dicarboxylic acid **DB-OH**. A sample of 4-acetoxybenzophenone was also prepared as model compound to analyze the properties of the triplet senstitzer.[47]

All four Dewar benzene derivatives prepared for this study were characterized by standard analytical methods and the results are included in the Synthetic Procedures section. **DB-OBPh** proved to

be crystalline after purification. Melting with concomitant reaction to the valence-bond isomerized product was shown to occur at ca. 109 °C. Diffraction data from cubic prisms obtained by slow evaporation from diethyl ether were solved in the space group $P2_1/n$ with 4 molecules per unit cell. Molecules of **DB-OBPh** crystallize with the Dewar benzene fragments disordered over two positions alternating their concave and convex faces with occupancies of 64% and 36%. The disorder extends to the carboxylate groups, which connect to the corresponding benzophenones in a manner that they themselves are not disordered, as illustrated in **Figure 2.1**.

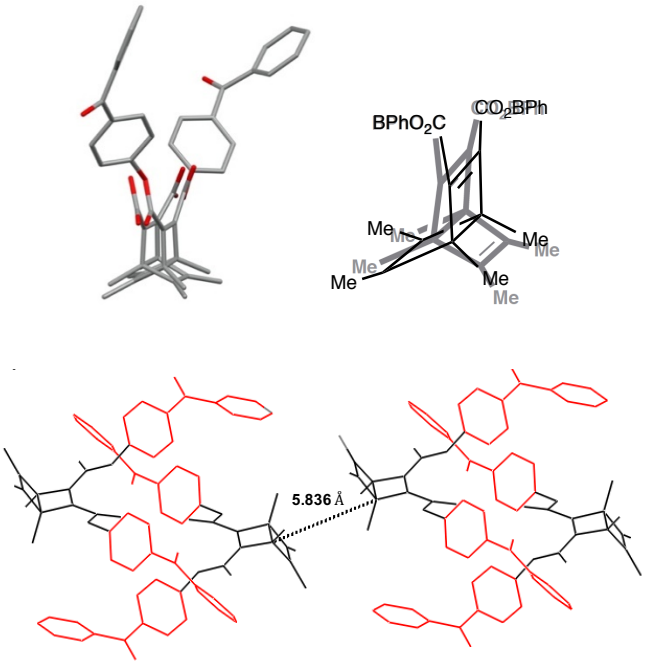

Figure 2.1. (Upper left) Bar diagram of the X-ray molecular structure of **DB-OBPh** illustrated the disorder of the Dewar benzene group and, (upper right) line structure illustrating its two orientations. (Bottom) Packing view illustrating the interdigitated benzophenone arrangement between pairs of molecules, and the closest distance between neighboring Dewar benzenes, which may be related to the distance for energy transfer.

2.3.2 Nanocrystalline Suspension

Knowing that the determination of an efficient quantum chain must be established by measuring the quantum yield of reaction, which is given by the number of product molecules formed per photon absorbed, we had to ensure that samples of **DB-OBPh** are able to form stable nanocrystalline suspensions. In fact, it is well known that spectroscopic methods based on measurements of the transmission of light in bulk solids are extremely challenging due to their high optical density, scattering, birefringence, and dichroism that characterize single crystals and polycrystalline samples. These effects also make it very difficult to measure the number of photons absorbed by the sample, which is essential for quantum yields measurements. To address these challenges, we have previously shown that crystals with sizes that are equal or smaller than the wavelength of light are able to mitigate these optical challenges, making it possible to measure transmission spectra, and to determine quantum yields with particle loadings that are high enough to trap every photon from a calibrated light source. It is now well established that many compounds are able to form aqueous nanocrystalline suspensions of well-defined crystals with average dimensions on the order of 50-500 nm, depending on the specific sample and experimental parameters. In our case, concentrated MeCN solutions of **DB-OBPh** were slowly added to a rapidly stirring solution of cetyl trimethyl ammonium bromide (CTAB) at concentration that is 1/50th of its critical micelle concentration (CMC) in Millipore water. Size determination by dynamic light scattering (DLS, DLS section) and scanning electron microscopy revealed prismatic crystals in the range ca. 200 nm to ca. 1 μm in size (**Figure 2.2**).

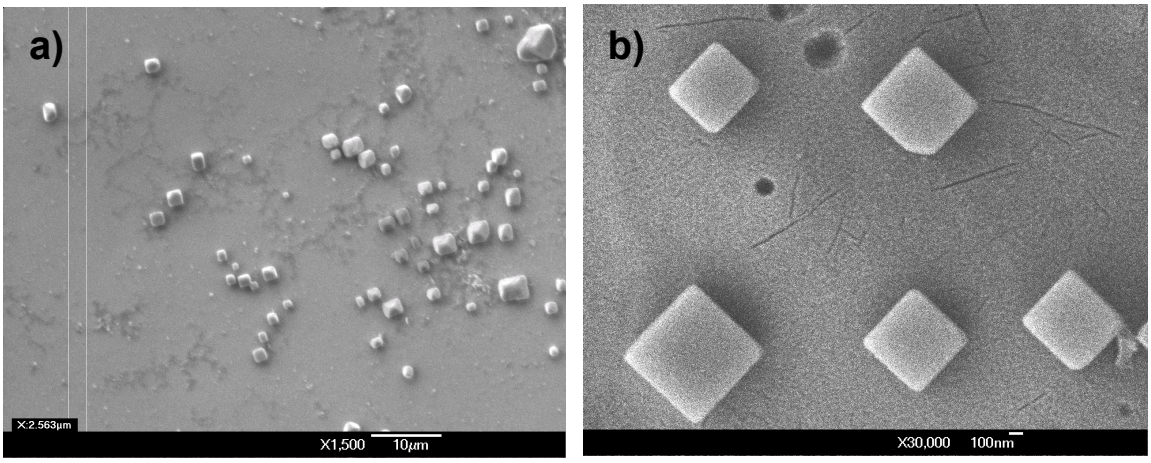

Figure 2.2 SEM images of **DB-OBPh** ca. 1 mm size crystals obtained from a dried suspension on a Si surface. Scale bars of a) 10 micron and b) 100 nm are shown.

2.3.3 Product Analysis in Solution and in Powder Samples.

Dilute (ca. 0.1 M) degassed acetonitrile solutions of **DB-OH**, **DB-OMe/OH** and **DB-OBPh** exposed to UV light with $\lambda \geq 295$ nm resulted on full conversion to the corresponding Huckel benzenes **HB-OH**, **HB-OMe/OH** and **HB-OBPh** as the only product. Similar results were observed with dry powders placed between two glass slides, indicating that the reaction can proceed as a solid-to-solid transformation. Reactions of **DB-OBPh** carried out in solution in the presence of oxygen lead to the formation of a new product consistent with the formation of an endoperoxide by reaction of the Dewar benzene with singlet oxygen. As expected, reactions carried out with **DB-OBPh** powders and nanocrystalline suspensions were not affected by the presence of oxygen. Samples of **HB-OBPh** could be crystallized and were shown to melt at 142 ^{o}C, which is a higher temperature than that of the melting point of the **DB-OBPh** reactant (ca. 109 °C). This suggests the possibility of a solid-to-solid reaction. Powder X-ray diffraction analysis of samples of **DB-OBPh** before and after reaction revealed that the reaction proceeds by amorphization, rather than a potential single-crystal to single-crystal transformation, or a more common solid-to-solid

reaction by a reconstructive phase transition. Unfortunately, we were not able to get diffraction quality single crystals of the Hückel photoproduct **HB-OBPh**.

2.3.4 Spectroscopic Characterization

Included in Figure 2.3 is a comparison of the UV spectra of the sensitizer-linked Dewar benzene **DB-OBPh** (purple dotted line) along with those of samples containing equimolar Dewar benzene methyl ester **DB-OMe** (blue solid line), two equivalents of 4-acetoxybenzopheone (**4-AcOBPh**, green, dashed line) that was used as a model chromophore, and a 2:1 mixture of **4-AcOBPh** and **DB-OMe** (black, dashed-dotted line). A relatively weak interaction of the two proximal benzophenone esters and the Dewar benzene can be inferred by noting that the UV spectrum of **DB-OBPh** (purple, dotted line) is more intense and slighter broader than the spectrum

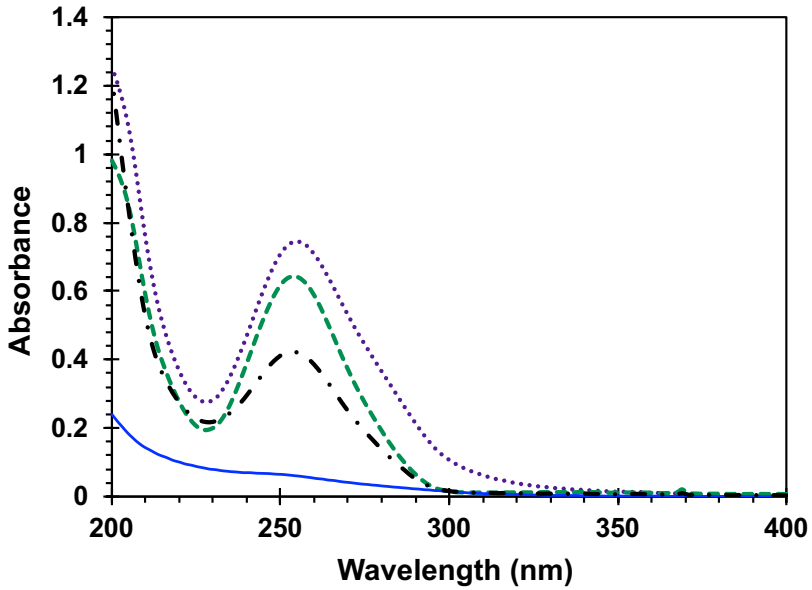

Figure 2.3 Absorption spectra in MeCN of 2.08×10^{-5} M **DB-OMe** (blue), 4.16×10^{-5} M 4-acetoxybenzophenone (green, dashed line), 1.65×10^{-5} M **DB-OBPh** (purple, dotted line), and a solution with 1:2 molar ratio of the **DB-OMe** and 4-acetoxybenzophenone (black, dashed-dotted line).

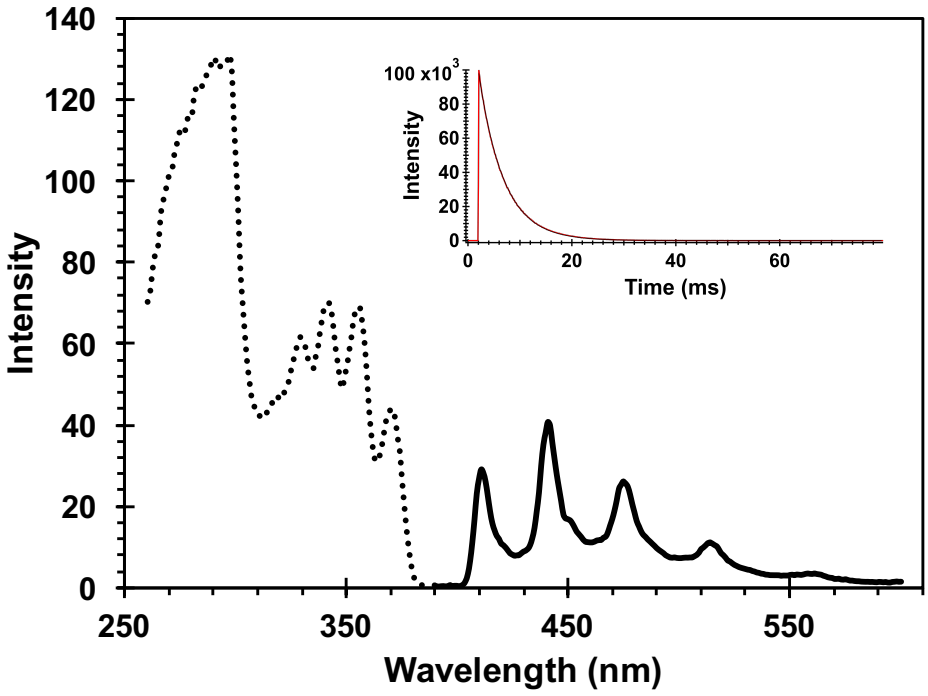

Figure 2.4 Phosphorescence excitation (dashed line) and emission (solid line) spectra of **HB-OBPh** in a methyl-cyclohexane glass at 77 K. The excitation spectrum detected at 441 nm and the emission obtained by excitation at 343 nm. The phosphorescence decay shown in the inset occurs with a time constant of 4.8 ms.

obtained when the two independent chromophores are mixed in the same molar ratio (Figure 2.3). We determined the triplet energy of the benzophenone sensitizer by measuring the phosphorescence spectrum of Hückel benzene **HB-OBPh** in dilute 2-methyltetrahydrofuran glass at 77 K (Figure 2.4). A characteristic emission with vibrational resolution and a relatively short (4.8 ms) lifetime typical of an n,π* excited state were obtained, along with a triplet energy of ca. 65 kcal/mol obtained from the onset of the 0-0 vibrational band.

2.3.5 Laser Flash Photolysis Detection of the Quantum Chain Carrier

In order to gain information on the evolution of the excited states and a potential triplet chain carrier we performed nanosecond laser flash photolysis experiments using a Brilliant B Quantel Nd-YAG laser operating at 355 nm with a pulse width of ca. 8 ns as the excitation source. Samples were introduced to a mounted 1 cm quartz flow cell through a continuous flow system to ensure that only unreacted material was continuously sampled. Samples were sparged with Argon for at least an hour prior to flowing into the flow cell and remained continuously sparged for the entire experiment. The characteristic triple-triplet absorption of the benzophenone sensitizer was determined by measuring the triplet absorption and lifetime of **4-AcOBPh**. As shown by the green

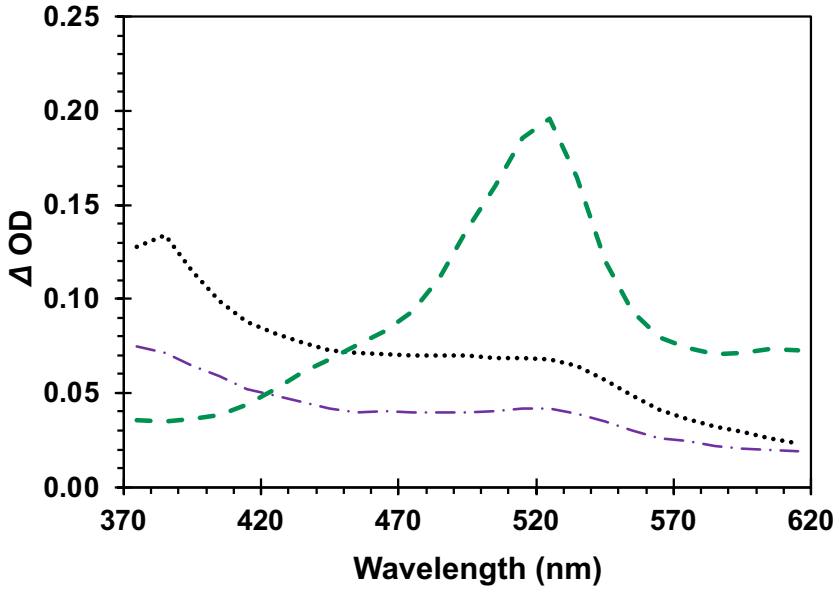

Figure 2.5 Transient absorption spectra of 5 mM 4-acetoxybenzphenone (green, dashed), the Dewar benzene reactant **DB-OBPh** (purple, dashed-dotted), and its photoproduct **HB-OBPh** (black, dotted) in Ar saturated MeCN.

dashed line in Figure 2.5, the triplet ketone has the characteristic triplet benzophenone absorption with a λ_{max} = 520 nm, and an oxygen-dependent lifetime of the order of 5 μs in dilute MeCN solution. The spectrum obtained from solutions of **DB-OBPh** (purple, dashed-dotted) was significantly different with broad absorption bands at ca. 480 and 520 nm. It was shown that the spectrum of **DB-OBPh** can be quenched with oxygen, and that it decays homogeneously, as expected for a single transient intermediate. Subsequent experiments carried out with Huckel benzene **HB-OBh** (black, dotted line) showed that the same transient is formed within the 8 ns pulse, suggesting that identity of the spectrum obtained upon irradiation of **DB-OBPh** is indeed the triplet state **^{3}HB-OBPh*** formed adiabatically from the original **^{3}DB-OBPh***, in agreement with steps 1 and 2 in Scheme 2. It was shown that transients from **DB-OBPh** and **HB-OBh** were also very similar.

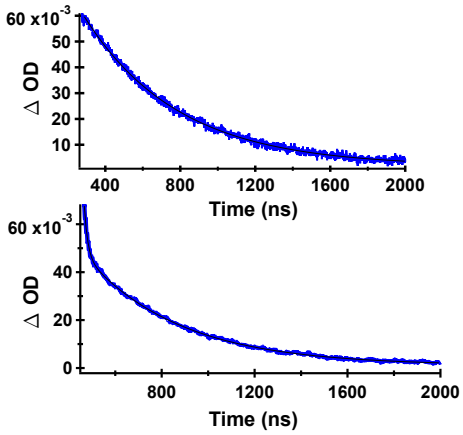

Figure 2.6 Decay curves of **DB-OBPh** in Ar saturated MeCN detected at 385 nm (Top) and at 530 nm (Bottom). The data points are sown in blue and the corresponding fit with a black line.

The decay data obtained from **HB-OBPh** were essentially identical, indicating that they arise from the same species (**Table 2.1** and **Figure 2.6**)

Decays measured at 380-420 nm for **DB-OBPh** showed a clean monoexponential decay (top of Figure 2.6) with a lifetime of 450 ns, as summarized in Table 2.1. Interestingly, absorption decays for

Table 2.1 Transient Lifetimes and Pre-exponential Factors of **DB-OBPh** and **HB-OBPh** in Ar-saturated MeCN

Compound (λ_{det})[1]	**A_1**	**τ_1** (%w)[2]	**A_2**	**τ_2** (%w)[2]	**χ^2 (10^4)**
DB-OBPh (530 nm)	0.024	16.2 (2%) ns	0.046	420 (98%) ns	5.67
DB-OBPh (385 nm)	-	-	0.058	450 ns	2.23
HB-OBPh (530 nm)	0.022	14.5 (2%) ns	0.14	419 (98%) ns	11.51
HB-OBPh (385 nm)	-	-	1	465	6.47

[1]Detection wavelength in parentheses. [2]Percentage weighted contribution of component "*i*" is given by $\%w_i = 100\,[(A_i\tau_i)\,/\,(A_{1i}\tau_1 + A_{2i}\tau_2)]$.

the same sample measured at 530 nm required a double exponential with a short-lived component of ca. 16 ns, that accounts for only 2% of the decay, and a majority (98%) long-lived component of 420 ns. As indicated in **Table 2.1**, the decay kinetics obtained from samples of **HB-OBh** were very similar. We tentatively assign the short-lived component at 530 nm as originating from a residual fraction of the originally excited benzophenone-centered triplet state, in the process of transferring its triplet energy to the Hückel benzene chromophore. A monoexponential behavior at the shorter wavelength is

consistent with having no significant absorption from the benzophenone chromophore at 385 nm, suggesting that it corresponds to the benzophenone-linked triplet benzene.

The importance of the intramolecular benzophenone sensitizer for the formation of the triplet state chain carrier was also demonstrated with samples of the Dewar benzene methyl ester **DB-OMe**, which failed to produce an observable triplet transient on its own, as expected for a fast non-adiabatic singlet state reaction and a low triplet yield that results from an inefficient intersystem crossing. However, the spectroscopic signature of the suggested chain carrier was obtained using the ground state Hückel benzene **HB-OMe** as a quencher of triplet 4-acetoxybenzophenone (**4-AcOBPh**). As shown in Figure 2.7, the spectrum of triplet **^{3}4-AcOBPh*** evolved into that of **^{3}HB-OMe*** as the concentration of the ground state Hückel benzene increased from 0 to 100 mM. The relatively intense signal of **^{3}4-AcOBPh*** with a maximum at ca. 520 nm is replaced by a red shifted weaker signal with a $\lambda_{max} \approx 530$ nm accompanied by an increase of the absorption intensity at 365 nm. Stern-Volmer analysis using changes in the decay rate as a function of increasing quencher concentration (Figure 2.7, inset) revealed a bimolecular quenching rate constant of $k_q = 6.3 \times 10^7\ M^{-1}s^{-1}$, which is about two orders of magnitude slower than diffusion control.[48]

2.3.6 Quantum Chain Reaction in Solution

Quantum yield determinations require a measurement of the moles of product molecules formed as a function of the moles of photons absorbed. The quantum yields of product formation from **DB-OBPh** ($\Phi_{HB\text{-}OBPh}$) were determined using the photodecarbonylation of dicumyl ketone (**DCK**) as a chemical actinometer.[49] We selected **DCK** because that it has a known quantum yield both in solution and in the solid state.[49] Thus, photochemical excitation of **DCK** in benzene solution at λ=312 nm leads

to the consumption of starting material with a quantum yield of $\Phi_{DCK\ (soln)}$ = 0.20±0.04. Similarly, photochemical reaction in the crystalline state using optically dense nanocrystalline suspensions proceeds with the exclusive formation of dicumene (**DC**) with quantum yield of $\Phi_{DC\ (Cryst)}$ = 0.20±0.02 (**Scheme 2.5**).

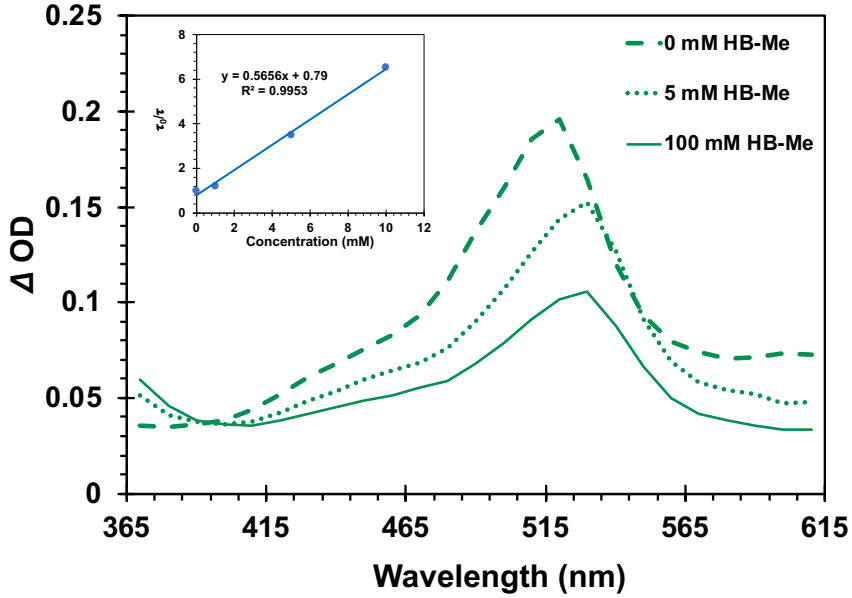

Figure 2.7 Evolution of the transient absorption of 4-acetoxybenzophenone as a function of added Hückel benzene **HB-OMe**. Inset: Stern-Volmer plot built with the lifetime of triplet 4-acetoxybenzophenone with increasing concentrations of **HB-OMe**. A bimolecular rate constant k_q= $6.3x10^7\ M^{-1}s^{-1}$ can be estimated from this analysis.

Scheme 2.5 Photodecarbonylation of Dicumyl ketone (DCK) actinometer with known nanocrystalline suspension quantum yield

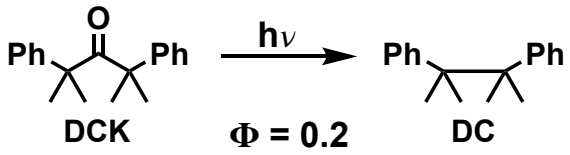

Knowing that the efficiency of a quantum chain reaction in solution depends on the efficiency of a concentration-dependent energy transfer step, one should expect the observed quantum yield to increase as a function of reactant concentration. With that in mind, we carried out quantum yield determinations with **DB-OBPh** concentrations varying from ca. 3 to 15 mM in MeCN. Optically dense, deoxygenated samples of the Dewar benzene and the actinometer were irradiated in parallel at 312 nm in 5 mL Pyrex tubes to assure that all photons entering each sample were absorbed, making sure that all samples are similarly exposed to the light source. Samples were sparged with Argon and sealed prior to irradiation. The moles of product (N) formed from each sample and the actinometer were calculated using internal standards by ^{1}NMR for **DB-OBPh** ($N_{HB\text{-}OBPh}$) and GC-MS for **DCK** (N_{DCK}). Further details for the experimental setup and calculations are described in the Supporting Information. Equation 4 was utilized to calculate quantum yields,

$$\Phi_{QC} = \frac{A_{DB\text{-}OBPh}}{A_{DCK}} \cdot \frac{N_{HB\text{-}OBPh}}{N_{DCK}} \cdot \frac{\eta_{MeCN}}{\eta_{Benz}} \qquad \text{Eq. 4}$$

where $A_{\mathbf{DB\text{-}OBPh}}$ refers to the absorbance of **DB-OBPh**, A_{DCK} is the absorbance of **DCK**, $N_{HB\text{-}OBPh}$ are the number of moles of isomerized product **HB-OBPh**, N_{DCK} is the number of moles of reacted DCK and η_{MeCN}, $\eta_{Benzene}$ are the refractive indices of MeCN and benzene, respectively. Experiments were run up to five

times over different reaction times with conversion values ranging from ca. 10% to 30%. **Figure 2.8** displays the quantum yield of formation of **HB-OBPh** photoproduct as a function of the initial concentration of **HB-OBPh**, varying from 3 mM to 15 mM. An intial value of $\Phi_{HB\text{-}OBPh}$ = 1.8±0.2 with a 3 mM of Dewar benzene increased up to $\Phi_{HB\text{-}OBPh}$ = 2.9±0.4 with a reactant

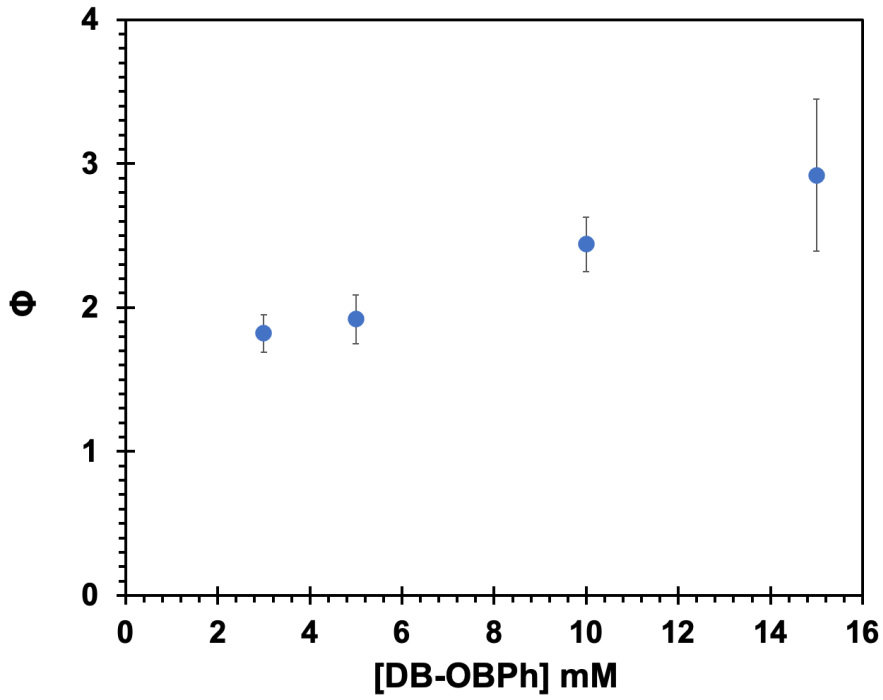

Figure 2.8 Quantum yield vales of **DB-OBPh** at 3, 5, 10, and 15 mM in MeCN solution.

concentration of 15 mM. We note that an increase of ca. 1.6 times in the quantum yield value within this concentration range is consistent with a bimolecular energy transfer rate of ca. $7x10^8$ $M^{-1}s^{-1}$, which is qualitatively consistent with the fast decay component measured by laser flash photolysis (**Figure 2.6** and **Table 2.1**) that we tentatively assigned to the last vestiges of the energy transfer step from the sensitizer to the benzene chromophores.

2.3.7 Quantum Chain Reaction in Nanocrystalline Suspension

Aqueous nanocrystalline suspensions of **DB-OBPh** and **DCK** were generated by the reprecipitation method.[50] Sample loadings were adjusted to generate optically dense suspensions of **DB-OBPh** and **DCK** that were optically matched, as indicated by a UV-Vis immersion probe. Suspensions were irradiated in 3 mL Pyrex tubes at 312 nm. Initial experiments revealed complete conversion of **DB-OBPh** at the shortest irradiation time of 10 seconds. A modified setup required suspensions of **DB-OBPh** and **DCK** to be irradiated with the former placed behind a 5 x 5 cm neutral density filter with a 1% transmission at 312 nm, so that the photon dose reaching the Dewar benzene was 100 times weaker (images of the setup can be found in the Quantum Yield Measurements section). The results shown in **Figure 2.9** reveal that quantum yields of product formation in the suspension sample have values that range from ca. $\Phi_{HB\text{-}OBPh}$ = 90 to $\Phi_{HB\text{-}OBPh}$ = 120, as the extent of reaction increases from 22% to 60% conversion. An increase in the observed quantum yield as a function of accumulated product suggests that the **HB-OBPh** product is a better absorber and potentially a more effective sensitizer. Alternatively, it is also possible that the efficiency of the solid state adiabatic reaction is improved once the crystals of the reactant are perturbed by the presence of the photoproduct.

While the large reactivity and high quantum yields observed in Figure 9 support the expectation of an efficient a quantum chain reaction, quantum yields on the order of 90-120 are far from the optimum if we assume a radiative triplet state lifetime on the order a few milliseconds (**Figure 2.4**, inset), a fast adiabatic reaction, and exciton hoping in the picosecond time scale. If an adiabatic reaction in the nanosecond time scale were the limiting factor, one should expect chain lengths as high as 10^6, given by the number of reactions that can occur within a few milliseconds. Notably, all our attempts towards the optical detection of the proposed chain carrier ^{3}**HB-OBPh*** in the solid state led to no signal detection under conditions where nanocrystals of 4-acetoxy benzophenone, used as a model compound, gave a

strong signal with a relatively short 0.8 μs lifetime (Transient Absorption section). The lack of an observable transient suggests that all 90 to 100 reactions in the chain take place within the ca. 8 ns laser pulse, suggesting that a quenching event may be the chain-limiting factor. In fact, we have previously shown that crystalline benzophenones are susceptible of efficient self-quenching mechanisms.[51]

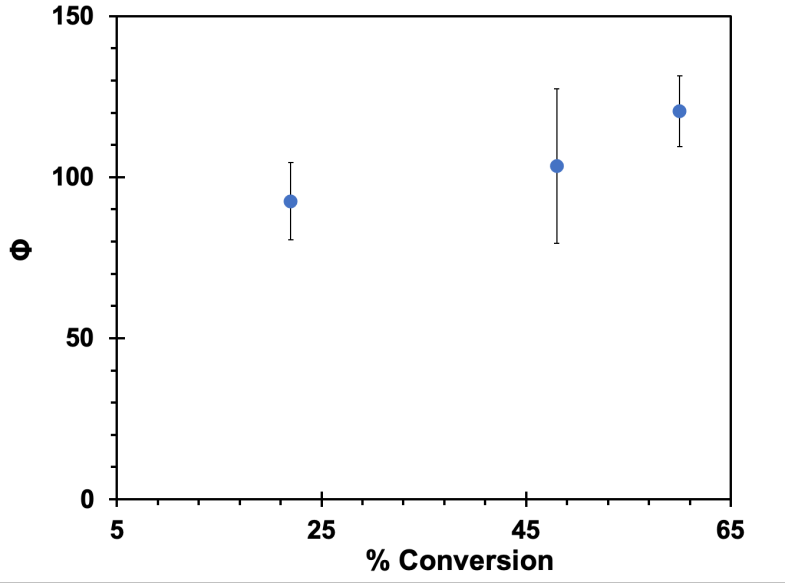

Figure 2.9 Quantum yields of formation of **HB-OBPh** in the solid state using suspensions prepared by the re-precipitation method.

An alternative explanation based on the quality of the sample was explored by X-ray powder diffraction analysis of centrifuged and dried suspension samples of **DB-OBPh**. The results revealed a largely amorphous powder, suggesting that the main sample population in suspension is not crystalline, even though one is able to find crystalline specimens by scanning electron microscopy (**Figure 2.2**). In order to determine whether the use of a higher quality, more crystalline sample can have a greater effect on the quantum chain, we carried out experiments to compare the extent of reaction between

polycrystalline powders suspended in surfactant-containing water, and the nanocrystalline suspensions generated by the re-precipitation method. While aggregates sizes are different, and microcrystals are prone to multiple excitations and triple-triplet annihilation, we reasoned that a greater conversion in suspended polycrystalline powders would qualitative confirm a greater efficiency for an exciton-mediated quantum chain amplification. Thus, suspended polycrystalline powder samples were prepared by dispensing 10 mg of accurately weighed **DB-OBPh** into 3 mL of a vortexing submiceller CTAB solution and nanocrystalline suspensions generated by the re-precipitation method could be obtained with loading values up to ca. 2 mg in 3 ml of submiceller CTAB. The two sample types were irradiated while stirring using an immersion 302-nm pen lamp. Analyzing the total amount of product generated under such similar conditions revealed that the suspended polycrystalline powder has a reactivity that is ca. 3-5 times greater than that of the mainly amorphous sample obtained by the re-precipitation method. This result qualitatively confirms that exciton-mediated energy transfer in the crystalline phase has the potential of increasing the quantum amplification in the triplet-sensitized reaction of Dewar benzenes.

2.4 Conclusions

Taking advantage of a crystalline tetramethyl Dewar benzene diester with 4-hydroxybenzophenone groups that acting as intramolecular triplet sensitizers, we were able to show that triplet quantum chain reactions in the crystalline state display quantum yields of product formation in the range of Φ_{QC}=100-300, which are two orders of magnitude greater than those measured in in dilute acetonitrile solutions (Φ_{QC}=1.5-2.0). The adiabatic and triplet state nature of the valence-bond isomerization reaction was confirmed in solution by using laser flash photolysis, where the same transient was observed from both the Dewar and the Hückel benzene isomers. The lack of an observable

transient in the solid state is interpreted in terms of a quantum chain reaction that occurs within the ca. 8 ns laser pulse, suggesting a quenching mechanism as a limiting factor for the quantum chain. Another contributing factor for the lower than expected quantum chain was unveiled when we showed that samples obtained by reprecipitation are formed as semicrystalline aggregates with coexisting amorphous and crystalline phases. With work in progress in our group we are addressing the roles of excited state quenching and crystallinity to find conditions where exciton-mediated reactions can produce quantum chain reactions with values that extend into thousands or millions of reactions per photon.

2.5 Experimental

2.5.1 General Information

All Dewar benzene derivatives were synthesized under an inert argon atmosphere unless otherwise specified. Nuclear magnetic resonance (NMR) spectra for ^{1}H and ^{13}C were obtained using 500 MHz Bruker NMR spectrometer. All chemical shifts are reported in ppm using natural abundance isotopes of reference solvents. Infrared (IR) spectra was collected using the Perkin-Elmer 1000 Series FT-IR spectrometer.

2.5.2 Synthetic Procedures

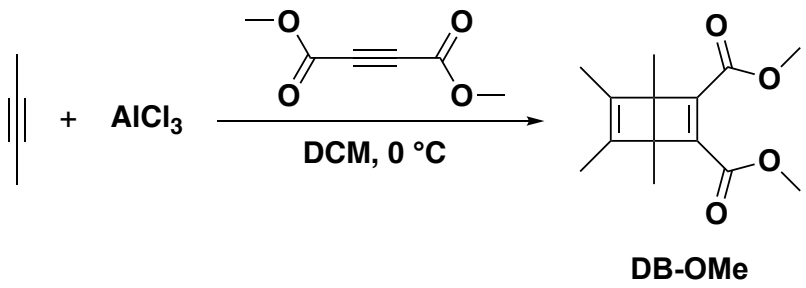

DB-OMe

Koster, J. B.; Timmermans, G. J.; Bekkum, H. V. *Synthesis* **1971**, *19*, 139–140.

Synthesis of DB-OMe: A 25 mL 3-neck round bottom flask was flame dried and charged with a stir bar and a $AlCl_3$ (0.090 g, 0.647 mmol, 1 equiv). This was followed by the addition of 1 mL anhydrous dichloromethane (DCM). 2-Butyne was then added dropwise (0.070 g, 101 μL, 1.29 mmol, 2 equiv) and allowed to stir for 10 minutes at 0 ^{o}C. This was followed by the dropwise addition of dimethyl acetylene dicarboxylate (60 μL, 0.480 mmol, 0.74 equiv). This was allowed to stir for 30 minutes at room temperature. Dimethylsulfoxide (DMSO) was then added dropwise (650μL), followed by the addition of anhydrous DCM (1 mL). The reaction was then washed with deionized water, brine, and then extracted in ether. The organic layer was dried over sodium sulfate, filtered, then concentrated under pressure to yield a yellow oil. The crude oil was purified using vacuum filtration between 70-75 ^{o}C and for 3 hours. The collected fraction was washed with hexanes and further purification involved precipitating the product out of hexanes at -78 ^{o}C as a white solid. The impurities within the layer of hexanes was carefully decanted, leaving a white powdery solid at -78 ^{o}C. The product was isolated as an oil at room temperature. ^{1}H NMR (500 MHz, CDCl3): δ = 3.78 (s, 6H), 1.63 (s, 6H), 1.28 (s, 6H).

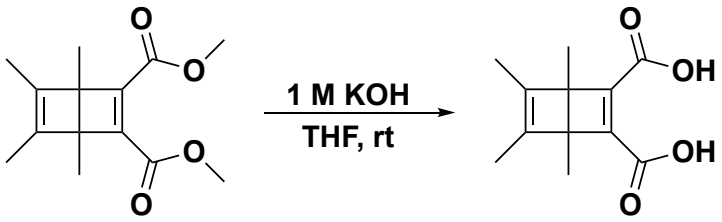

DB-OMe **DB-OH**

Ferrar, L.; Mis, M.; Dinnocenzo, J. P.; Farid, S.; Merkel, P. B.; Robello, D. R. *J. Org. Chem.* **2008**, *73*, 5683–5692

Synthesis of DB-OH: DB-OMe was dissolved in 20 mL THF and 20 mL 1 M KOH within a 500 mL round bottom flask. The reaction was allowed to stir overnight. Product was washed with ether and extracted in deionized water. The water layer was acidified with 1 M HCl, then extracted with ethyl acetate. The organic layer was dried over magnesium sulfate, filtered, then concentrated under pressure to yield a yellow solid. No further purification was required. ^{1}H NMR (500 MHz, CDCl3): δ = 2.17 (s, 18H), 1.67-1.63 (m, 18H), 1.29 (s, 6H); ^{13}C NMR (126 MHz, CDCl3) δ = 161.25, 152.32, 143.38, 81.21, 55.84, 41.49, 36.21, 30.86, 11.05, 9.94. m.p.: 165 ^{o}C

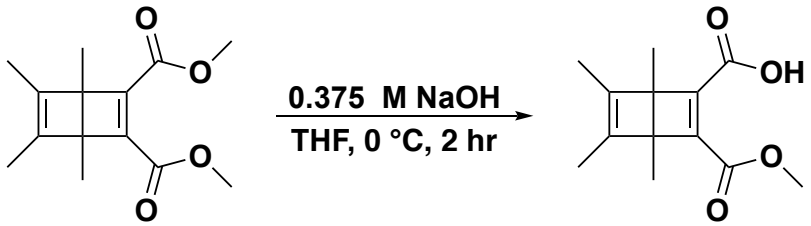

DB-OMe **DB-OMe/OH**

Ferrar, L.; Mis, M.; Dinnocenzo, J. P.; Farid, S.; Merkel, P. B.; Robello, D. R. *J. Org. Chem.* **2008**, *73*, 5683–5692

Synthesis of DB-OMe/OH: DB-OMe was dissolved in 20 mL THF and 20 mL 0.375 M NaOH within a 500 mL round bottom flask. The reaction was allowed to stir for 2 hours cold at 0 °C. Product was washed with ether and extracted in deionized water. The water layer was acidified with 1 M HCl, then extracted with ethyl acetate. The organic layer was dried over magnesium sulfate, filtered, then concentrated under pressure to yield a pale yellow solid. The crude product was purified using column chromatography. Utilizing a gradient solvent system composed of hexanes: ethyl acetate (50:1, 20:1, 15:1). Purified product was isolated as white powder. ^{1}H NMR (500 MHz, CDCl3): δ = 2.17 (s, 18H), 1.67-1.63 (m, 18H), 1.29 (s, 6H); ^{13}C NMR (126 MHz, CDCl3) δ = 161.25, 152.32, 143.38, 81.21, 55.84, 41.49, 36.21, 30.86, 11.05, 9.94. m.p.: 103 ^{o}C

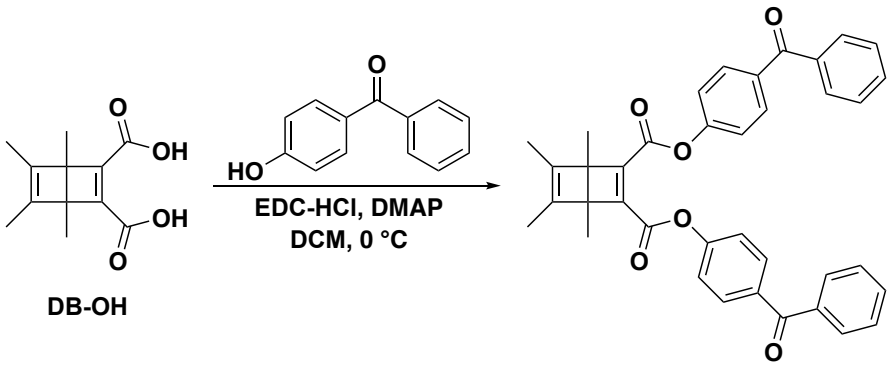

Synthesis of DB-OBPh: A 25 mL 3-neck flask round bottom flask was flame dried and charged with compound **4** (0.050 g, 0.225 mmol, 1 equiv), 4-hydroxybenzophenone (0.054g, 0.270 mmol, 1.2 equiv), a catalytic amount of 4-(dimethylamino)pyridine (0.003 g, 0.023 mmol, 0.1 equiv) and a stir bar. This was followed by the addition of 2 mL anhydrous DCM and 1-ethyl-3-(3-dimethylaminopropyl)carbodiimide hydrochloride (EDC·HCl) stirring at 0 °C. The reaction was allowed to stir cold for at least 2 hours. The reaction was subjected to column chromatography without workup utilizing a gradient solvent system composed of hexanes: ethyl acetate (100:0, 50:1, 25:1, 20:1). The purified product was isolated as a white. ^{1}H NMR (500 MHz, CDCl3): δ = 7.93 – 7.83 (m, 4H), 7.79 (dt, *J* = 8.4, 1.5 Hz, 4H), 7.64 – 7.56 (m, 2H), 7.54 – 7.45 (m, 4H), 7.35 – 7.29 (m, 4H), 1.75 (s, 6H), 1.47 (s, 6H ; ^{13}C NMR (126 MHz, CDCl3) δ = 195.50, 159.59, 153.45, 152.74, 143.44, 137.42, 135.32, 132.55, 131.74, 129.98, 128.37, 121.34, 57.06, 11.24, 10.04. Rf = 0.4 in hexanes: ethyl acetate (4:1). m.p.: 109 °C

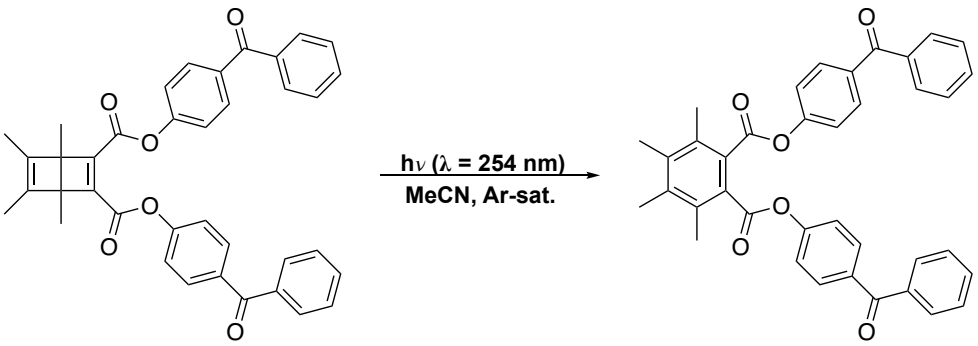

DB-OBPh **HB-OBPh**

Synthesis of HB-OBPh: A 25 mg sample of DB-OBPh was irradiated at 254 nm light in Argon-saturated MeCN for 1.5 hours. Product was purified by recrystallization to give HB-OBPh in quantitative yield. ^{1}H NMR (500 MHz, $CDCl_3$): δ = 7.86 – 7.81 (m, 4H), 7.78 (dt, *J* = 8.4, 1.5 Hz, 4H), 7.60– 7.56 (m, 2H), 7.50 – 7.45 (m, 4H), 7.30 – 7.26 (m, 4H), 2.50 (s, 6H), 2.36 (s, 6H) ; ^{13}C NMR (126 MHz, CDCl3) δ = 195.50, 167.12, 153.84, 139.39, 137.39, 135.38, 132.69, 132.56, 131.75, 129.97, 129.01, 128.38, 121.49, 17.88, 16.89. Rf = in hexanes: ethyl acetate (4:1). m.p.: 142 ^{o}C

2.5.3 ^{1}H and ^{13}C NMR Spectra for DB-OBPh and HB-OBPh

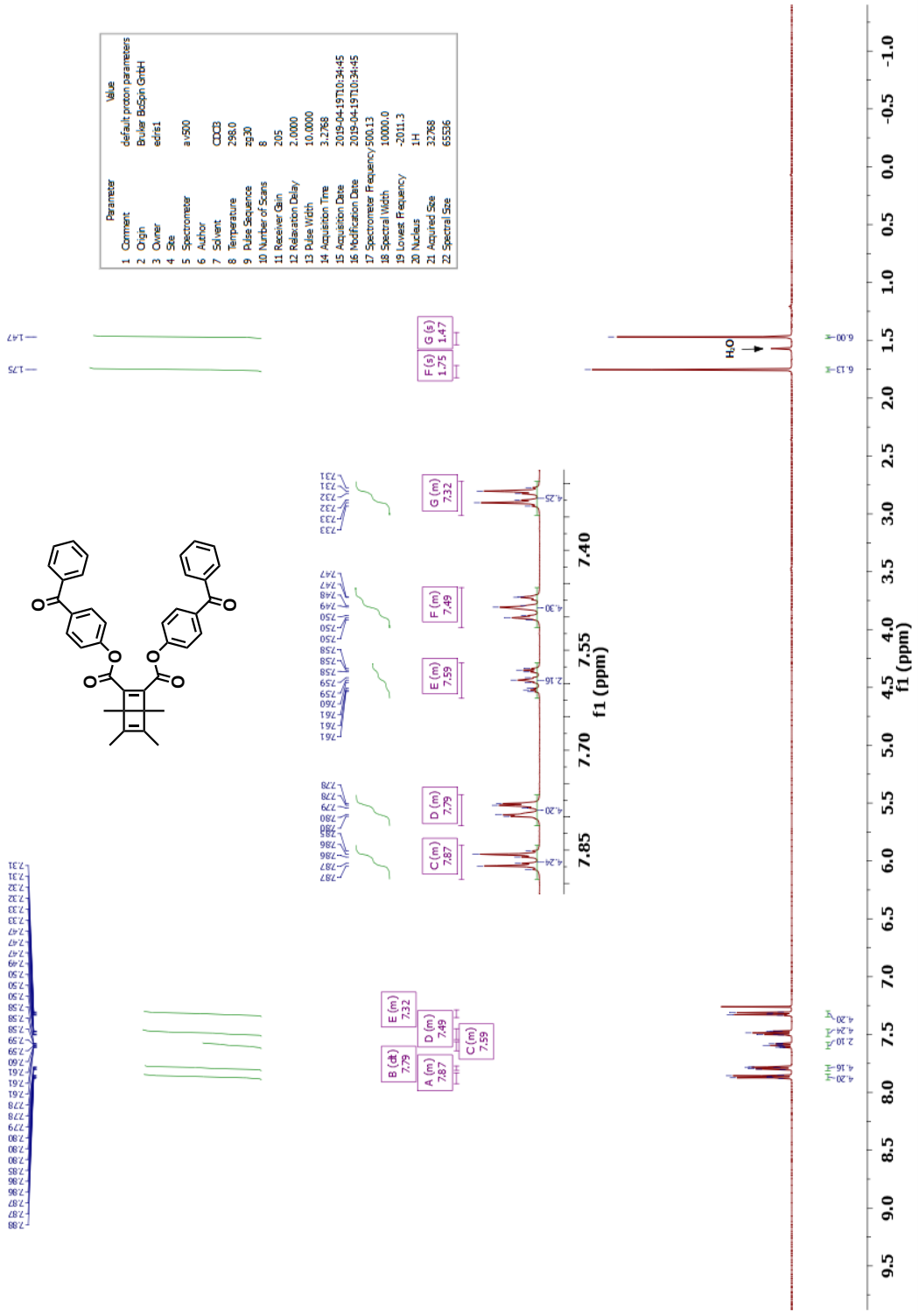

Figure 2.10 ^{1}H NMR of **DB-OBPh** in $CDCl_3$ at 500 MHz

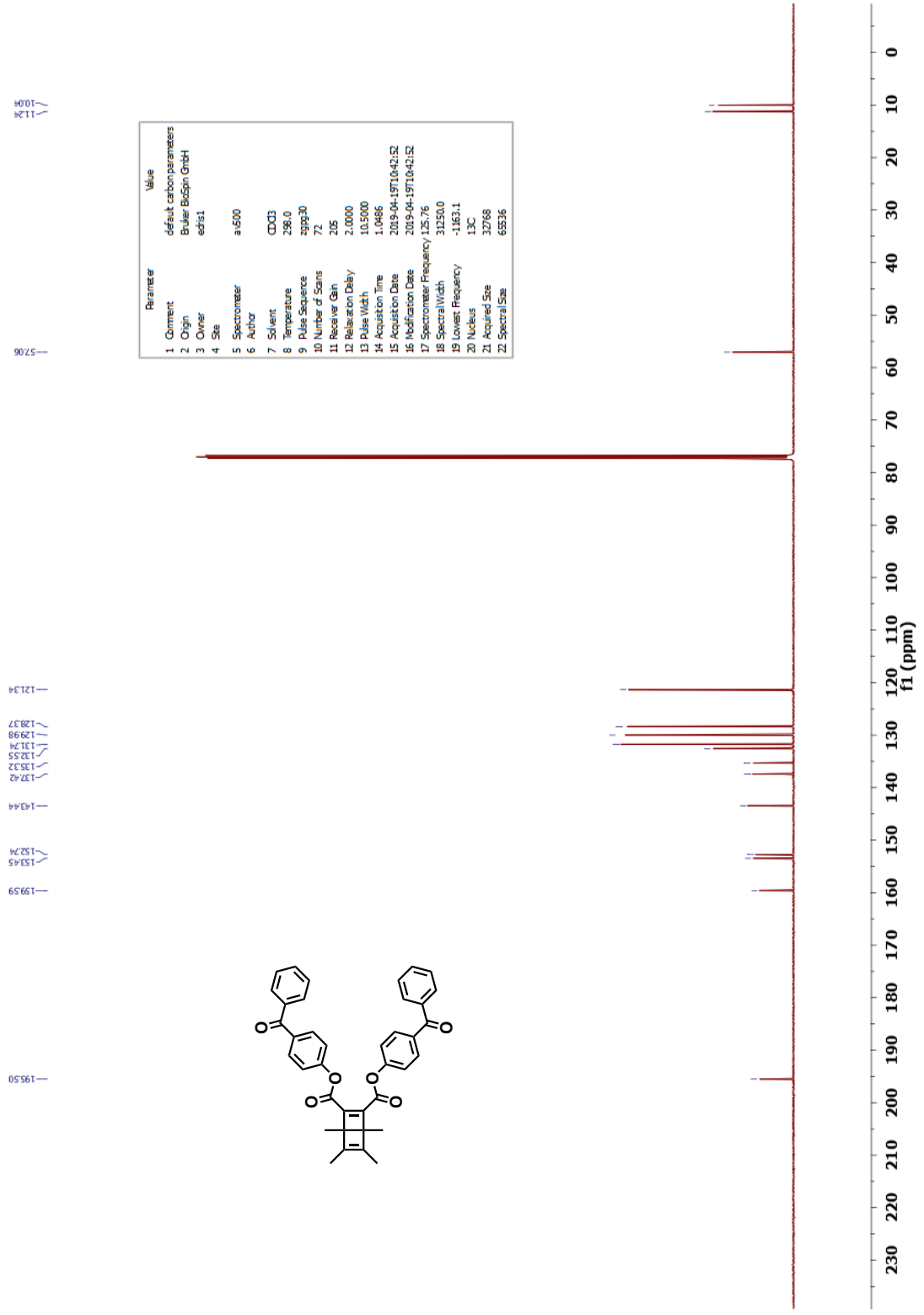

Figure 2.11 $^{13}C\{^{1}H\}$ NMR of **DB-OBPh** in $CDCl_3$ at 126 MHz

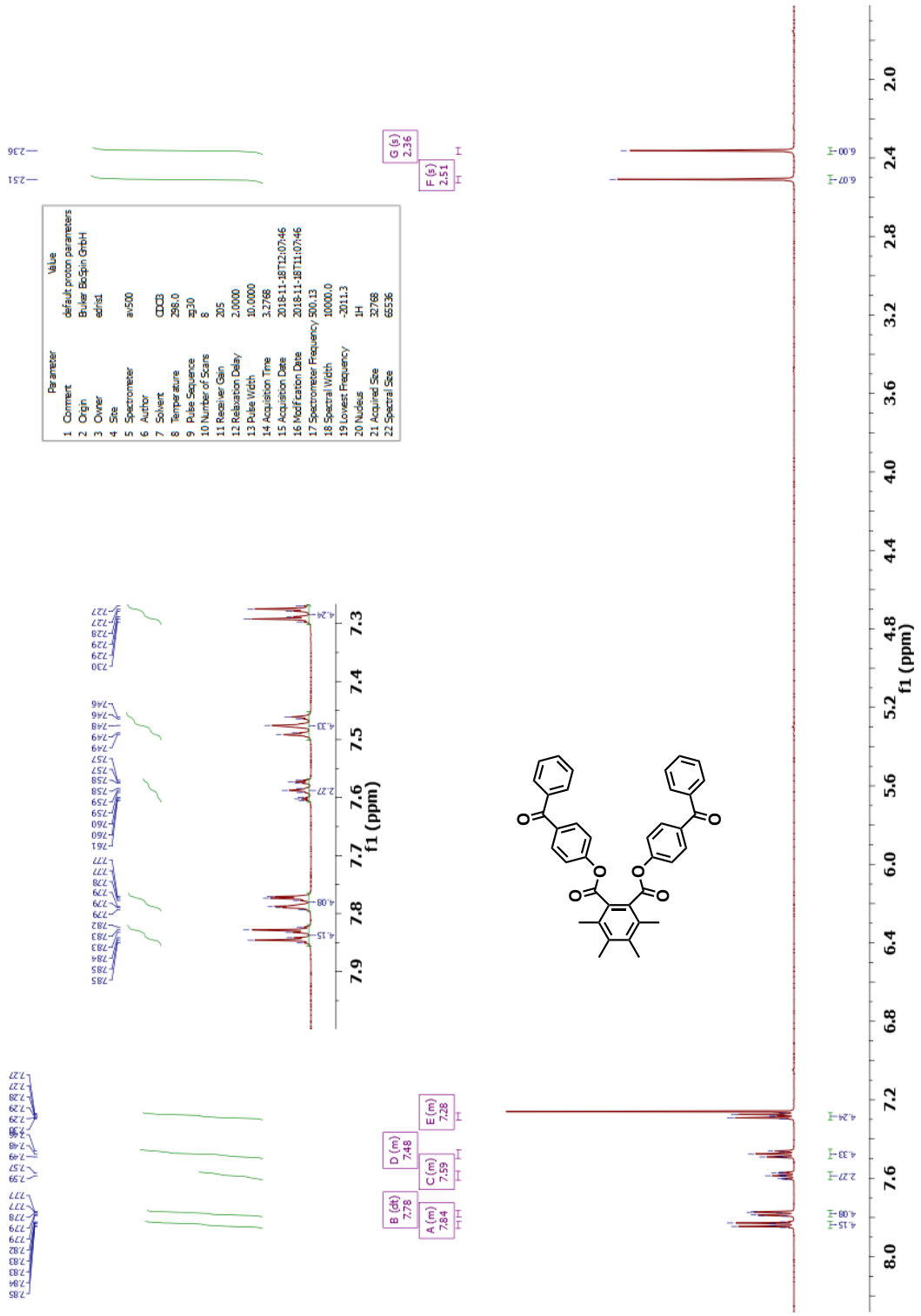

Figure 2.12 ^{1}H NMR of **HB-OBPh** in $CDCl_3$ at 500 MHz

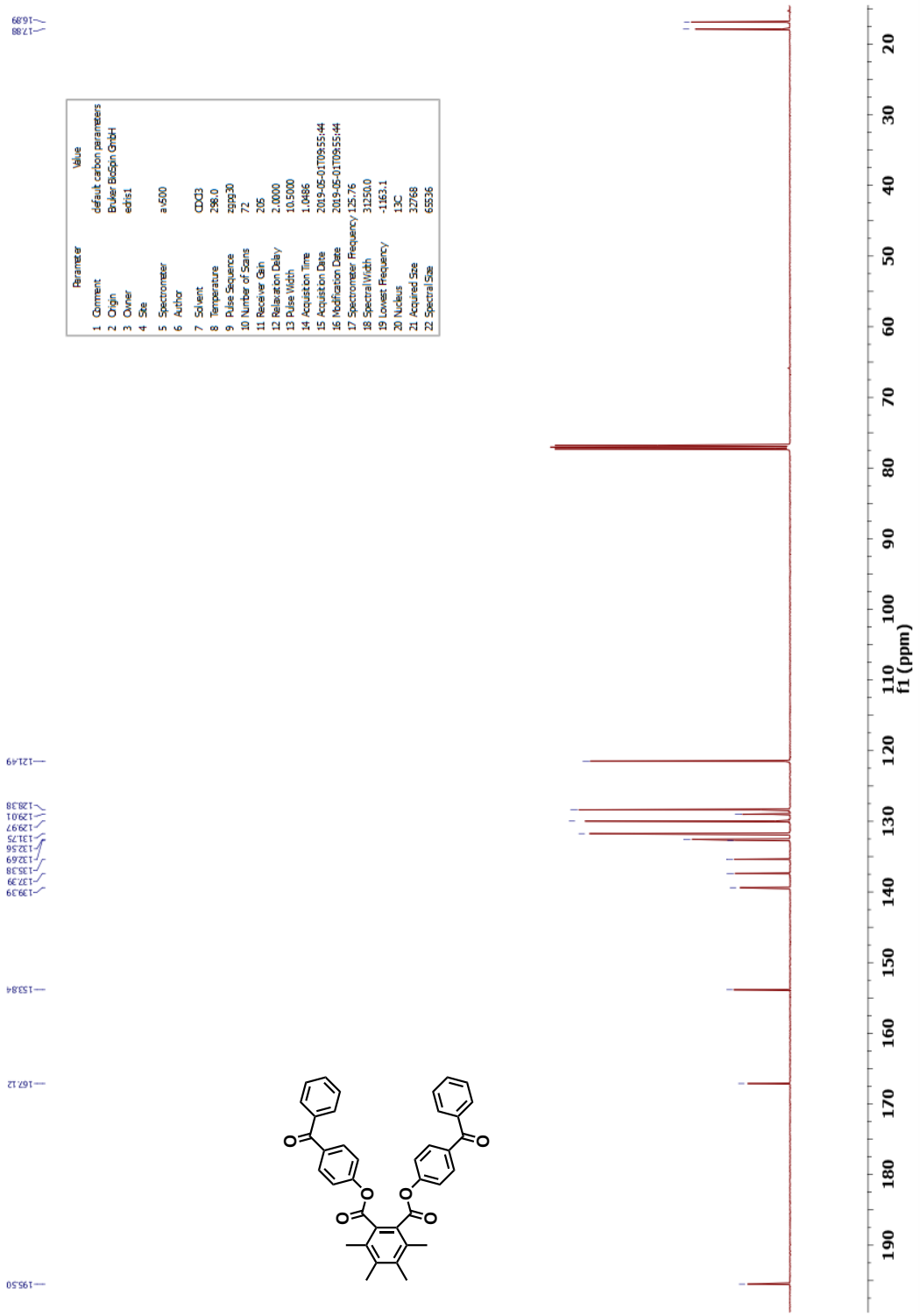

Figure 2.13 $^{13}C\{^{1}H\}$ NMR of **DB-OBPh** in $CDCl_3$ at 126 MHz

2.5.4 IR Spectra

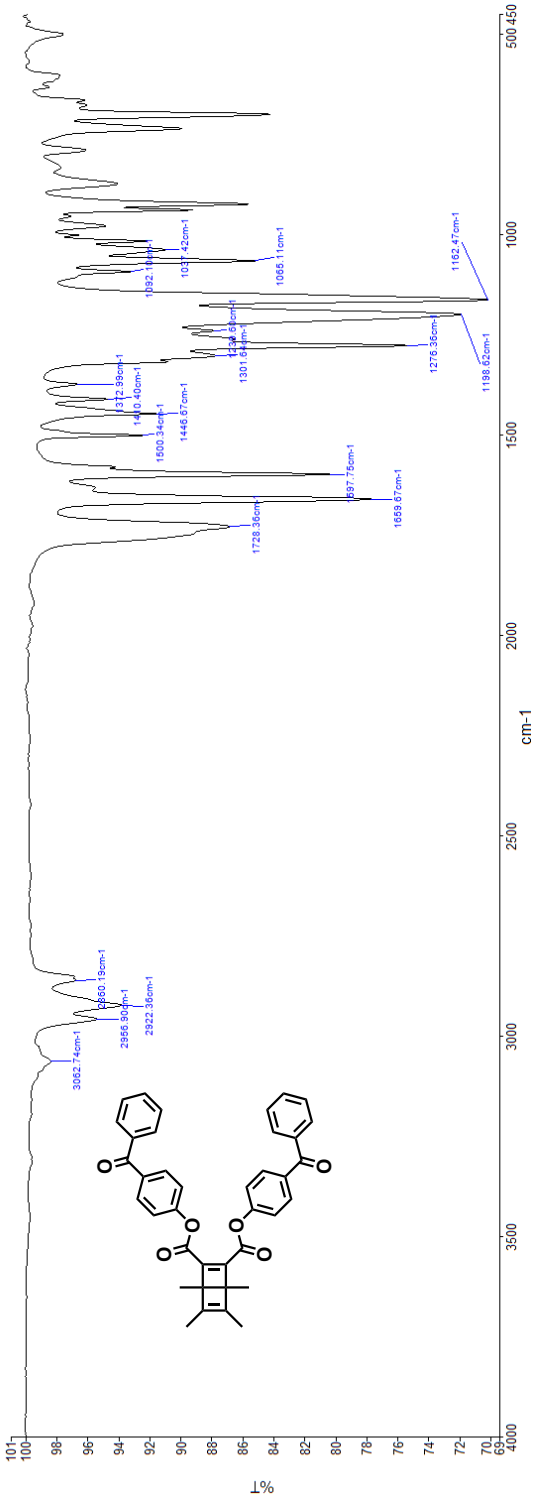

Figure 2.14 FTIR of **DB-OBPh**

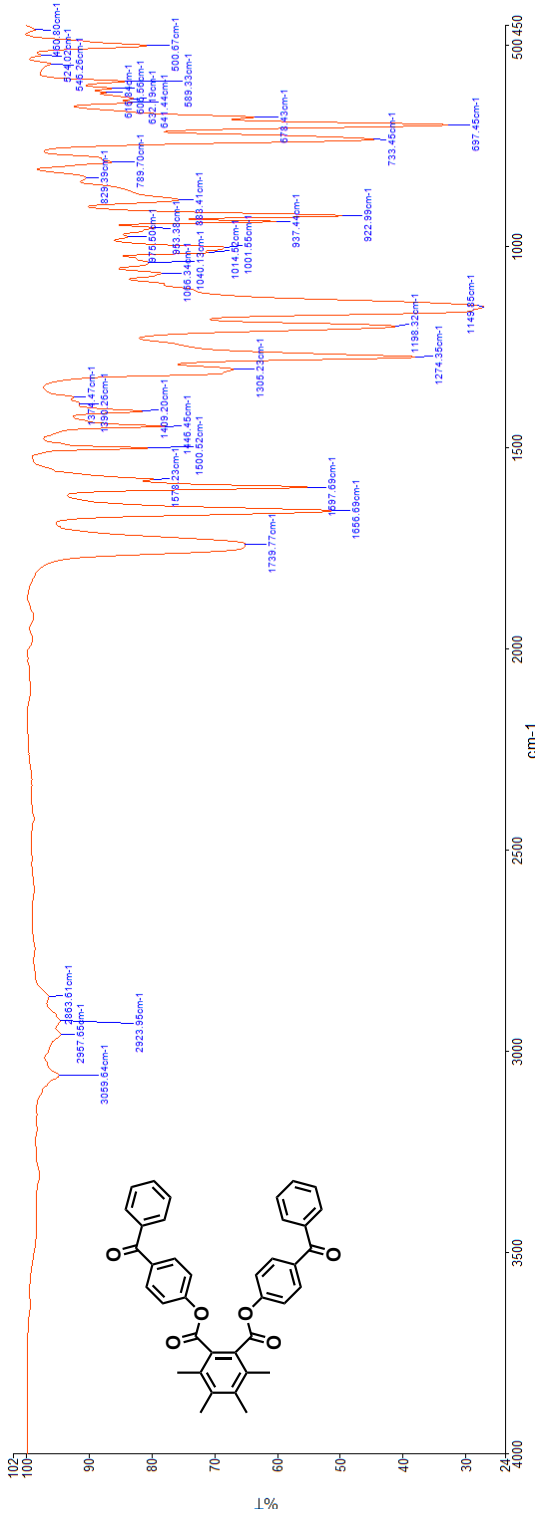

Figure 2.15 FTIR of **HB-OBPh**

2.5.5 UV-Vis

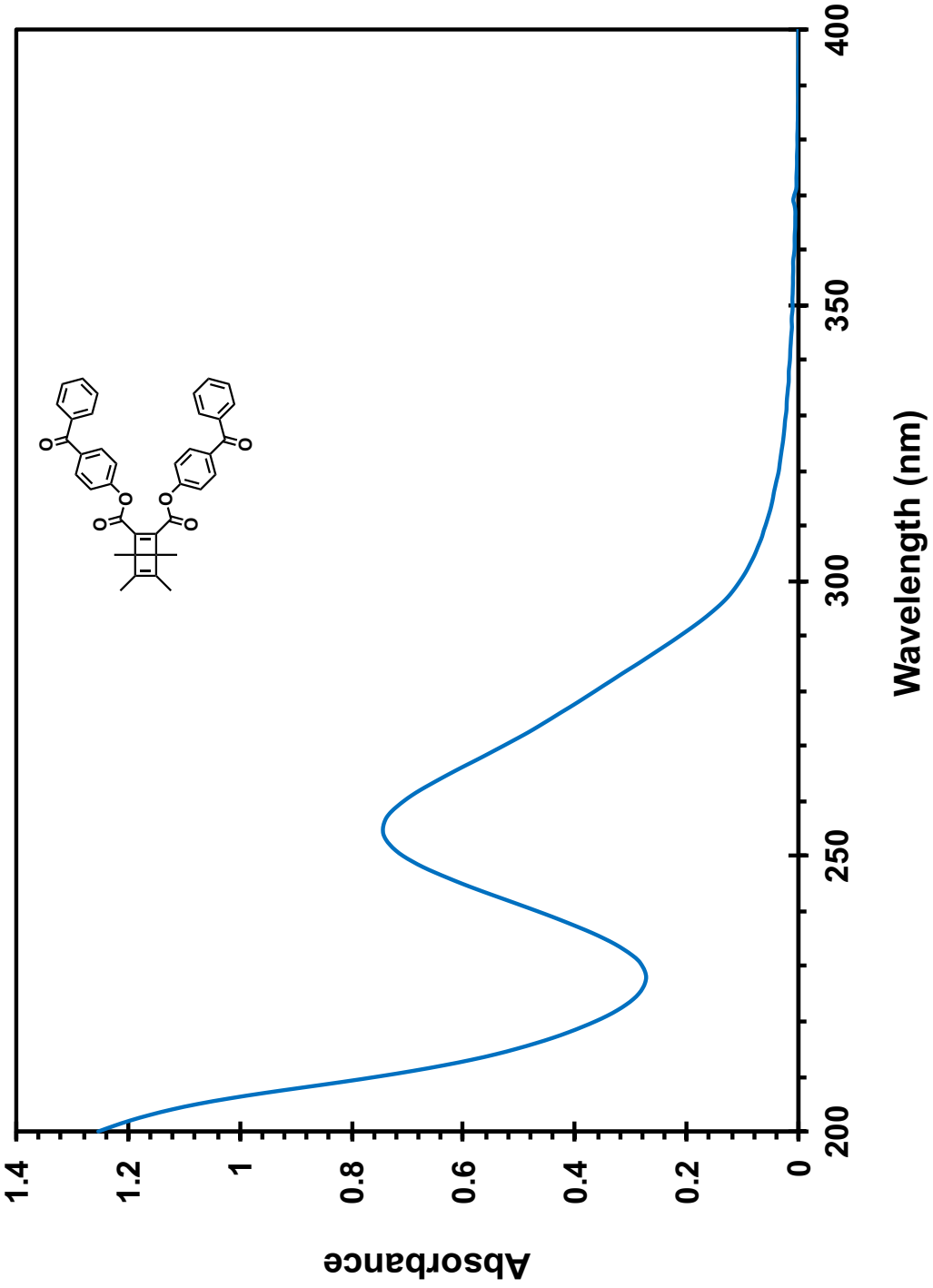

Figure 2.16 UV absorbance spectra of DB-OBPh (1.65 x 10^{-5} M in MeCN)

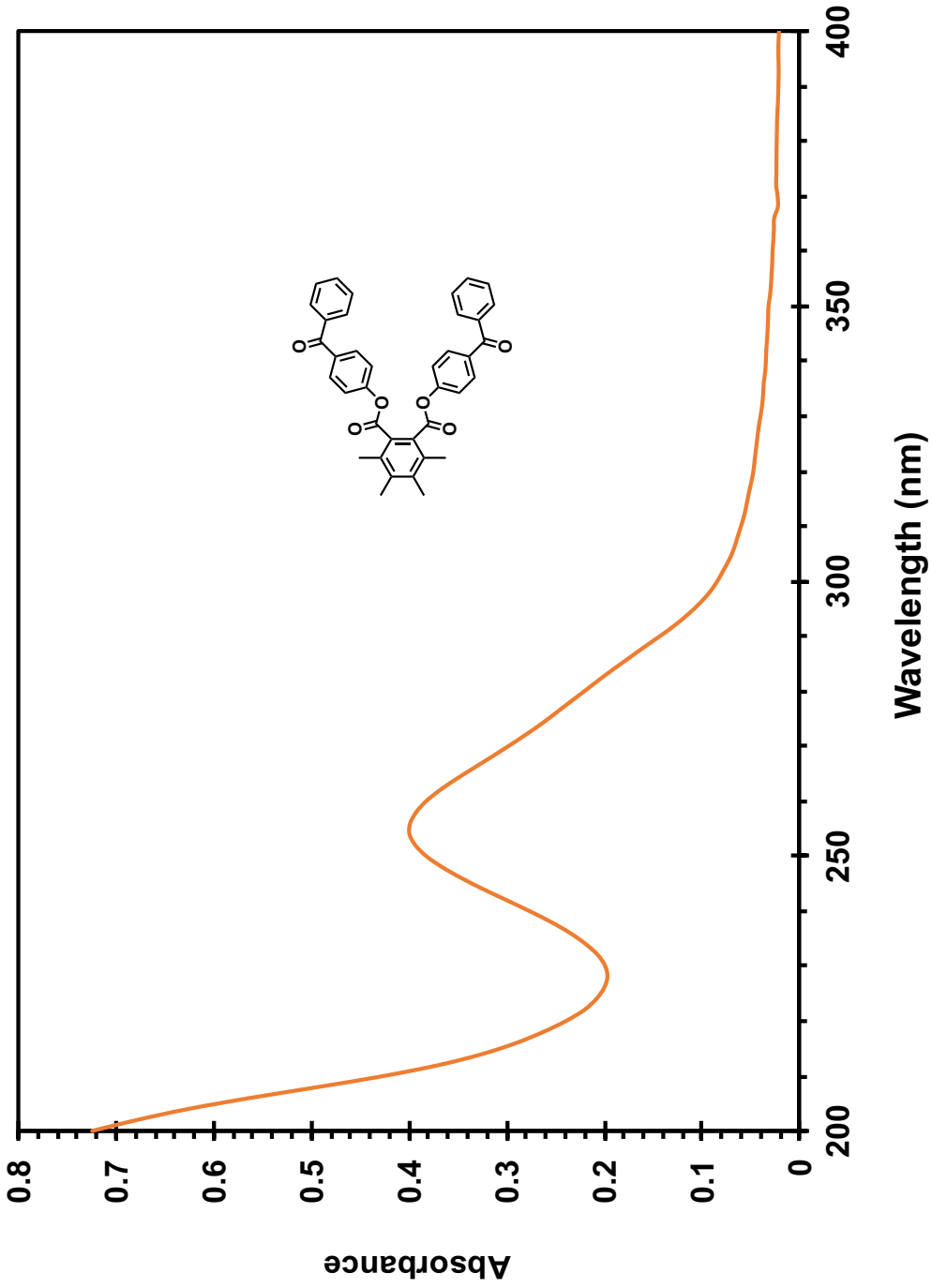

Figure 2.17 UV absorbance spectra of **HB-OBPh** (1.3 x 10^{-5} M in MeCN)

2.5.6 Dynamic Light Scattering (DLS)

Record	Z-Ave (d.nm)	PdI	Mean (d.nm)	Area (Percent)	Scattering Angle (°)	Size Peak (d.nm)	Size Analysis Version
Trial 1	174.2	0.068	189.9	100	173	58.12	1.2
Trial 2	187.9	0.066	203.7	100	173	60.24	1.2
Trial 3	198.7	0.072	217.9	100	173	69.4	1.2

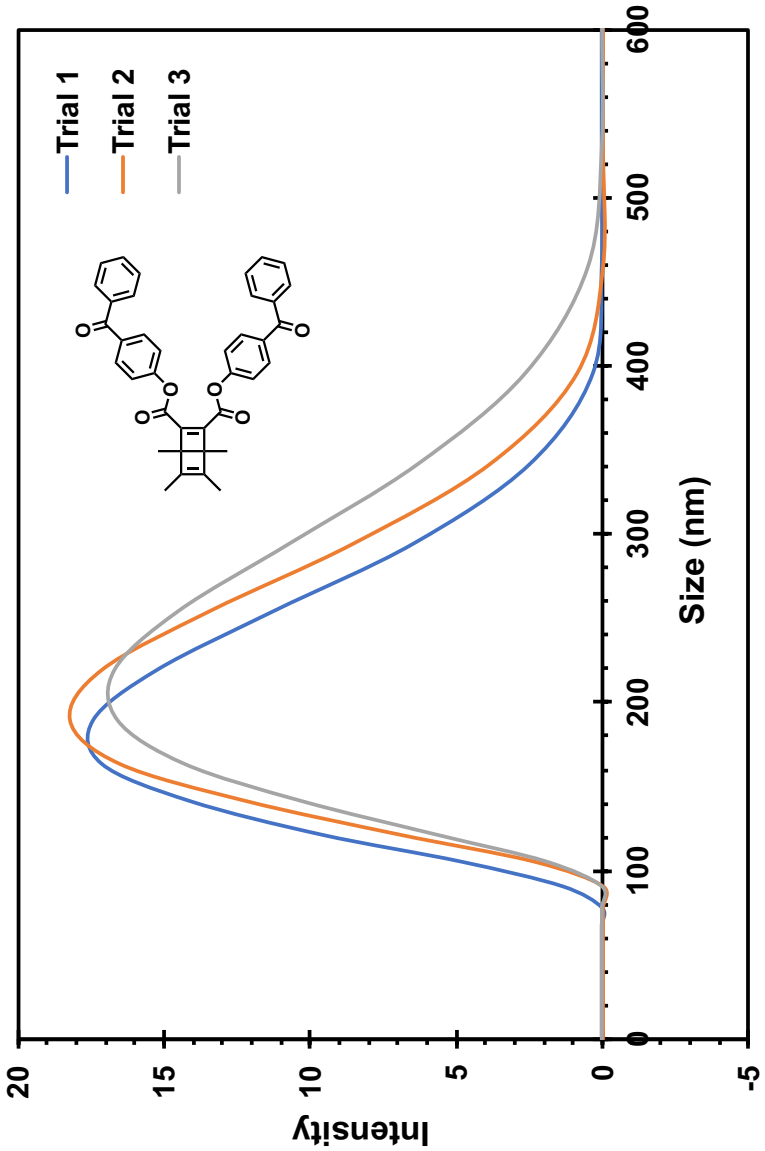

Figure 2.18 DLS of **DB-OBPh**

2.5.7 pXRD

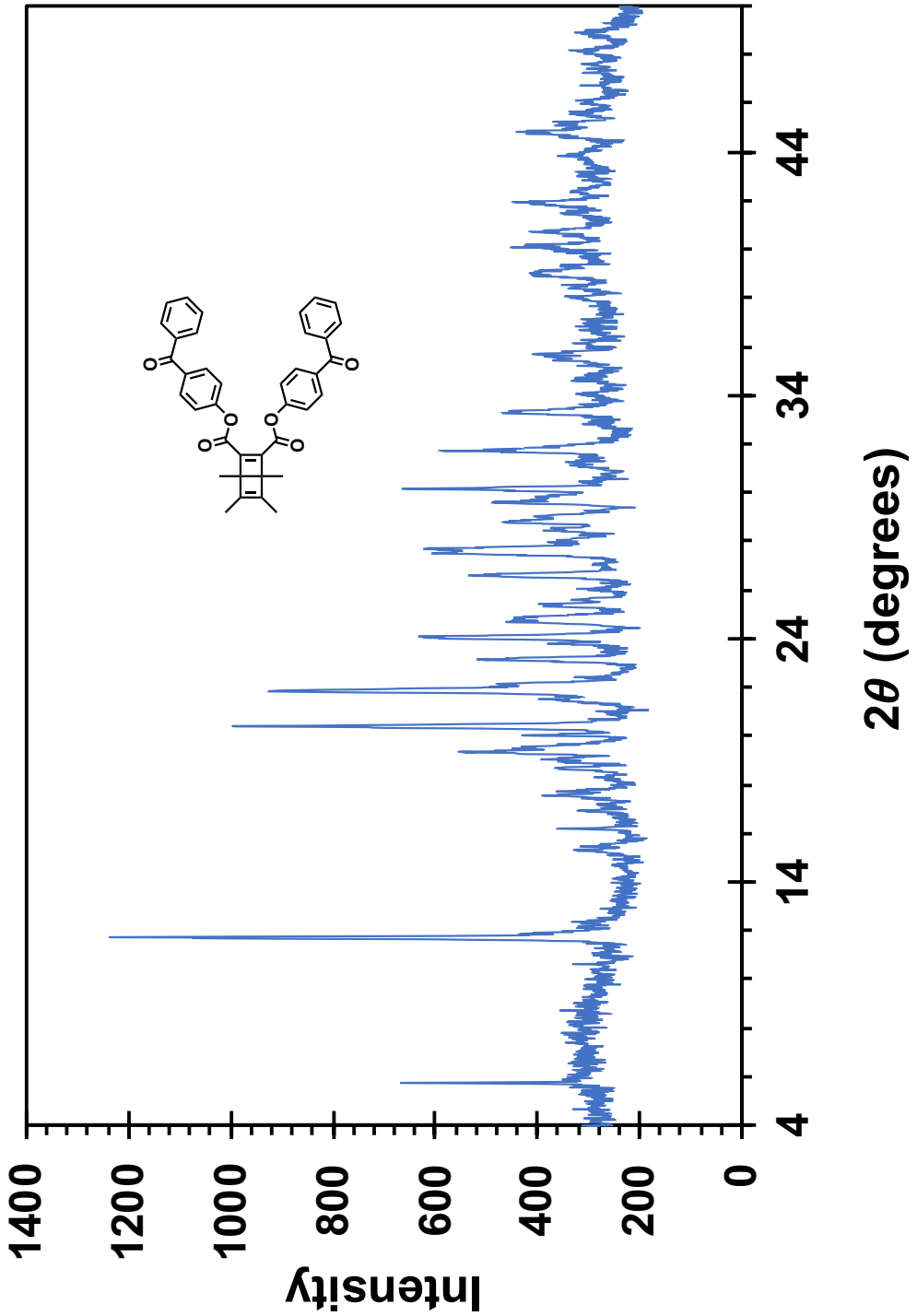

Figure 2.19 pXRD of **DB-OBPh**

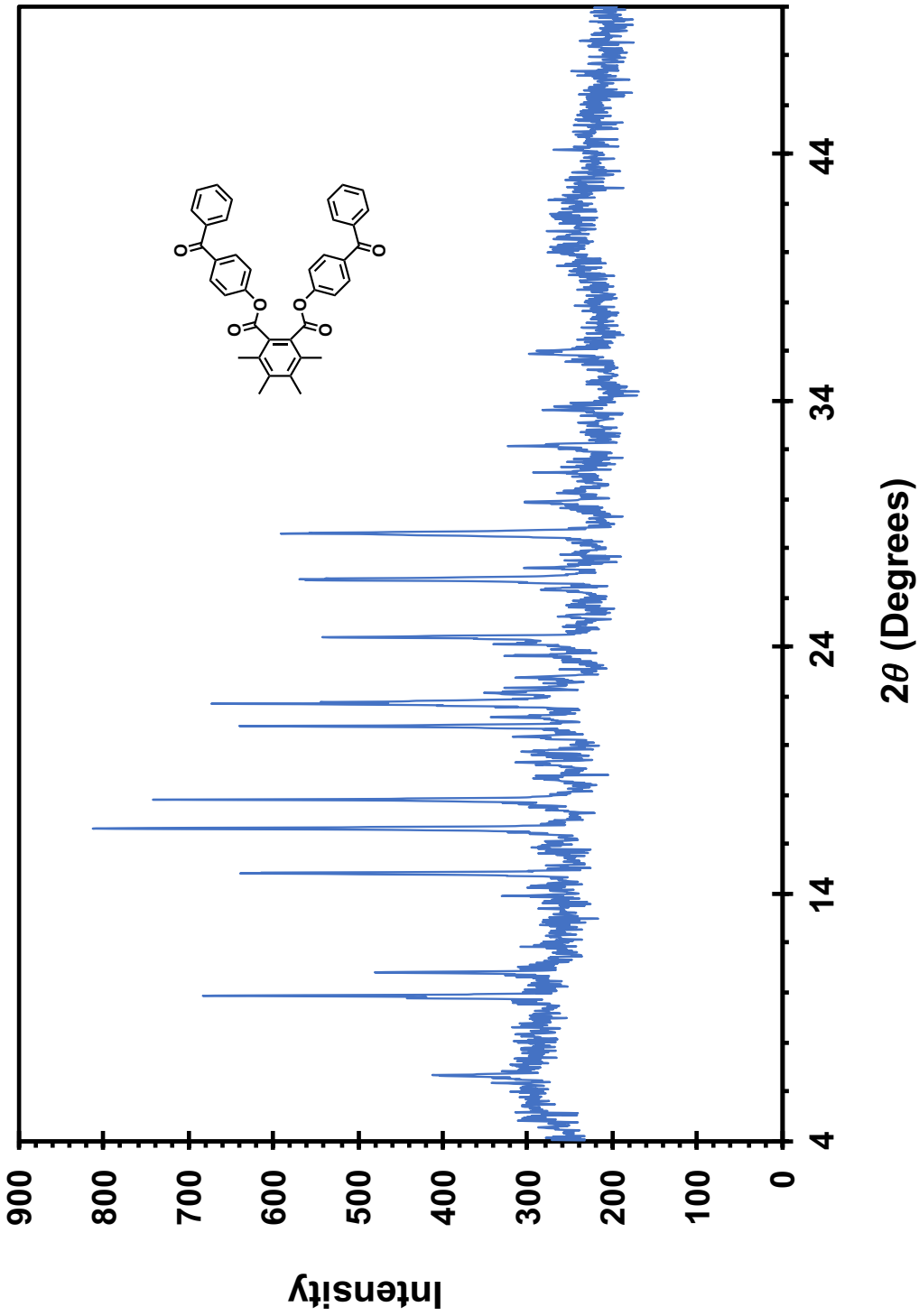

Figure 2.20 pXRD of **HB-OBPh**

2.5.8 Transient Absorption Spectroscopy

4-acetoxybenzophenone NC suspension

Preparation: A 33 mg/mL stock solution was utilized to prepare a stock aqueous crystalline suspension of 4-acetoxybenzophenone based on the reprecipitation method. A 100 μL aliquot of the stock suspension was then resuspended in 12 mL of 0.1932 mM CTAB solution and introduced to the sample cell of the laser through a flow cell.

Reaction of 4-acetoxybenzophenone with 355 nm laser excitation

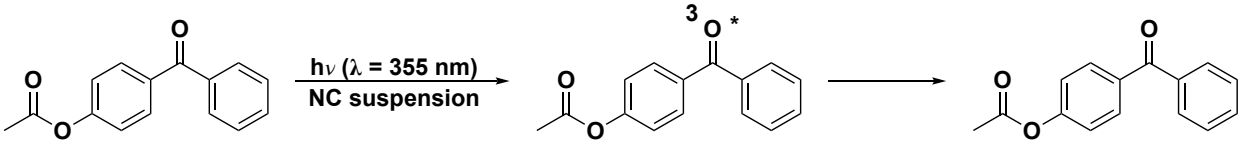

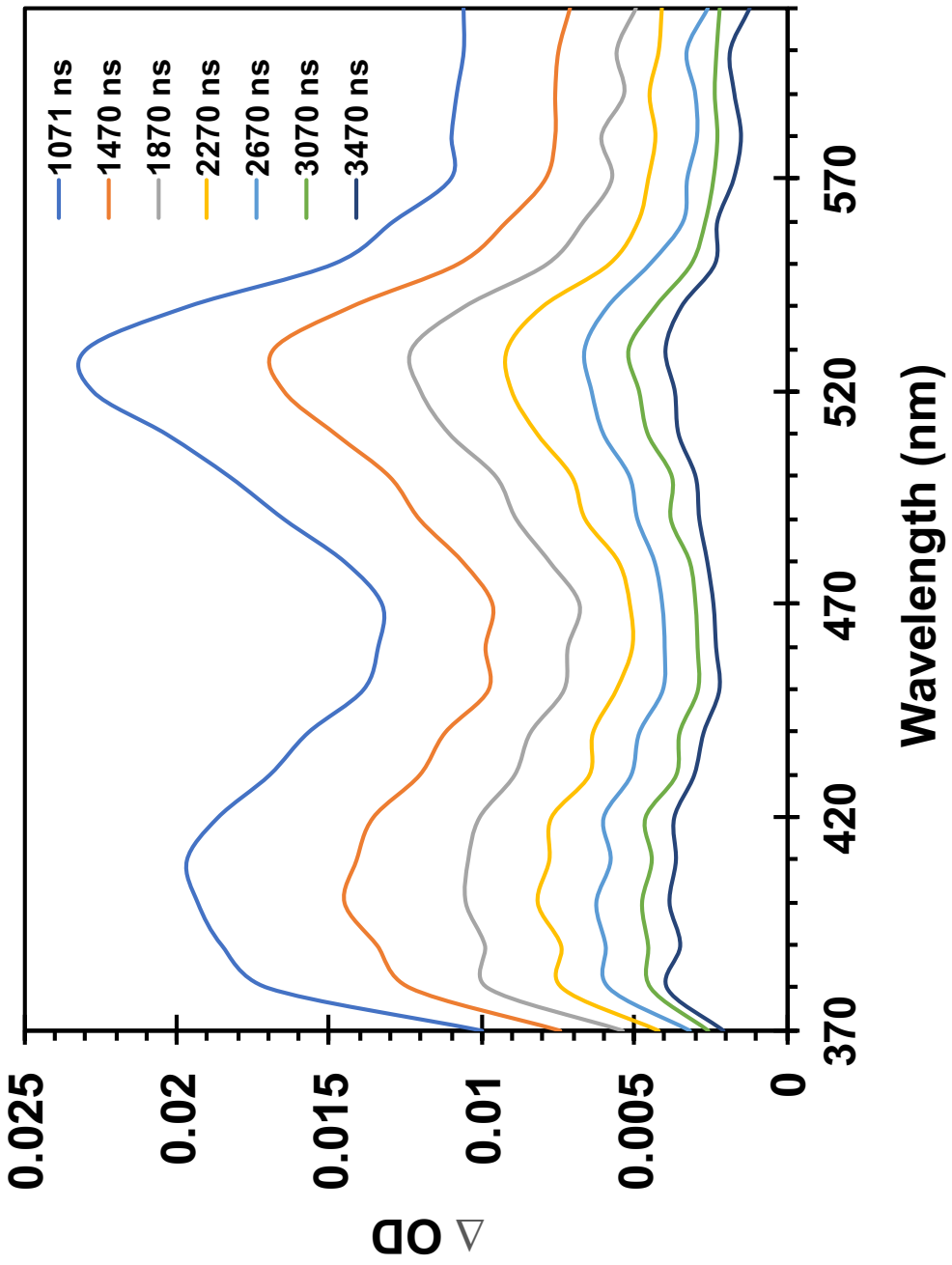

Figure 2.21 Transient Absorption (370-610 nm) of 4-acetoxybenzophenone in nanocrystalline suspension

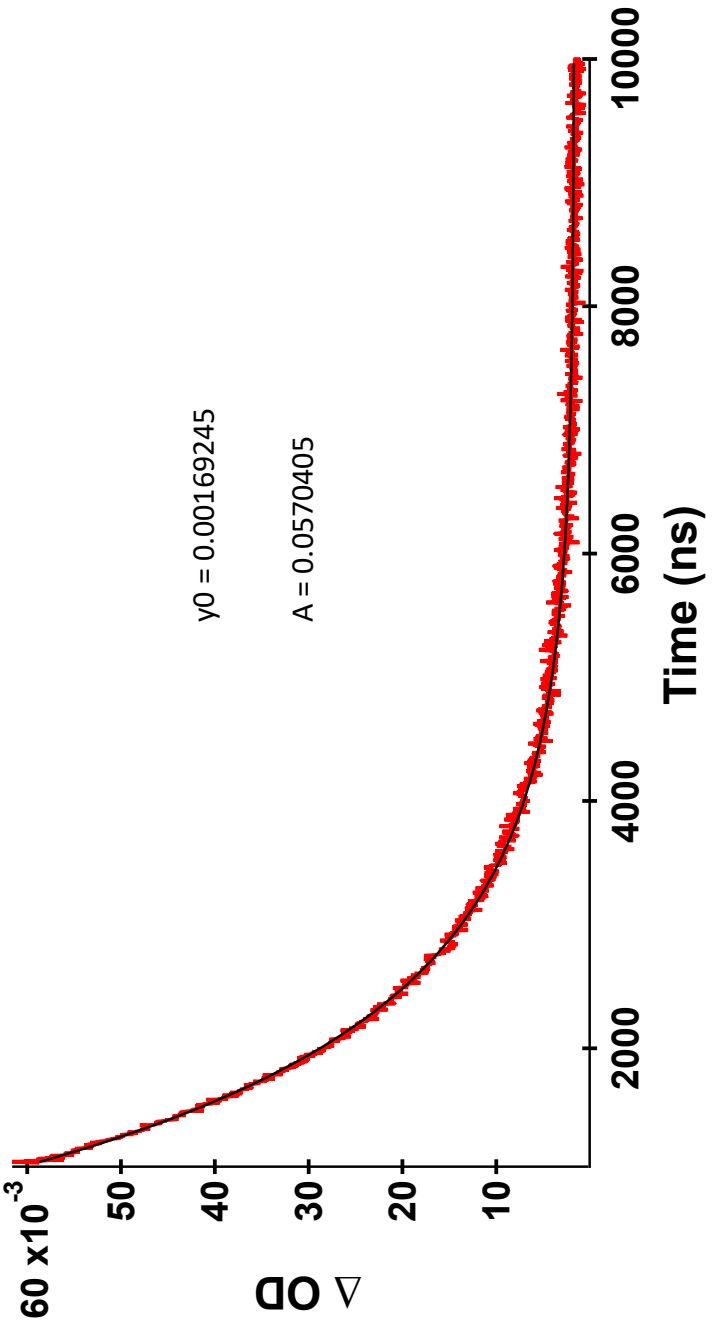

Figure 2.22 Transient Lifetime (530 nm) of 4-acetoxybenzophenone in the nanocrystalline suspension

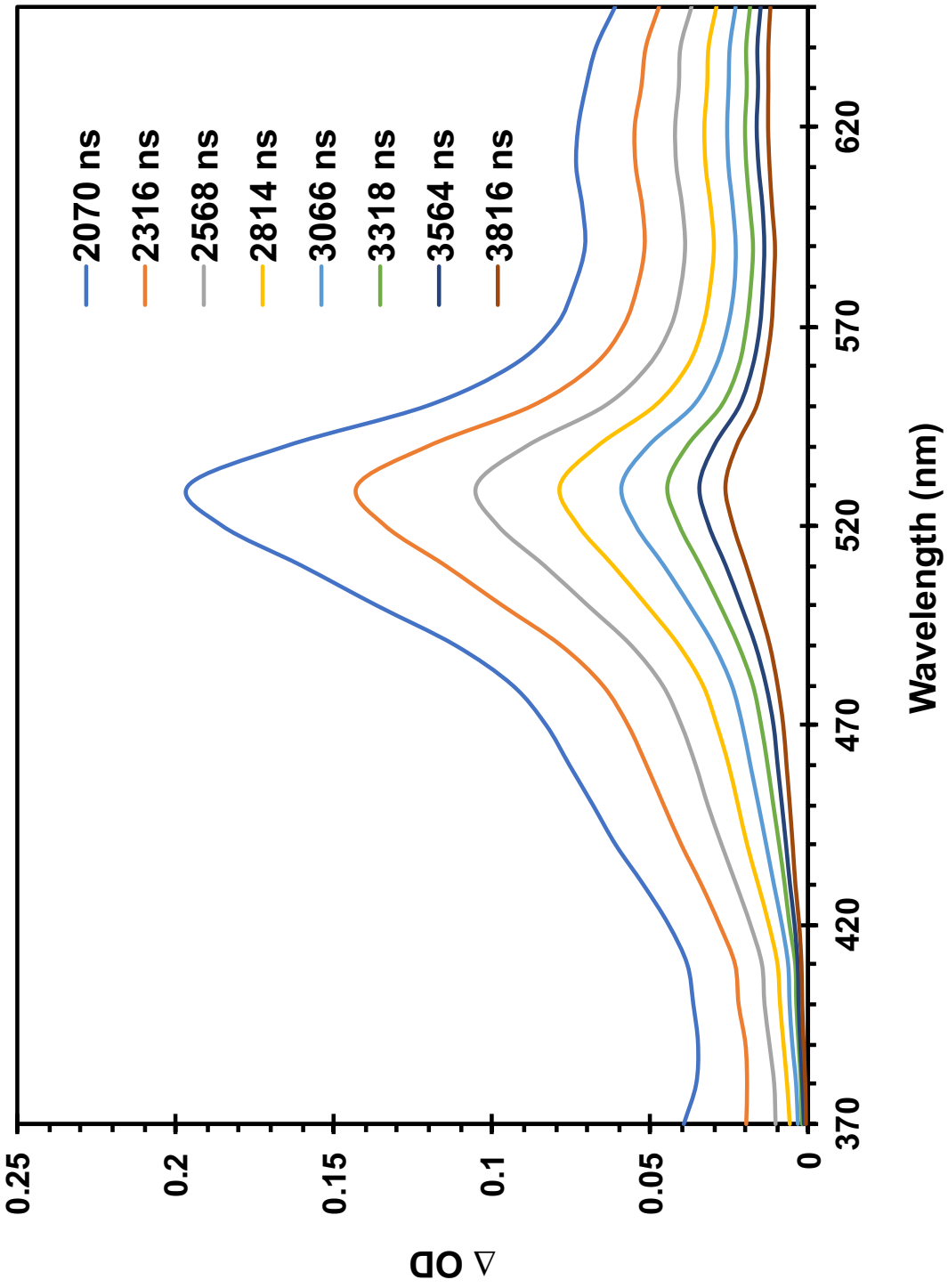

Figure 2.23 Transient Absorption of 4-acetoxybenzophenone in solution

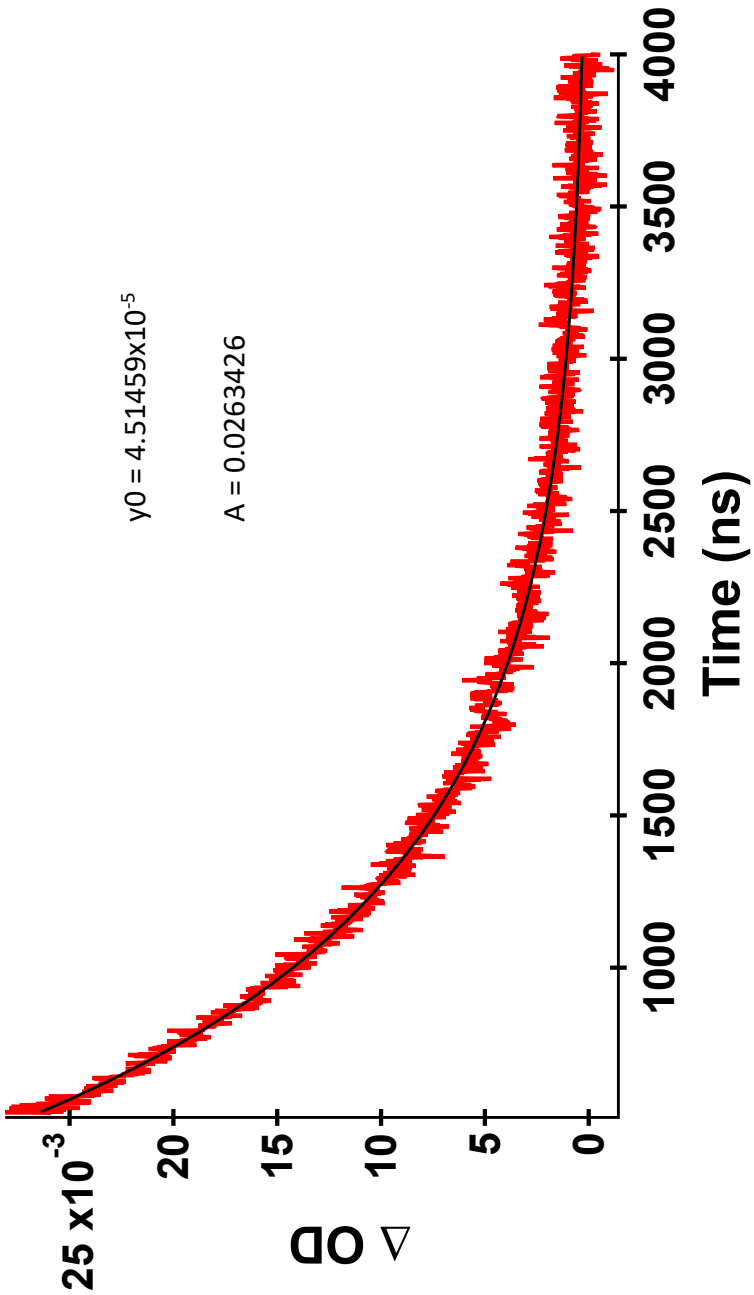

Figure 2.24 Transient Lifetime (530 nm) of 4-acetoxybenzophenone in solution

2.5.9 Quantum Yields in Solution vs. Suspension

In solution

Stock solutions of **DB-OBPh** (3, 5, 10, 15 mM) and DCK (31 mM) were prepared in acetonitrile and benzene, respectively. A 1mL aliquot of each sample was sparged with Argon in separate Pyrex tubes and sealed with a septum for six minutes each. Sparged samples were irradiated simultaneously for 5, 10, and 15 seconds using the Rayonet photochemical reactor containing eight 12 inch 8W (BLE-8T312) 312 nm bulbs. All samples were optically dense and were reproduced in triplicate. A pictorial representation of the experimental setup is provided below.

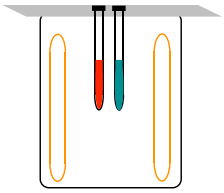

Rayonet with cardboard on top (grey) to hold samples (red and green) in place while irradiated with eight 312 nm bulbs (orange).

2-methoxynaphthalene was used an external standard to determine the number of product moles formed. ^{1}H NMR and GC-MS were used to monitor product formation from DB-OBPh and DCK, respectively. An example calculation to determine quantum yields is provided below:

Quantum yield: $\Phi_{DB\text{-}OBPh} = (A_{DB\text{-}OBPh}/A_{DCK})(mol_{HB\text{-}OBPh}/mol_{DC})\Phi_{DCK}$

$A_{DB\text{-}OBPh}$: Absorbance of DB-OBPh at given concentration

A_{DCK}: Absorbance of DCK at given concentration

$mol_{HB\text{-}OBPh}$: moles of DB-OBPh photoproduct

mol_{DC}: moles of DC photoproduct

Φ_{DCK}: Quantum yield of DCK (0.2 in benzene)

The equation was modified to consider the difference in refractive indices between actinometer (DCK) and analyte (DB-OBPh) solvents:

$$\Phi_{DB\text{-}OBPh} = (A_{DB\text{-}OBPh}/A_{DCK})(mol_{HB\text{-}OBPh}/mol_{DC})(\eta_{Acetonitrile}/\eta_{Benzene})\Phi_{DCK}$$

$\eta_{Acetonitrile}$: 1.3441

$\eta_{Benzene}$: 1.5011

A table for solvent refractive indices was provided by: http://www.raeco.com/training/refractive-index-values.htm

Irradiation of the analyte an actinometer can be irradiated as a mixture if both samples are prepared in the same solvent; however, I chose to irradiate them in separate vessels since the quantum yield of DCK was determined in benzene.

Veerman, M.; Resendiz, M.; Garcia-Garibay, M.A. *Org Lett*, **2006**, *12*, 2615-2617.

https://pubs.acs.org/doi/full/10.1021/ol060978m

Degassed samples were irradiated on a maximum time scale of 15 seconds; starting at 5 seconds and increasing by 5 second increments. Experiments were run directly in deuterated solvents. Once irradiation was completed, a known concentration of 2-methoxynaphthalene was added to the reaction as an external standard. Quantum yields for DB-OBPh were determined using ^{1}H NMR integrations. An example of a 3mM solution of DB-OBPh (A = 4.12) is provided below:

Table 2.2 H NMR Integrations of **DB-OBPh** from quantum yield experiment

Time (sec):	5	10	15
Trial 1	0.58	0.77	0.92
Trial 2	0.59	0.71	1.04
Trial 3	0.54	0.75	0.9

The moles of product formed was then determined as a ratio between the integrations of the analyte and internal standard. Explicit information for this reasoning can be found on this website: http://www.organ.su.se/bo/Gruppfiler/NMR%20yield%20calculation.pdf

Table 2.3 Integrations for DB-OBPh and 2-methoxynaphthalene to determine moles of **HB-OBPh**

Time (sec)	5	10	15
ES integration	1	1	1
ES protons	3	3	3
Sample integrations	0.58, 0.59, 0,54	0.77, 0.71, 0.75	0.92, 1.04, 0.90
Sample protons	6	6	6
rA/ES	0.285	0.372	0.477
nES (mmol)	0.000790	0.000790	0.000790
nES*(rA/ES)	0.0002291 0.0002331 0.0002133	0.0003042 0.0002805 0.0003963	0.0003635 0.0004109 0.0003556

$rA/ES = (DB\text{-}OBPh_{int}/DB\text{-}OBPh_{protons})/(ES_{int}/ES_{protons})$

$nES = ((5mg/(158.2mg/mol))/(0.002mL))*(50/750)*750x10^{-6}L$

GC-MS was used to determine the moles of product formed from irradiation of a 31mM DCK sample (A = 2) based on product integrations with respect to the internal standard integration. A calibration curve was then generated to measure the concentration with respect to the response factor ratio of internal standard/DC signal.

Calibration curve details:

Mass IS = 0.0053g

Stock Conc. of IS (M) = (0.0053g/(158.2g/mol))/0.003L = 0.0115 M IS

Mass DC = 0.0056g

Stock Conc. of DC (M) = (0.0056g/(238.37g/mol))/0.003L = 0.00783 M DC

Table 2.4 2-methoxynaphthalene to dicumene ratio to determine standard calibration

Sample #	IS signal	DC signal	ES/DC signal	[DC] M	[ES/DC]
1	9067695	11517613	0.787289432	0.000783096	1.584493458
2	8747473	2626678	3.330241849	0.000195774	6.337973833
3	8842462	619684	14.26930823	4.89435E-05	25.35189533
4	8547186	131272	65.11050338	1.22359E-05	101.4075913
5	8575641	32527	263.6468472	3.05897E-06	405.6303253
6	8292412	4509	1839.080062	7.64742E-07	1622.521301

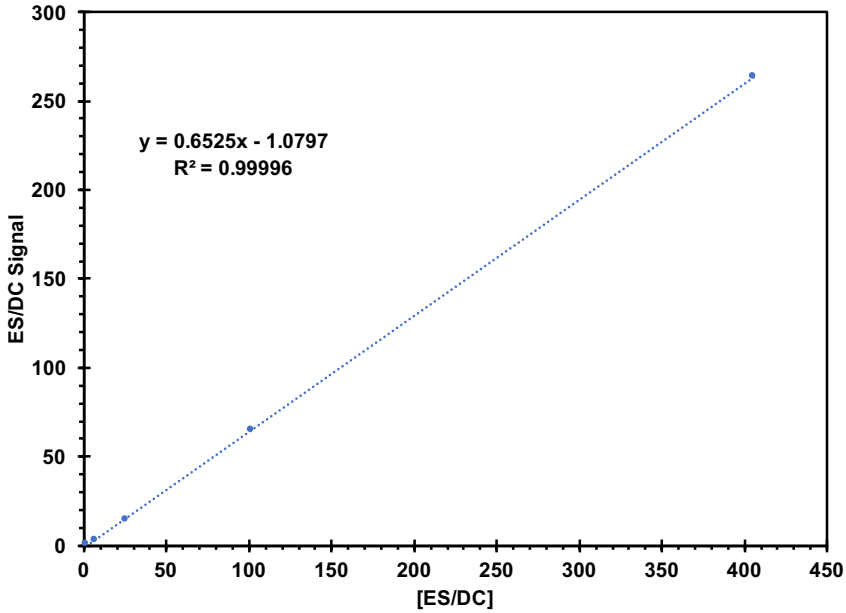

Figure 2.25 Standard curve oh 2-methoxynaphthalene and dicumene

Determining mmol of DC:

ES/DC Signal = Slope*concentration + y-int

Slope = 0.6525

Y-int = -1.0797

ES mass = 0.0098g

Stock Conc. (M) = (0.0098g/(158.2g/mol))/0.002L = 0.0310 M

Conc. in tube (M) = 0.0310*(50/750) = 0.00206 M

Conc .in GC vial (M) = 0.000248 M

ES mass in GC vial (g) = (0.000248mol/L)*0.001L*(158g/mol) = 0.0000392 g

Table 2.5 Calculated mmol of dicumene for 15 seconds for 5 second time intervals

Time	IS integration	DC integration	mmol DC
5	2334212	2820437	$8.47x10^{-5}$
	2468450	2255775	$7.43x10^{-5}$
	2733398	2473281	$7.40x10^{-5}$
10	2290771	2733527	$8.43x10^{-5}$
	2601903	2485423	$7.60x10^{-5}$
	2280171	2453113	$8.04x10^{-5}$
15	2737909	2732095	$7.76x10^{-5}$
	2458716	2426480	$7.72x10^{-5}$
	2740744	24922293	$7.41x10^{-5}$

Quantum yield were calculated for the triplicates at each time point. The values were then averaged and a standard deviation was calculated.

Table 2.6 Calculated quantum yields of **DB-OBPh** at 3mM

Time	5	10	15
	0.997	1.33	1.72
	1.16	1.36	1.96
	1.06	1.35	1.77
Ave	1.07	1.35	1.82
Std	0.08	0.02	0.12

In suspension

Suspensions of DB-OBPh and DCK were made by the reprecipitaiton method (Kasai, H.; Nalwa, H. S.; Oikawa, H.; Okada, S.; Matsuda, H.; Minami, N.; Kakuta, A.; Ono, K.; Mukoh, A.; Nakanishi, H. *Jpn. J. Appl. Phys. 2,* **1992**, *31*, L1132-L1134.). Stock solutions of DB-OBPh (0.0345 M) and DCK (0.0807 M) were made in acetonitrile and acetone, respectively. A 110 uL aliquot of DB-OBPh stock solution was added to 12 mL vortexting 0.1932 mM CTAB solution. A 120 uL aliquot of DCK stock solution was added to 12 mL vortexting 4.2 mM SDS solution. Optically dense suspensions of DB-OBPh and DCK were added into separate Pyrex tubes since the conversion rate of DB-OBPh was much greater than that of DCK. The conversion rate of DB-OBPh in suspension was so fast that DB-OBPh suspension samples were irradiated behind a 5x5 cm neutral density filter (2 OD, 1% T). Suspensions were irradiated within the black box setup (shown below) in the Rayonet photochemical reactor containing eight 12 inch 8W (BLE-8T312) 312 nm bulbs. Samples were irradiated for 10, 15, and 20 seconds in triplicate.

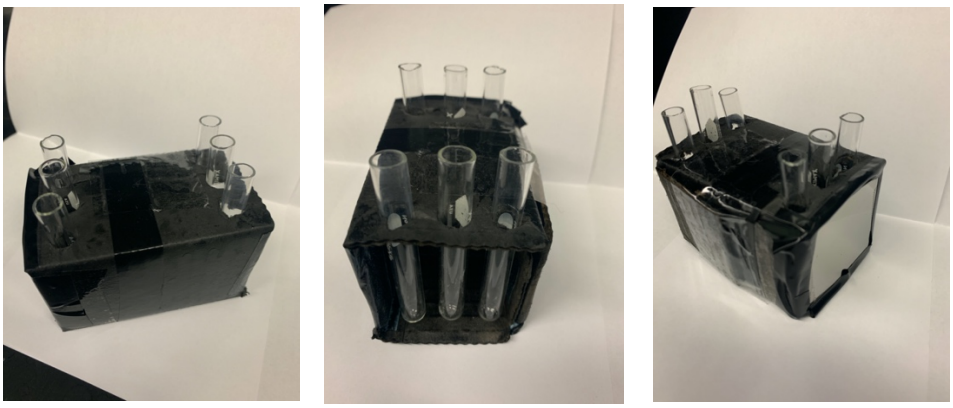

Figure 2.26 Suspension setup for irradiation. There Is a divider in the middle of the black box that does not allow light to travel through from either side.

After irradiation, samples were dried in large culture by sparging with air. Dry samples of **DB-OBPh** were redissolved in deuterated chloroform (700 μL) for ^{1}H NMR. Dry samples of DCK were redissolved in DCM (950 μL) for GC-MS. 50 μL of a 4.5 mM stock solution 2-methoxynaphthalene (external standard) was added to each sample before analytical analysis.

Quantum yields for suspensions were calculated similarly to the solution protocol described above. Below is an example calculation for 0.313 mM DB-OBPh (A = 2.22) and 0.800 mM DCK (A = 2.00) suspensions based on ^{1}H NMR and GC-MS integrations

Table 2.7 Integrations and product moles for 0.313mM loading **DB-OBPh** in suspension

Time (sec)	10	15	20
Trial 1	0.39	0.61	0.72
Trial 2	0.45	0.59	0.70
Trial 3	0.42	0.55	0.77

Time	10	15	20
ES integration	1	1	1
ES protons	3	3	3
DB-OBPh protons	6	6	6
rA/ES	0.195 0.225 0.21	0.305 0.295 0.275	0.36 0.35 0.385
nES (mmol)	0.000252845	0.000252845	0.000252845
nES*(rA/ES)	$4.93x10^{-5}$ $5.69x10^{-5}$ $5.31x10^{-5}$	$7.71x10^{-5}$ $7.46x10^{-5}$ $6.95x10^{-5}$	$9.10x10^{-5}$ $8.85x10^{-5}$ $9.73x10^{-5}$

Table 2.8 Integrations and product moles for 0.800mM loading in **DCK** suspension

Time (sec)	ES integration	DC integration	mmol DC
10	2302860	198117	$1.30x10^{-5}$
	1913072	14421	$1.15x10^{-5}$
	2422266	190871	$1.19x10^{-5}$
15	1856272	227164	$1.78x10^{-5}$
	1846016	226475	$1.78x10^{-5}$
	2227453	163082	$1.12x10^{-5}$
20	1829953	224681	$1.78x10^{-5}$
	1733605	169636	$1.46x10^{-5}$
	1781779	197158	$1.63x10^{-5}$

ES mass = 0.0016g

Stock conc (M) = (0.0016g/(158.2g/mol))/0.002L = 0.00505689mol/L

Conc in GC vial (M) = (0.00505689mol/L)*(50/1000) = 0.000252845mol/L

ES mass in GC vial = (0.000252845mol/L)*0.001L*158.2g/mol = 0.00004g

Table 2.9 Quantum yields of **DB-OBPh** in suspension

Time	10	15	20
	0.809	0.921	1.08
	1.05	0.889	1.29
	0.944	1.32	1.27
Ave	0.934	1.04	1.22
Ave*99	92.5	103.4	120.4
Std	0.12	0.24	0.11

2.5.10 Polycrystalline Powder Suspension vs. Reprecipitated Suspension Conversion

The polycrystalline suspension was prepared by suspending DB-OBPh polycrystalline powder (11mg) into 3 mL of vortexing 0.2mM CTAB solution. The reprecipitated suspension was prepared by dissolving DB-OBPh (15mg) in 250μL MeCN and adding 30 μL of the stock into 3 mL vortexing 0.2mM CTAB. Both samples were irradiated with 312 nm light for 6 minutes and the conversion was monitored by ^{1}H NMR.

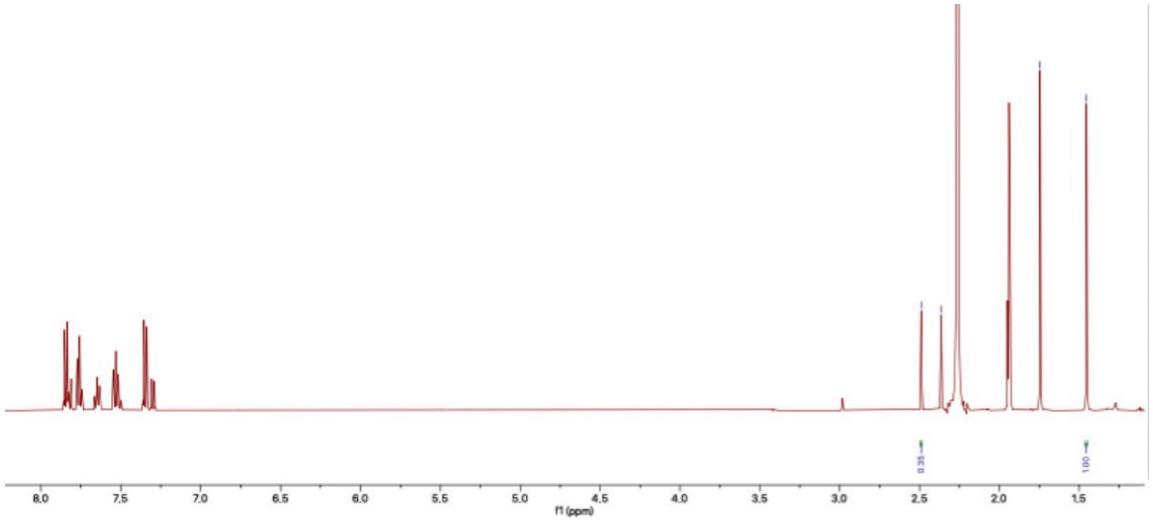

Figure 2.27 Irradiation of **DB-OBPh** polycrystalline powder

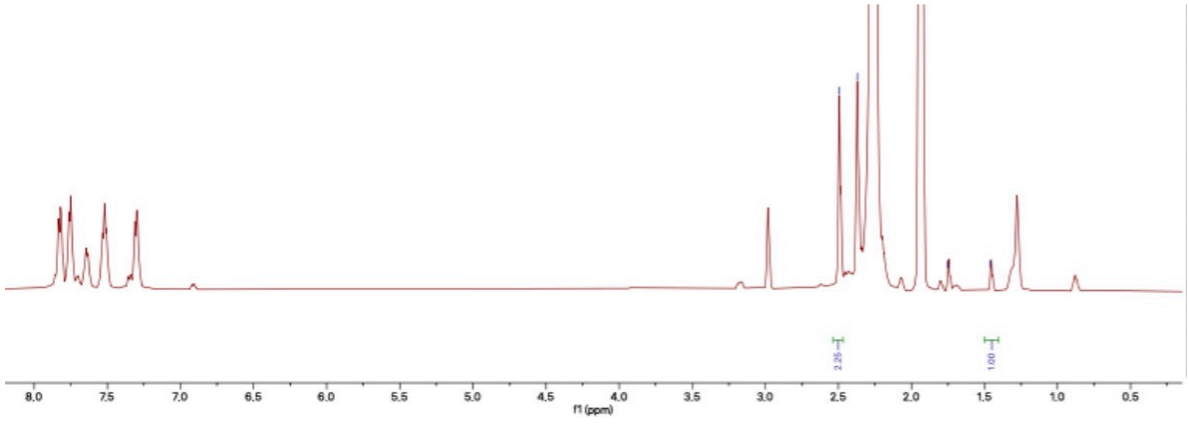

Figure 2.28 Irradiation of **DB-OBPh** reprecipitated suspension

Table 2.10 Conversion values for comparing polycrystalline powder and reprecipitated suspension

Trial	Polycrystalline P product (mg)	Reprecipitated Susp product (mg)
1	2.9 (27)	1.8 (70)
2	4.18 (38)	1.82 (72)
3	3.63 (33)	1.98 (95)

(Values in parentheses denote %conversion of sample)

2.6 References

1) Lechtken, P.; Breslow, R.; Schmidt, A. H.; Turro, N. J. Thermal rearrangement of Dewar benzenes of benzene triplet states. Examples of spin forbidden nonadiabatic pericyclic reactions *J. Am. Chem. Soc*. **2010**, *132*, 16302-16303.

2) Johnson, J. C.; Nozik, A. J.; Michl, J. Triplet Yield from Singlet Fission in a Thin Film of 1,3-Diphenylisobenzofuran. J. Am. Chem. Soc. **2010**, *132*, 16302-16303.

3) Jin, S.; Son, H.-J.; Farha, O. K.; Wiederrecht, G. P.; Hupp, J. T. Energy Transfer from Quantum Dots to Metal-Organic Frameworks for Enhances Light Harvesting. *J. Am. Chem. Soc.* **2013**, *135*, 955–958.

4) Manna, M. K,; Shokri, S.; Wiederrecht, G. P.; Gosztola, D. J.; Ayitou, A. J. New perspectives for triplet-triplet annihilation based photon upconversion using all-organic energy donor & acceptor chromophores. *Chem. Commun.*, **2018**, *54*, 5809-5818.

5) Congreve, D. N.; Lee, J.; Thompson, N. J.; Hontz, E.; Yost, S. R.; Reusswig, P. D.; Bahlke, M. E.; Reineke, S.; Voorhis Van, T.; Baldo, M. A. External quantum efficiency above 100% in a singlet-exciton-fission-based organic photovoltaic cell. *Science.* **2013**, *340*, 334-337.

6) Joubert, M.–F. Photon avalanche upconversion in rare earth laser materials, *Opt. Mater.* **1999**, *11***,** 181-203.

7) Scaiano; J. C.; Johnston, L. J.; McGimpsey, W. G.; Weir D. Photochemistry of organic reaction intermediates: novel reaction paths induced by two-photon laser excitation *Acc. Chem. Res.* **1988**, *21*, 22–29.

8) Singh-Rachford, T. N.; Castellano, F. N. Photon upconversion based on sensitized triplet–triplet annihilation. *Coord. Chem, Rev*. **2010**, *254*, 2560-2573

9) Miyata, K.; Conrad-Burton, F. S.; Geyer, F. L.; Zhu, X.-Y. Triplet Pair States in Singlet Fission. *Chem. Rev.* **2019**, *119*, 4261-4292

10) Smith, M. B.; Michl, J. Singlet Fission. *Chem. Rev.* **2010**, *110*, 6891–6936.

11) Hyndman, H.L.; Monroe, B.M.; Hammond, G.S. "Mechanisms of photochemical reactions in solution. LX. Photochemical isomerization of 2,4-hexadiene via a quantum-chain mechanism", *J. Am. Chem. Soc.*, **1969**, *91*, 2852-2859. 12) Turro, N. J.; Mcvey, J.; Ramamurthy, V.; Lechtken, P. Adiabatic Photoreactions of Organic Molecules *Angew. Chem. Int. Ed. Eng.* **1979**, *18*, 572–586.

13) Forster, T. Diabatic and Adiabatic Processes in Photochemistry *Pure Appl. Chem*, **1970**, *24*, 443-449.

14) Forster, T.; Excimers, *Angew. Chem., Int. Ed. Engl.*, **1969**, *8*, 333.

15) Turro, N. J.; Lechtken, P.; Lyons, A.; Hautala, R. R.; Carnahan, E.; Katz, T. J. Molecular photochemistry. LXIV. Photochemical generation of electronically excited organic products in adaiabatic pericyclic photoreactions. Unexpected propensity toward spin inversion in a retrocycloaddition and in a valence isomerization *J. Am Chem. Soc.*, **1973**, *95*, 2035-2037.

16) Saltiel, J.; Townsend, D. E.; Sykes, A. Quantum chain process in the sensitized cis-trans photoisomerization of 1,3 dienes *J. Am. Chem. Soc*. **1973**, *95*, 5968-5973.

17) Saltiel, J.; D'Agostino, J.; Megarity, E. D.; Metts, L.; Neuberger, K. R.; Wrighton, M.; Zafiriou, O. C. The cis-trans photoisomerization of olefins, Org. Photochem. **1973**, *3*, 1-113.

18) Yee, W. A.; Hug, S.J.; Kliger, D.S. Direct and sensitized photoisomerization of 1,4-diphenylbutadienes *J. Am. Chem. Soc*. **1988**, *110*, 2164-2169.

19) Ganapathy, S.; Liu, R.S.H. Photoisomerization of polyenes. 30. Quantum chain processes in photoisomerization of the all-trans, 7-cis, and 11-cis isomers of retinal *J. Am. Chem. Soc.* **1992**, *114*, 3459-3464.

20) Sundahl, M.; Wennerstrom, O. Catalysis of a photochemical reaction; a cis-trans isomerization proceeding by a quantum chain process *J. Photochem. and Photobio. A.* **1996**, 98, 117-120.

21) Brink, M.; Jonson, H.; Sundahl, M. Catalysis of triplet state cis-trans isomerizations making a quantum chain process more efficient *J. Photochem and Photobio. A.* **1998**, 112, 149-153.

22) Whitten, D. G.; Mercer-Smith, J. A. Photosensitization o Stilbene Isomeriation by Palladium and Platinum Porphyrins, an Intermolecular Quantum Chain Process *J. Am. Chem. Soc.* **1978**, *110*, 2620-2625.

23)Gopal, V. R.; Reddy, M.A.; Rao, V. J. Wavelength Dependent Trans to Cis and Quantum Chain Isomerizations of Anthrylethylene Derivatives *J. Org. Chem.* **1995**, *60*, 7966-7973.

24) Saltiel, J.; Wang, S.; Ko, D.; Gormin, D. A. Cis-Trans Photoisomerization of the 1,6-Diphenyl-1,3,5-hexatrienes in the Triplet State. The Quantum Chain Mechanism and the Structure of the Triplet State *J. Phys. Chem. A.* **1998**, *102*, 5383-5392.

25) Crandall, J. K.; Mayer, C. F. Benzene-photosensitized transformations of the four geometrical isomers of 1,5,9-cyclododecatriene *J. Am. Chem. Soc.*, **1967**, *89*, 4374-4380.

26) Kazakov, V. P.; Voloshin, A. I.; Shavaleev. Chemiluminescence in visible and infrared spectral regions and quantum chain reactions upon thermal and photochemical decomposition of adamantylideneadamantane-1,2-dioxetane in the presence of chelates $Pr(dpm)_3$ and $Pr(fod)_3$ *J. Photochem and Photobio*. **1998**, *11*, 177-186.

27) Lechtken, P.; Yekta, A.; Turro, N. J. Tetramethyl-1,2-dioxetane. Mechanism for an autocatalytic decomposition. Evidence for a quantum chain reaction. *J. Am. Chem. Soc.* **1973**, *95*, 3027-3028.

28) Turro, N. J.; Schore, N. E.; Yekta. Quantum chain processes. Novel procedure for measurement of quenching parameters. Evidence that exothermic triplet-triplet energy transfer is not diffusion limited and an estimation of the efficiency of exothermic quenching in a solvent cage *J. Am. Chem. Soc*. **1974**, *96*, 1936-1938.

29) Turro, N.J.; Waddell, W. H. Quantum chain processes. Direct observation of high quantum yields in the direct and photosensitized excitation of tetramethyl-1,2-dioxetane *Tetrahedron Letters.* **1975**, *25*, 2069-2072.

30) Schuster, G. B.; Turro, N. J.; Steinmetzer, H.; Schaap, A. P.; Faler, G.; Adam, W.; Liu, J. C. Adamantylideneadamantane-1,2-dioxetane. Chemiluminescence and decomposition kinetics of an unusually stable 1,2-dioxetane *J. Am. Chem. Soc.* **1975**, *97*, 7110-7117.

31) Wilson, T.; Schaap, A. P. Chemiluminescence from cis-diethoxy-1,2-dioxetane. Unexpected effect of oxygen *J. Am. Chem. Soc.* **1971**, *93*, 4126-4136.

32) Turro, N. J.; Lechtken, P.; Schore, N. E.; Schuster, G.; Steinmetzer, H.; Yekta, A. Tetramethyl-1,2-dioxetane. Experiments in chemiexcitation, chemiluminescence, photochemistry, chemical dynamics, and spectroscopy *Acc. Chem. Res.* **1974**, *7*, 97-105.

33) Carr, R.V.; Kim, B.; McVey, J.K.; Yang, N.C.; Gerhartz, W.; Michl, J. Photochemistry and Photophysics of 1,4-dewarnaphthalene Chem. Phys. Lett., **1976**, 39, 57-60.

34) Yang, N.C.; Carr, R.V.; Li, E.; McVey, Rice, S. A. 2,3-Naphtho-2,5-bicyclo[2.2.0]hexadiene *J. Am. Chem. Soc.,* **1976**, 96, 2297-2298.

35) Powel, R. C; Soos, A.G. Singlet exciton energy transfer in organic solids *J. Lumin.* **1975**, *11*, 1-45.

36) Swenberg, C.E.; Gaecintov, N.E. in *Organic Molecular Photophysics*, Volume 1, Birks, J.B. Ed., John Wiley and Sons, London, 1973. 37) Yoon, Z.S.; Yoon, M.-C.; Kim, D. Excitonic Coupling in covalently linked multiporphyrin systems by matrix diagonalization *J. Photochem. Photobiol., C* **2005**, *6*, 249-263.

38) Swenberg, C. & Pope, M. *Electronic Processes in Organic Crystals and Polymers* Oxford University Press (1999).

39) Soos, Z.; Powell, R. Generalized Random-Walk Model for Singlet-Exciton Energy Transfer. *Phys. Rev. B* **1972**, *6*, 4035–4046.

40) Kuzmanich, G.; Natarajan, A.; Chin, K. K.; Veerman, M.; Mortko, C. J.; Garcia-Garibay, M. A. Solid-state photodecarbonylation of diphenylcyclopropenone: a quantum chain process made possible by ultrafast energy transfer *J. Am. Chem. Soc.* **2008**, *130*, 1140-1141.

41) Kuzmanich, G.; Gard, M. N.; Garcia-Garibay, M. A. Photonic amplification by a singlet-state quantum chain reaction in the photodecarbonylation of crystalline diarylcyclopropenones. *J. Am. Chem. Soc.* **2009**, *131*, 11606–11614.

42) Wakasa, M.; Yago, T.; Sonoda; Y.; Katoh, R. Structure and dynamics of triplet-exciton pairs generated from singlet fission studied via magnetic field effects *Communications Chemistry,* **2018**, *1*, 1-6.

43) Ryasnyanskiy, A.; Biaggio, I. Triplet exciton dynamics in rubrene single crystals. *Phys. Rev. B*, **2011**, *84*, 193203.

44) Turro, N. J.; Ramamurthy, V.; Katz, T. J. Energy Storage and Release. Direct and sensitized photoreactions of dewar benzene and prismane. *Nouveau Journal de Chimie* **1978**, *1*, 363–365.

45) Kiau, S.; Liu, G.; Shukla, D.; Dinnocenzo, J. P.; Young, R. H.; Farid, S. Kinetics of Isomerization via Photoinduced Electron Transfer. I. Spectral Analysis and Structural Reorganization of Hexamethyl Dewar Benzene Exciplexes *J. Phys. Chem. A* **2003**, *107*, 3625-3632.

46) Ferrar, L.; Mis, M.; Dinnocenzo, J. P.; Farid, S.; Merkel, P. B.; Robello, D. R. Quantum Amplified Isomerization in Polymers Based on Triplet Chain Reactions *J. Org. Chem.* **2008**, *73*, 5683-5692.

47) Tomasulo, M.; Kaanumal, S. L.; Sortino, S.; Raymo, F. M. Synthesis and Properties of Benzophenone−Spiropyran and Naphthalene−Spiropyran Conjugates *J. Org. Chem.* **2007**, *72*, 595-605.

48) The bimolecular diffusion rate constant in acetonitrile is MeCN= 6.83×10^9 $M^{-1}s^{-1}$. CRC Handbook of Chemistry and Physics, ed. R.C. Weast, CRC Press, Inc., Boca Raton, FL, 68th edn., 1987–1988.

49) Veerman, M.; Resendiz, M. J. E.; Garcia-Garibay, M. A. Large Scale Photochemical Reactions of Nanocrystalline suspensions: A Promising Green Chemistry Method *Org. Lett.* **2006**, *8*, 2615-2617.

50) Kasai, H.; Nalwa, H. S.; Oikawa, H.; Okada, S.; Matsuda, H.; Minami, N.; Kakuta, A.; Ono, K.; Mukoh, A.; Nakanishi, H. A Novel Preparation Method of Organic Microcrystals *Jpn. J. Appl. Phys. 2,* **1992**, *31*, L1132-L1134

51) Kuzmanich, G.; Simoncelli, S.; Gard, M. N.; Spanig, F.; Henderson, B. L.; Guldi, D. M.; Garcia-Garibay, M. A. Excited State Kinetics in Crystalline Solids: Self-Quenching in Nanocrystals of 4,4'-Disubstituted Benzophenone Triplets Occurs by a Reductive Quenching Mechanism J. Am. Chem. Soc. **2011**, *43*, 17296-17306.

CHAPTER THREE

Effect of Crystal Packing on Triplet Quantum Chain reactions of Crystalline Dewar Benzenes

Edris Rivera, Ieva Liepuonute, Garett Ruesch, Olivia Friedl, and Miguel A. Garcia-Garibay

3.1 ABSTRACT

We have previously studied the quantum chain reactions of benzophenone-linked Dewar benzenes (**DB-OBPh**) and the ability to utilize the solid state as a chain amplification technique, promoting ultrafast energy transfer between neighboring molecules within a close-packed, uniform arrangement. Although we were able to achieve quantum yields of ca 90-120 in the solid state, we are far from realizing its full potential in achieving a quantum chain of 10^6. Our initial analysis determined that the semicrystalline suspensions are less reactive than the polycrystalline powder form, showcasing potential quantum yields ca. 100-300. In this work we further explore the extent of the **DB-OBPh** quantum chain using alkyl substituted Dewar benzenes to ensure crystallinity and unique packing. We confirmed unique crystal packing using pXRD and generate a single crystal for the cyclohexyl **DB-OBPh** derivatives. After measuring quantum yields, we found that values ranged between 250-350 in **DB-OBPh** derivatives and an unexpected value of ~570 in mono-sensitizer-linked Dewar benzene nanocrystalline suspension. This work revealed that the crystal packing places a significant role on the extent of the quantum chain reaction.

3.2 Introduction

Quantum chain reactions are nonlinear photochemical processes that result in the formation of several photoproducts per photon via energy transfer events.[1-18] Dewar benzenes are known to undergo a quantum chain reaction upon triplet activation and are of particular interest due to their long-lived chain carrying species that propagates the energy transfer step.[19-21] Energy transfer in crystals based on the generation of triplet excitons are well documented in literature and we were interested in extending this reactivity to Dewar benzenes.[21-30] Since our previous work involving quantum chain amplification of **DB-OBPh**, much of this current work has focused on addressing limitations that resulted in low quantum yields. We have previously shown that **DB-OBPh** can achieve quantum yields of ca. 90-120 in suspension; however, the extent of this chain is much lower than our initial hypothesis. Further analysis of the dried suspension showed mostly amorphous material based on the lack of long ranged order revealed by pXRD. We were able to demonstrate the true potential for **DB-OBPh** through a comparative irradiation study between the amorphous suspension (generated by the reprecipitation method) and a polycrystalline powder suspended in CTAB; suggesting quantum yields of ca. 100-300 can be achieved in the crystalline solid state. In addition to this limitation, we were also interested in studying the impact of the crystalline solid state environment and the possibility of benzophenone self-quenching on quantum yield efficiency.[31-34] To address these limitations and further expand the quantum chain reaction of Dewar benzenes we were interested in exploring quantum chain reactions of alkyl-substituted **DB-OBPh**s and derivatives with only one covalently attached benzophenone sensitizer. The **DB-OBPh** derivatives were synthesized with t-butyl **3.1**, cyclohexyl **3.2** and adamantyl **3.3** substituents to ensure crystallinity and unique packing between

Dewar benzenes. We were interested in determining the role of benzophenone self-quenching by measuring quantum yields of derivatives **3.4** and **3.5** (**Figure 3.1**).

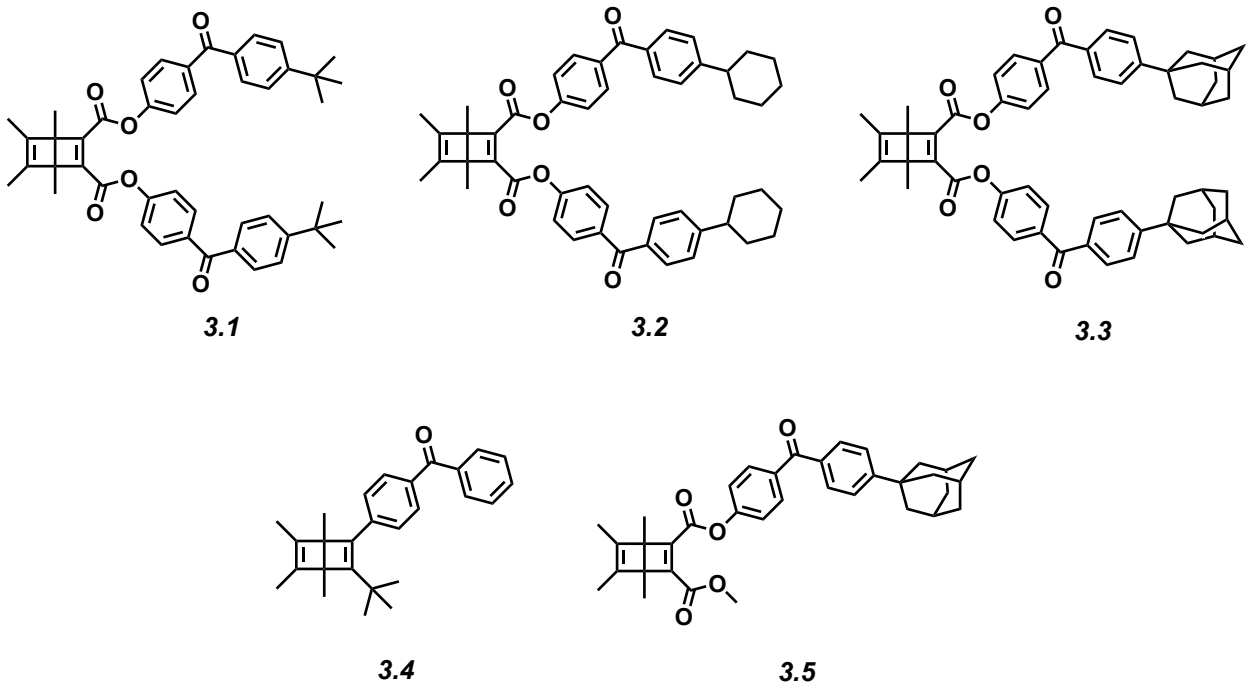

Figure 3.1 Alkyl-substituted **DB-OBPh** derivatives

3.3 Results and Discussion

The reaction for **DB-OBPh** derivatives **3.1** and **3.2** proceeds via acid chloride formation of *para*-alkyl benzoic acid with excess oxalyl chloride and a catalytic amount of anhydrous DMF. The acid chloride was not purified and was carried onto the next step after in vacuo reduction for 40 minutes. The resulting yellow oil was dissolved in dry DCM and added to a suspension of $AlCl_3$/DCM at -72 °C. After stirring for at least 10 minutes, anisole was slowly added to the reaction while stirring cold (-72 °C). The reaction was allowed to stir overnight and allowed to gradually

warm to room temperature. Derivative **3.3** was prepared similarly starting with *para*-methoxybenzoic acid to carry out a Friedel Crafts acylation with phenyladamantane. The resulting compound was extracted with ethyl acetate and washed with DI water. The organic layer was dried with $MgSO_4$, filtered, and reduced in vacuo. The resulting oil was purified via column chromatography and gave pure alkyl-substituted hydroxybenzophenones, HO-BPhR (Scheme 3.1A). [35,36]

Scheme 3.1 Synthesis of benzophenones A) for DB-OBPhs B) and monoDB-BPh C)

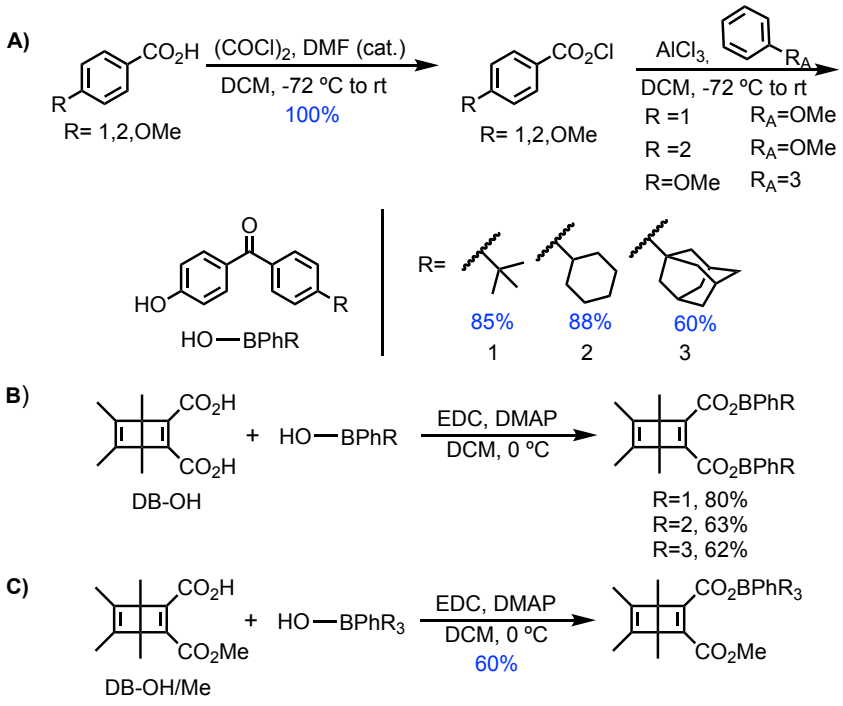

Compounds **3.1-3.3** and **3.5** were realized based on similar procedures attaching hydroxybenzophenone sensitizers onto the dicarboxylic acid (**Scheme 3.1B**) and monocarboxylic acid (**Scheme 3.1C**) Dewar benzene. Final products were obtained as white powders after

recrystallization in acetone and ether and had high melting points of 137 °C, 151 °C, 165 °C, and 145 °C, respectively. Compound **3.4** was achieved through Sonogashira coupling of 4-bromobenzophenone and t-butyl acetylene to give acetylene **3.6**.[37] This was utilized in the next reaction with 2-butyne and $AlCl_3$ which was stirred at 0°C for 10 minutes prior to the dropwise addition of **3.6**. After stirring for an hour, the cold reaction was quenched with the slow addition of DMSO (**Scheme 3.2**).

Scheme 3.2 Synthesis of **3.4**

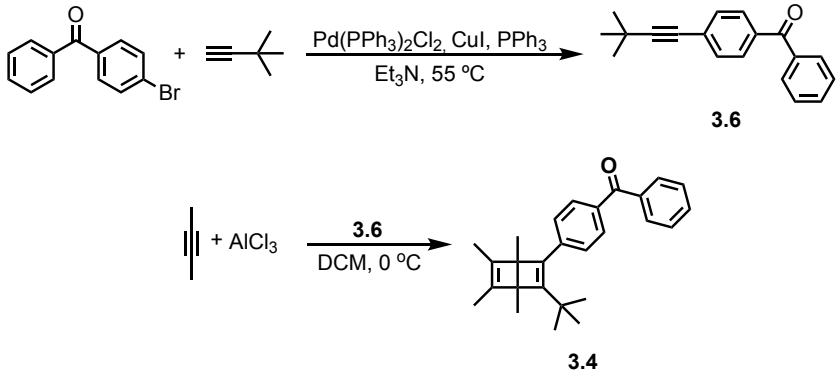

Compound **3.4** was washed with DI water and extracted in ethyl acetate. The organic layer was dried with $MgSO_4$, filtered, then dried in vacuo producing a crude oil. The compound proved difficult to purify and a viscous yellow oil. Due to the lack of crystallinity no further analysis was considered for **3.4**.

3.4 Solid state analysis of DB-OBPhs

We confirmed **3.1**, **3.2**, and **3.3** were crystalline via pXRD and obtained a crystal structure for **3.2** by single crystal x-ray diffraction (**Figure 3.2**).

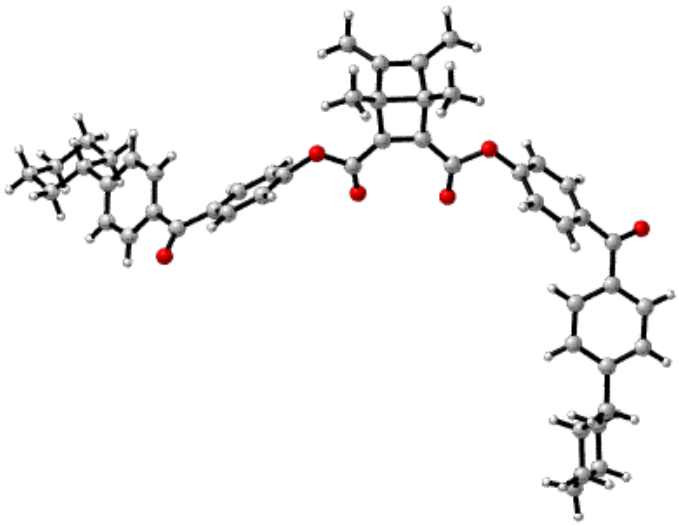

Figure 3.2 Crystal structure of compound **3.2**

Compound **3.2** takes up a P1/ triclinic space group with disorder about the Dewar benzene portion of the molecule, confirming unique crystal packing between DB-OBPh derivatives. While our previous work displayed quantum yield values of **DB-OBPh** in amorphous suspension, we were interested in measuring quantum yields of nanocrystalline suspensions. Compounds **3.1**, **3.2**, and **3.5** were prepared as nanocrystalline suspensions based on the reprecipitation method. This method proceeds by dissolving 2 mg/L of each compound in acetone and THF and adding 20 μL of each in vorterxing 0.5 mM CTAB solution. The suspensions were characterized using DLS (**Figure 3.3**) UV-vis (**Figure 3.4**), and crystallinity was confirmed using pXRD.

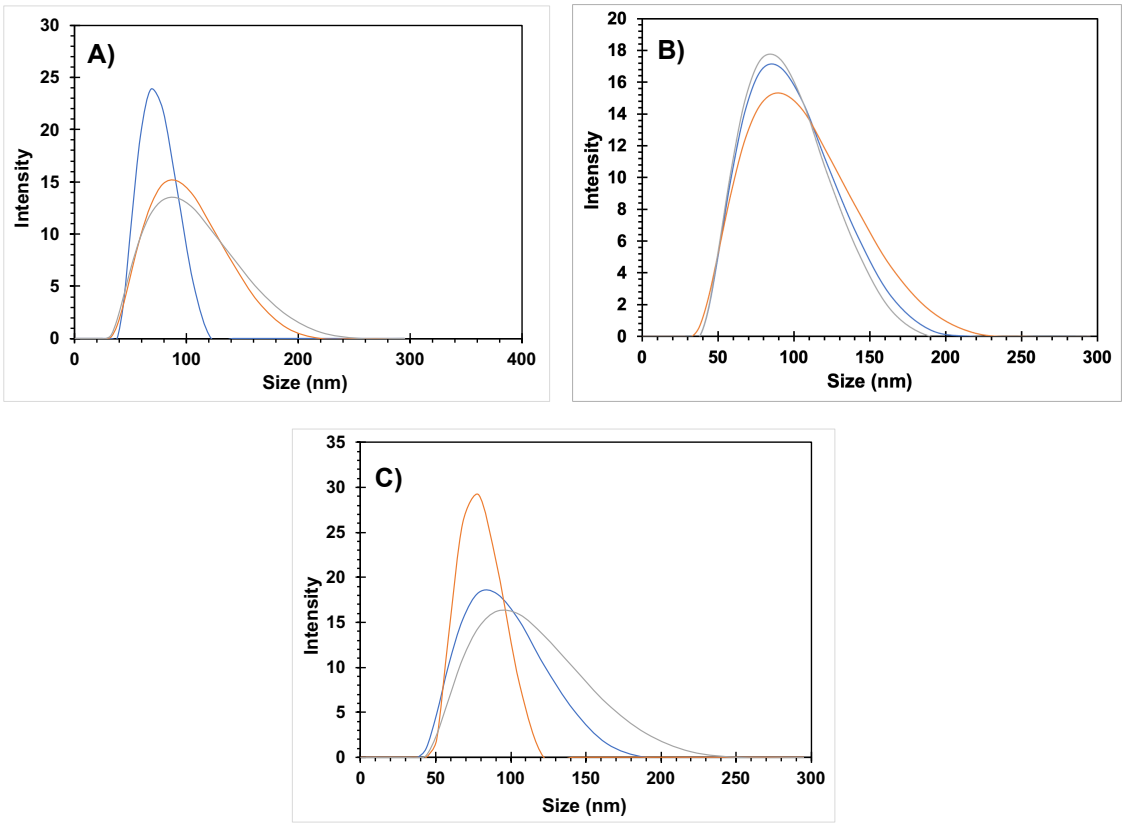

Figure 3.3 DLS measurement of compound 1 (A) , 2 (B), and 3 (C) with a size distribution of 101±30, 89±20, and 92±16 respectively

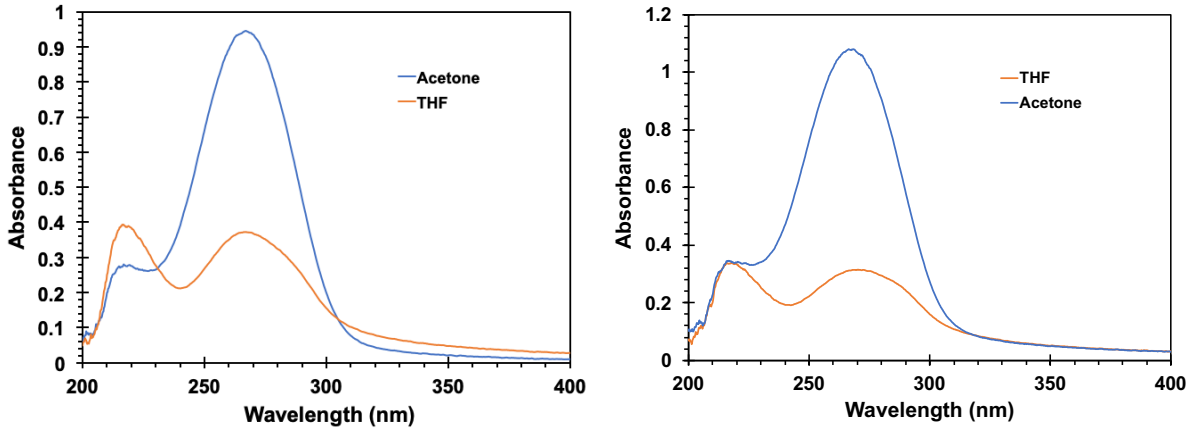

Figure 3.4 UV-vis of compound A) **3.1** and B) **3.2** as nanocrystalline suspensions prepared in 0.5mM CTAB solution.

Figure 3.5 shows the diffractogram of **3.2** in the polycrystalline powder (A) and dried crystalline suspension (B) revealing unique packing pattern between both forms. This indicates the evidence of polymorphism between the nanocrystalline suspension and bulk powder.

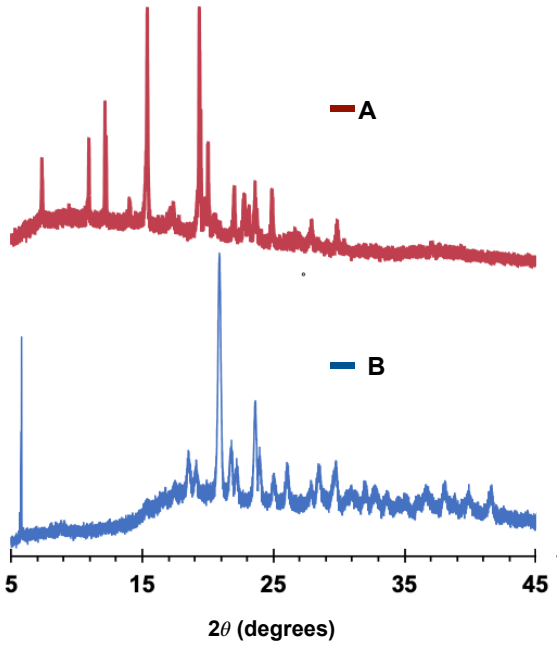

Figure 3.5 Diffractogram of compound 1 as a polycrystalline powder (A) and nanocrystalline suspension (B)

While we were unable to obtain a diffraction quality single crystal of compound **3.3** we assume that the crystal packing of the single crystal is likely different from that of the polycrystalline powder and/or the nanocrystalline suspension. This observation led to the investigation of polymorphism in **DB-OBPh**. To do this we generated polycrystalline powder samples of **DB-OBPh** out of various solvents and measured the powder pattern of each (**Figure 3.6**).

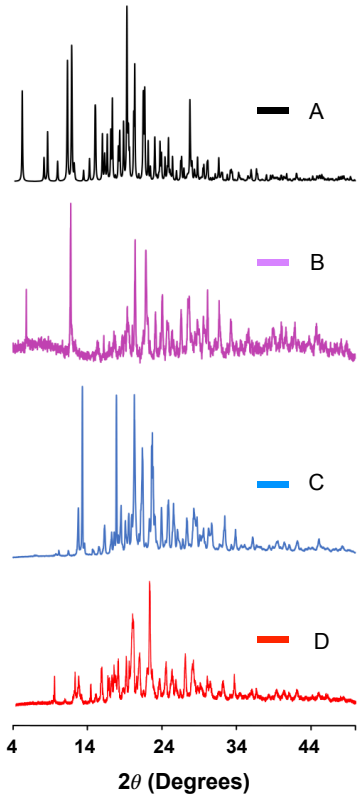

Figure 3.6 Polycrystalline powder pattern of **DB-OBPh** A) simulated, B)hexanes/ethyl acetate, C) ether, and D) acetonitrile

The data confirms polymorphism in **DB-OBPh** which may play a significant role in the efficiency of the quantum chain reaction of **DB-OBPh** derivatives.

We were also interested in investigating the transformation of the **DB-OBPh**s to **HB-OBPh** as we hypothesize a topotactic transformation may have significant impact on the extent of the quantum chain reaction, since maintenance of the crystalline environment will ensure excitonic energy transfer.

To study the isomerization of the solid state we monitored the transformation of **DB-OBPh**s using both light microscopy and pXRD. **Figure 3.7** shows macroscopic crystals of **3.2** under a polarized light microscope and the irradiation of **3.2** over 2 minutes. While showing a blue color under the 2nd order compensator, indicating anisotropic material prior to irradiation (t=0, A), subsequent irradiation indicating isomerization from Dewar to Huckel benzene resulted in isotropic material.

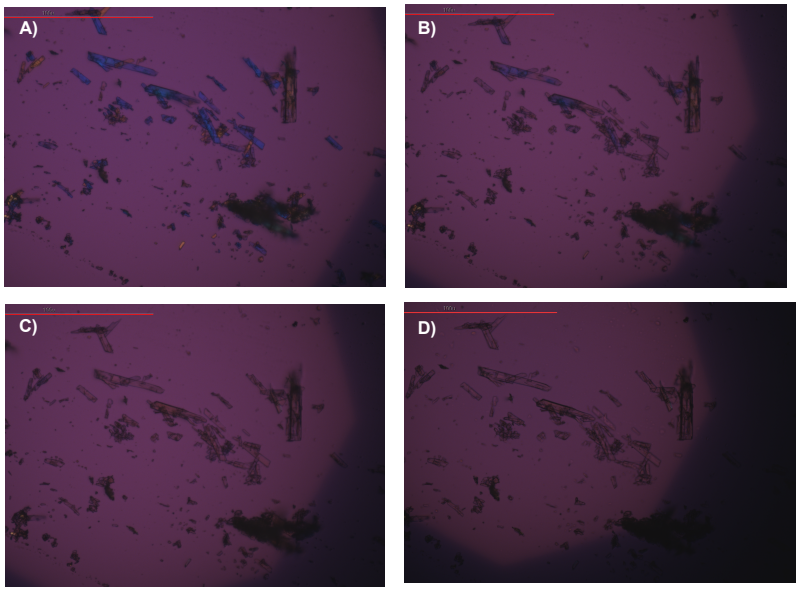

Figure 3.7 Compound 2 under 2nd compensator of polarized light microscope with irradiation time 0 min (A), 0.5 min (B), 1.0 min (C), and 2.0 min (D).

This was further confirmed by pXRD before and after full isomerization of **3.1** and **3.2** bulk powder revealing amorphous product formed after irradiation of polycrystalline powder. While this suggests an amorphization pathway, the lack of breaking or opaque texture of the macrocrystals may indicate a solid solution that proceeds through a reconstructive phase.

Previous work from our group determined possible routes of transformation of crystalline reactants to products.[38] High melting points of starting materials **3.1-3.3** and **3.5** and solid photoproduct indicate that the transformation is a solid-to-solid transformation. To determine if the transformation occurs along a reconstructive phase, we measured the glass transition, Tg, temperature of **3.2** using DSC (**Figure 3.8**). In order to confirm this transformation undergoes a reconstructive phase the irradiation must be conducted at the glass transition temperature.

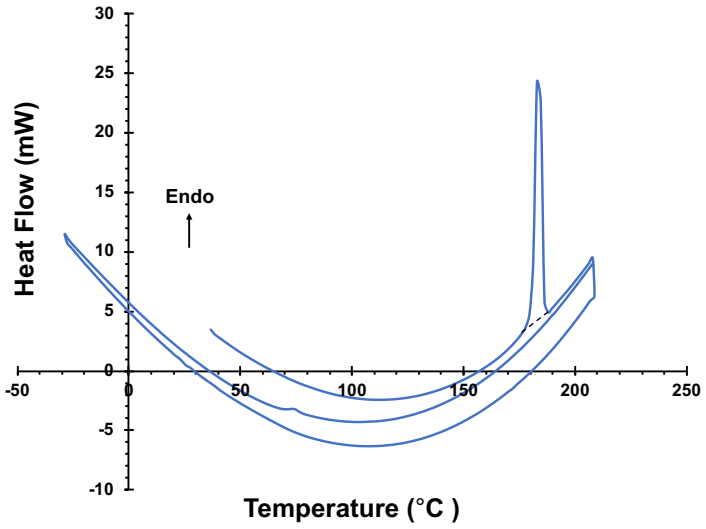

Figure 3.8 Thermogram of crystalline **3.2** photoproduct showing 3 cycles, heating from 30 to 210 °C, cooling from 210 to -30 °C, then heating from -30 to 210 °C

The thermogram shows an endotherm at 170 °C indicative of melting of crystalline compound **3.2** during the initial heating cycle from 30 °C to 210 °C. The subsequent cycle shows another endotherm at 70 °C indicative of the Tg. To explore the potential for the transformation to occur under a reconstructive phase, irradiation at temperatures above the Tg are necessary.

3.5 Quantum Yields of DB-OBPhs

After confirming unique crystal packing for **DB-OBPh** derivatives we were interested in determining the impact of the crystalline solid state packing environment on the extent of the quantum chain. To do so we measured quantum yields of **3.1**, **3.2**, and **3.5** as nanocrystalline suspensions. Samples **3.1**, **3.2**, and **3.**5 were prepared as 56 mg/mL, 62 mg/mL, and 76 mg/mL solutions in THF and 30 μL of each were separately injected into vortexting 0.5mM CTAB, respectively. All suspensions were optically dense and irradiated in tandem with DCK as an actinometer with a known quantum yield in suspension (Φ=0.2). Suspensions were irradiated in 3 mL Pyrex tubes behind a 5x5 neutral density filter via Rayonet with four 8W 312 nm bulbs. The neutral density filter only allowed 1% transmittance of light to slow the reaction by 100 times.

Quantum yields were measured using 2-methoxynaphthalene as an external standard, ^{1}H NMR and GC-MS. A detailed description of the calculations is presented at the end of the chapter. As shown in Figure **3.9**, compound **3.5** showed the greatest quantum yields of ca. 575, and quantum yields of ca. 274 and 343 for **3.1** and **3.2**.

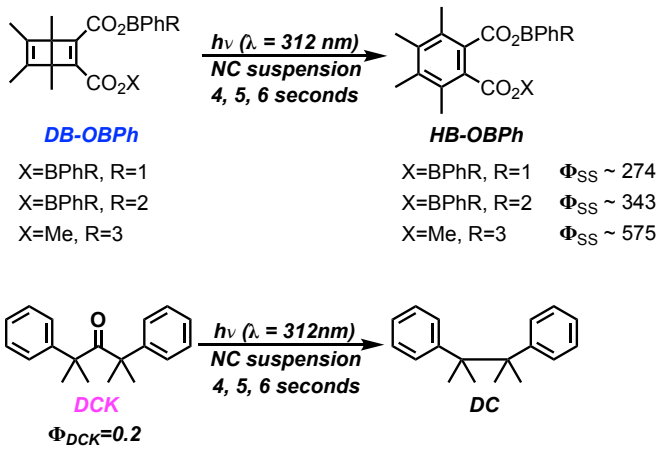

Figure 3.9 Quantum yield experiment for compounds **3.1**, **3.2**, and **3.5**

This proved our initial hypothesis that quantum yields of crystalline DB-OBPhs have the potential to reach 100-300 and that crystal packing plays a significant role in the efficiency of the quantum chain. More interesting was the extent of the chain reaction of 5 which possesses a single benzophenone sensitizer attached. This indicates significant interaction between benzophenones that are covalently attached. Further analysis will address the electronics of a **DB-OBPh**s with a single sensitizer covalently attached.

3.6 Conclusion

In this work we confirmed that the crystalline environment plays a role on the efficiency of the quantum chain reaction of **DB-OBPhs** by confirming unique crystal packing between derivatives, ensuring suspensions were crystalline, and measuring quantum yields. While we were only able to generate a crystal structure for **3.2** we are interested in obtaining crystal structures for the remaining derivatives to gain greater insight on crystal packing. We also observed that the chain reaction further extends when one sensitizer is covalently attached, addressing the possibility of benzophenone self-quenching and the development of a unique benzophenone scaffold. Moving forward we're interested in studying the lifetimes of such systems and others that may promote a long-lived excited species.

3.7 Experimental

3.7.1 General Information

All compounds were synthesized under an inert argon atmosphere unless otherwise specified. Nuclear magnetic resonance (NMR) spectra for ^{1}H and ^{13}C were obtained using 500 MHz Bruker NMR spectrometer. All chemical shifts are reported in ppm using natural abundance isotopes of reference solvents. Infrared (IR) spectra was collected using the Perkin-Elmer 1000 Series FT-IR spectrometer.

3.7.2 Synthetic Procedures

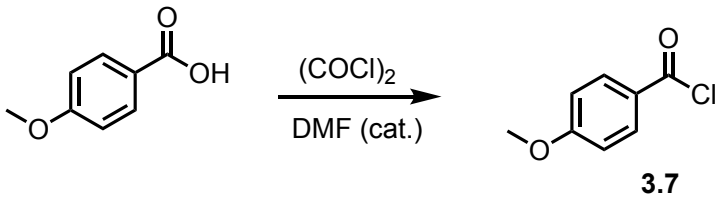

3.7

Synthesis of 3.7: A 250 mL round bottom flask was flame dried and charged with a stir bar, p-methoxybenzoic acid (1.10 g, 7.23 mmol) and placed under argon atmosphere. This was followed by the addition of 10 mL anhydrous dichloromethane (DCM). The reaction was placed in a -72 C bath and allowed to stir for a few minutes. Oxalyl chloride ($(COCl)_2$ 2.50 mL, 29 mmol, 4 equiv.) was added slowly to the flask while cold, followed by the addition of a few drops of anhydrous dimethylformamide (DMF). The reaction was then relieved from the -72 C bath and allowed to warm to room temperature while stirring. Upon warming the reaction will begin to bubble as the reactant begins to dissolve. After 30-40 min. reaction will turn pale yellow. The reaction was allowed to stir at room temperature overnight. The reaction resulted in yellow solution. The acid chloride was not purified via column chromatography, but was put under rigourous rotovapping

at high temperatures (45-50 C) in dry toluene to remove excess $(COCl)_4$. The resulting yellow oil was collected to be used for the following Friedel Crafts acylation.

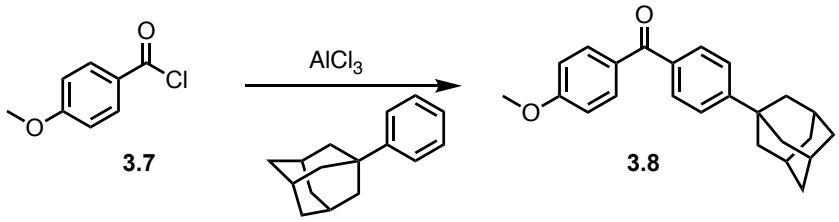

Synthesis of 3.8: A 150 mL three-neck round bottom flask was flamed dried, purged with argon, and charged with $AlCl_3$ (~2 g, 14.42 mmol, 2 equiv.). This was followed by the addition of ~7 mL of anhydrous DCM. The reaction was placed in a -72 C bath and allowed to stir for a few minutes to cool. The acid chloride was then separately dissolved in 5 mL dry DCM and transferred to the cold reaction flask slowly. The reaction was allowed to stir for ~10 minutes before dissolving phenyladamantane in dry DCM and slowly adding it to the reaction flask. The reaction went from a dark yellow to a bright red. The reaction was allowed to stir overnight. Product was washed with DI water and extracted in ethyl acetate. The organic layer was collected, dried over magnesium sulfate, filtered, then concentrated under pressure to yield a yellow oil. The crude product was purified using column chromatography with a gradient solvent system of hexanes: ethyl acetate. The resulting purified product was a white crystalline powder (50% yield). ^{1}H NMR (500 MHz, CDCl3): δ = 1.75-2.12 (m, 15H), 3.89 (s, 3H), 6.95,9.97 (d, 2H), 7.45,7.46 (d, 2H), 7.72,7.73 (d, 2H), 7.82,7.84 (d, 2H); ^{13}C NMR (126 MHz, CDCl3) δ = 195.41, 163.02, 155.74, 135.47,

132.49, 130.52, 129.87, 124.77, 113.47, 55.49, 42.97, 36.70, 28.84. HRMS (DART) calcd for C24H26O2 [M+H]**+** 347.22131, found 347.22167.

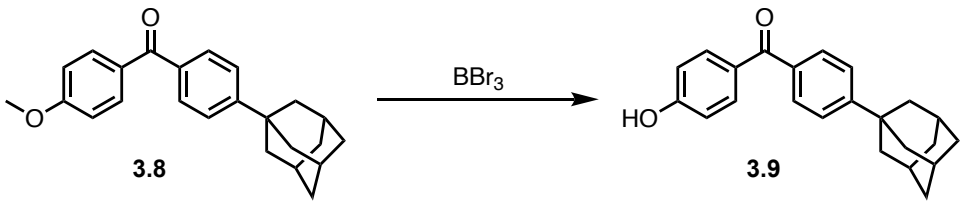

Synthesis of 3.9: A 100 mL one-neck round bottom flask was flame dried, flushed with argon and charged with a stir bar and compound **3.8** (1.8 g, 5.2 mmol). Was placed under argon atmosphere and the compound was fully dissolved in 10 mL dry DCM. The reaction was then placed in a -72 C bath and allowed to stir for a few minutes to cool. Then BBr_3 (15.60 mL, 15.60 mmol, 3 equiv) was slowly added to the reaction. The reaction was then relieved from the cold bath and allowed to warm to room temperature while stirring. Reaction was allowed to stir overnight. Product was washed with DI water and extracted in ethyl acetate. The organic layer was dried over magnesium sulfate, filtered, then concentrated under pressure to yield a pale pink oil. The crude product was purified using column chromatography. Utilizing a gradient solvent system composed of hexanes: ethyl acetate. Purified product was isolated as white powder ^{1}H NMR (500 MHz, CDCl3): δ = 1.41-1.95 (s, 15H), 6.95,9.97 (d, 2H), 7.45,7.46 (d, 2H), 7.72,7.73 (d, 2H), 7.82,7.84 (d, 2H); ^{13}C NMR (126 MHz, CDCl3) δ = 195.68, 159.69, 152.73, 135.72, 132.83, 130.52, 130.14, 126.73, 115.09, 44.69, 34.20, 26.77, 26.07. HRMS (DART) calcd for C23H24O2 [M+H]**+** 333.17606, found 332.17662.

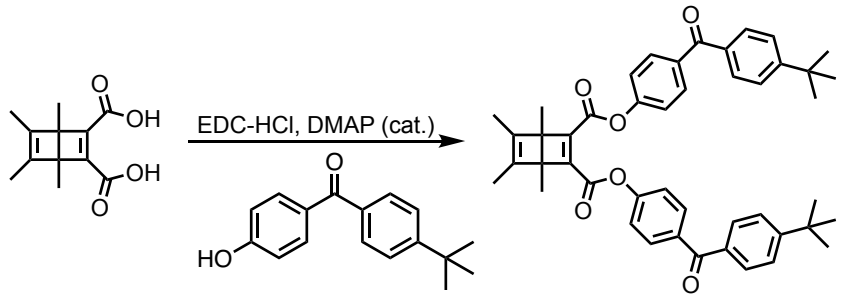

3.1

Synthesis of 3.1: A 25 mL 3-neck flask round bottom flask was flame dried and charged with DB-OH (0.050 g, 0.225 mmol, 1 equiv), 4-hydroxy-tbutyl-benzophenone (0.069g, 0.270 mmol, 1.2 equiv), a catalytic amount of 4-(dimethylamino)pyridine (0.003 g, 0.023 mmol, 0.1 equiv) and a stir bar. This was followed by the addition of 3 mL anhydrous DCM and 1-ethyl-3-(3-dimethylaminopropyl)carbodiimide hydrochloride (EDC·HCl) (0.108 g, 0.562 mmol, 2.5 equiv) stirring at 0 °C. The reaction was allowed to stir cold for at least 2 hours. The product was washed with brine and extracted in ethyl acetate. The organic layer was collected, dried with $MgSO_4$, then concentrated under pressure to give a brown/orange oil. The crude was subjected to column chromatography utilizing a gradient solvent system composed of hexanes: ethyl acetate. The purified product was isolated as a white. ^{1}H NMR (500 MHz, CDCl3): δ = 1.36 (s, 18H), 1.47 (s, 6H), 1.75 (s, 6H), 7.48 – 7.50 (d, 4H), 7.74 – 7.76 (m, 2H), 7.85, 7.86 (m, 4H), 7.87,7.88 (m, 4H ; ^{13}C NMR (126 MHz, CDCl3) δ = 195.21, 159.66, 156.37, 153.29, 1452.71, 143.46, 135.66, 131.64, 130.07, 125.34, 121.26, 57.07, 35.15, 31.15, 11.24, 10.04 m.p.: 137 °C

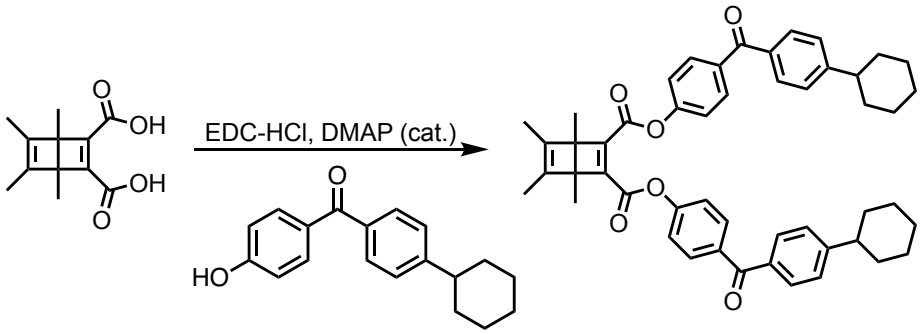

3.2

Synthesis of 3.2: A 25 mL 3-neck flask round bottom flask was flame dried and charged with DB-OH (0.050 g, 0.225 mmol, 1 equiv), 4-hydroxy-4-cyclohexyl-benzophenone (0.076g, 0.270 mmol, 1.2 equiv), a catalytic amount of 4-(dimethylamino)pyridine (0.003 g, 0.023 mmol, 0.1 equiv) and a stir bar. This was followed by the addition of 3 mL anhydrous DCM and 1-ethyl-3-(3-dimethylaminopropyl)carbodiimide hydrochloride (EDC·HCl) (0.108 g, 0.562 mmol, 2.5 equiv) stirring at 0 °C. The reaction was allowed to stir cold for at least 2 hours. The product was washed with brine and extracted in ethyl acetate. The organic layer was collected, dried with $MgSO_4$, then concentrated under pressure to give a brown/orange oil. The crude was subjected to column chromatography utilizing a gradient solvent system composed of hexanes: ethyl acetate. The purified product was isolated as a white. ^{1}H NMR (500 MHz, CDCl3): δ = 1.26-1.45 (m, 10H), 1.47 (s 6H), 1.76 (s, 6H), 2.57 – 2.61 (m, 2H), 7.30 – 7.32 (d, 8H), 7.73,7.75 (d, 4H), 7.85,7.86 (d, 4H ; ^{13}C NMR (126 MHz, CDCl3) δ = 195.26, 159.66, 153.33, 153.25, 152.71, 143.46, 135.72, 135.04, 131.62, 130.34, 126.88, 121.26, 57.06, 44.74, 34.16, 26.75, 26.06, 11.24 10.04. m.p.: 150 ^{o}C

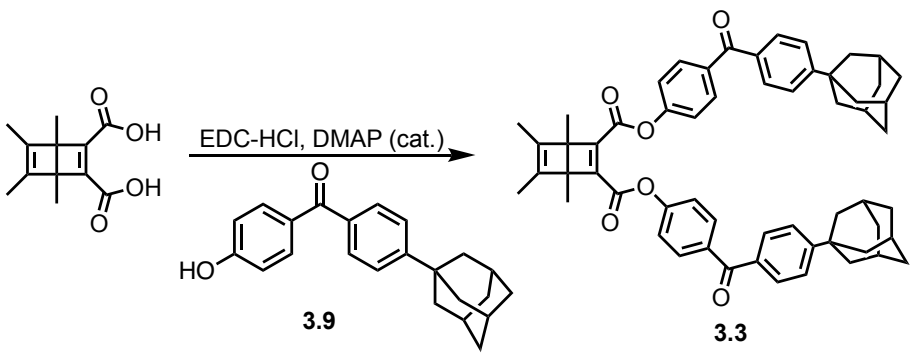

Synthesis of 3.3: A 25 mL 3-neck flask round bottom flask was flame dried and charged with compound **4** (0.050 g, 0.225 mmol, 1 equiv), 4-hydroxy-4-amantylbenzophenone (0.054g, 0.270 mmol, 1.2 equiv), a catalytic amount of 4-(dimethylamino)pyridine (0.003 g, 0.023 mmol, 0.1 equiv) and a stir bar. This was followed by the addition of 2 mL anhydrous DCM and 1-ethyl-3-(3-dimethylaminopropyl)carbodiimide hydrochloride (EDC·HCl) (0.108 g, 0.562 mmol, 2.5 equiv) stirring at 0 °C. The reaction was allowed to stir cold for at least 2 hours. The product was washed with brine and extracted in ethyl acetate. The organic layer was collected, dried with $MgSO_4$, then concentrated under pressure to give a brown/orange oil. The crude was subjected to column chromatography utilizing a gradient solvent system composed of hexanes: ethyl acetate. The purified product was isolated as a white. ^{1}H NMR (500 MHz, CDCl3): δ = 7.93 – 7.83 (m, 4H), 7.79 (dt, *J* = 8.4, 1.5 Hz, 4H), 7.64 – 7.56 (m, 2H), 7.54 – 7.45 (m, 4H), 7.35 – 7.29 (m, 4H), 1.75 (s, 6H), 1.47 (s, 6H ; ^{13}C NMR (126 MHz, CDCl3) δ = 195.50, 159.59, 153.45, 152.74, 143.44, 137.42, 135.32, 132.55, 131.74, 129.98, 128.37, 121.34, 57.06, 11.24, 10.04. Rf = 0.4 in hexanes: ethyl acetate (4:1). m.p.: 109 °C

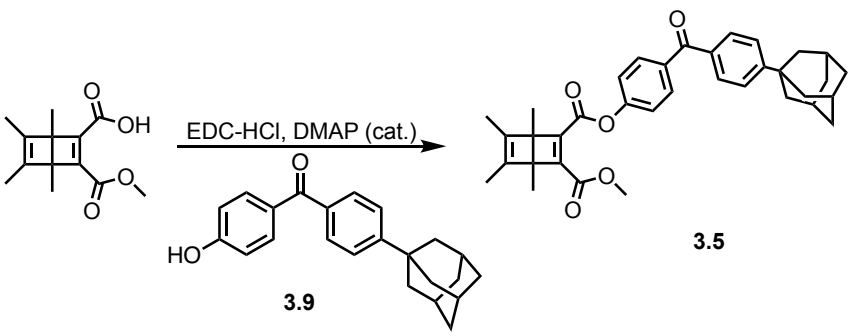

Synthesis of 3.5: A 25 mL 3-neck flask round bottom flask was flame dried and charged with compound **DB-OMe/OH** (0.050 g, 0.212 mmol, 1 equiv), 4-hydroxy-4-adamantylbenzophenone (0.084g, 0.254 mmol, 1.2 equiv), a catalytic amount of 4-(dimethylamino)pyridine (0.003 g, 0.021 mmol, 0.1 equiv) and a stir bar. This was followed by the addition of 2 mL anhydrous DCM and 1-ethyl-3-(3-dimethylaminopropyl)carbodiimide hydrochloride (EDC·HCl) (0.061 g, 0.317 mmol, 1.5 equiv) stirring at 0 °C. The reaction was allowed to stir cold for at least 2 hours. The product was washed with brine and extracted in ethyl acetate. The organic layer was collected, dried with $MgSO_4$, then concentrated under pressure to give a brown/orange oil. The crude was subjected to column chromatography utilizing a gradient solvent system composed of hexanes: ethyl acetate. The purified product was isolated as a white. ^{1}H NMR (500 MHz, CDCl3): δ = 7.93 – 7.83 (m, 4H), 7.79 (dt, *J* = 8.4, 1.5 Hz, 4H), 7.64 – 7.56 (m, 2H), 7.54 – 7.45 (m, 4H), 7.35 – 7.29 (m, 4H), 1.75 (s, 6H), 1.47 (s, 6H ; ^{13}C NMR (126 MHz, CDCl3) δ = 195.50, 159.59, 153.45, 152.74, 143.44, 137.42, 135.32, 132.55, 131.74, 129.98, 128.37, 121.34, 57.06, 11.24, 10.04. Rf = 0.4 in hexanes: ethyl acetate (4:1). m.p.: 109 ^{o}C

3.7.3 ^{1}H, ^{13}C-NMR Spectra

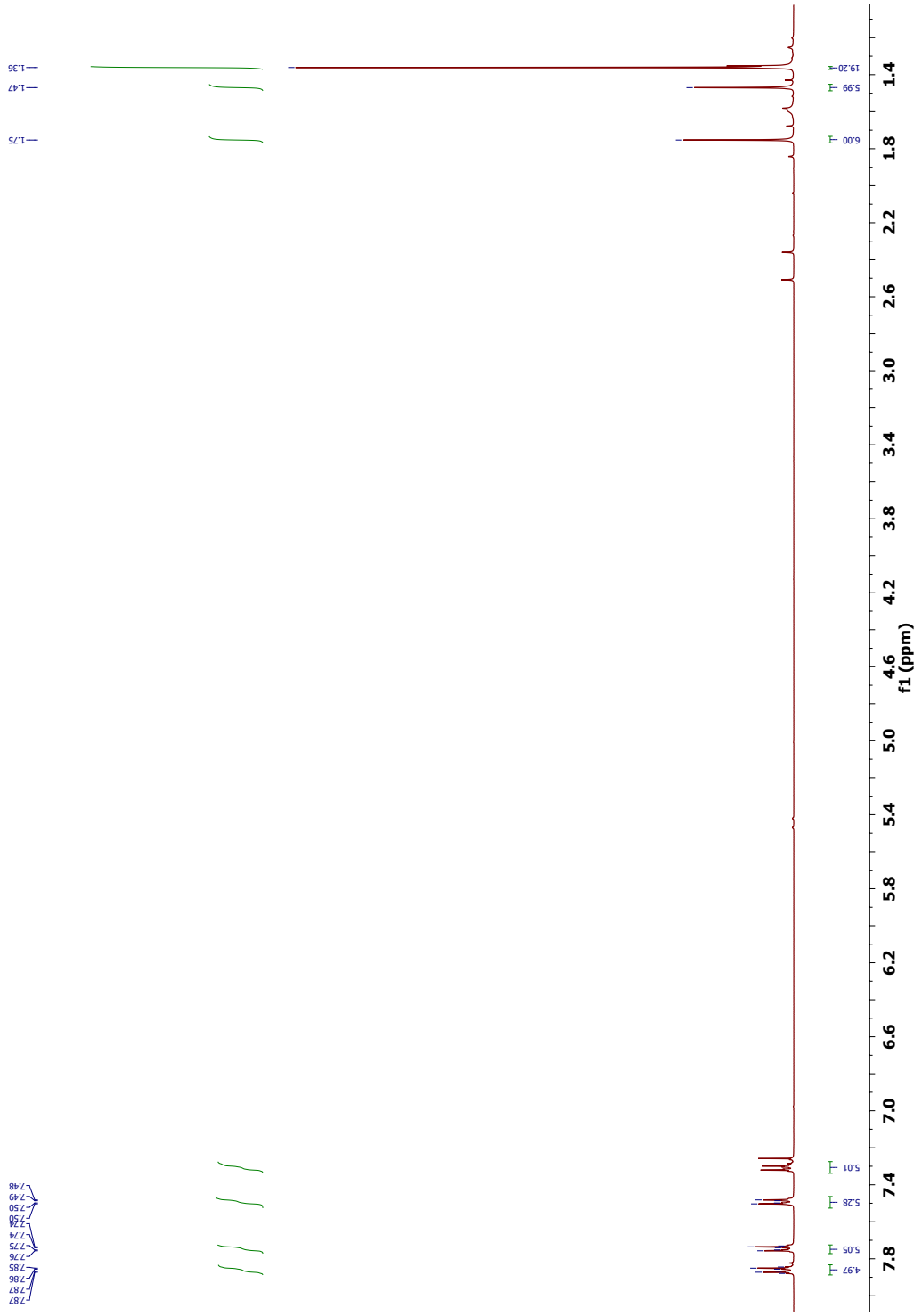

Figure 3.10 ^{1}H NMR of **3.1** in $CDCl_3$ at 500 MHz

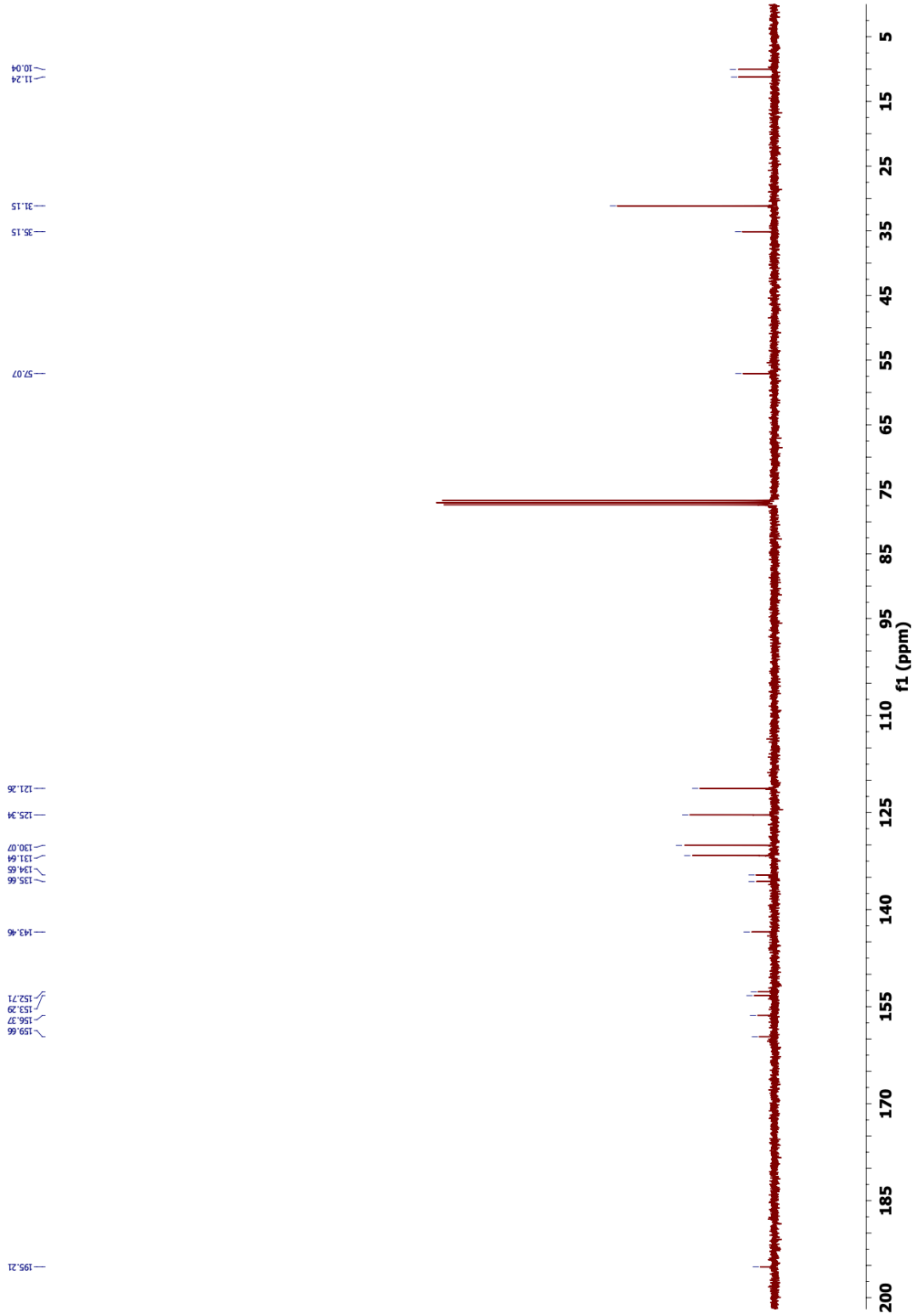

Figure 3.11 $^{13}C\{^{1}H\}$ NMR of **3.1** in $CDCl_3$ at 126 MHz

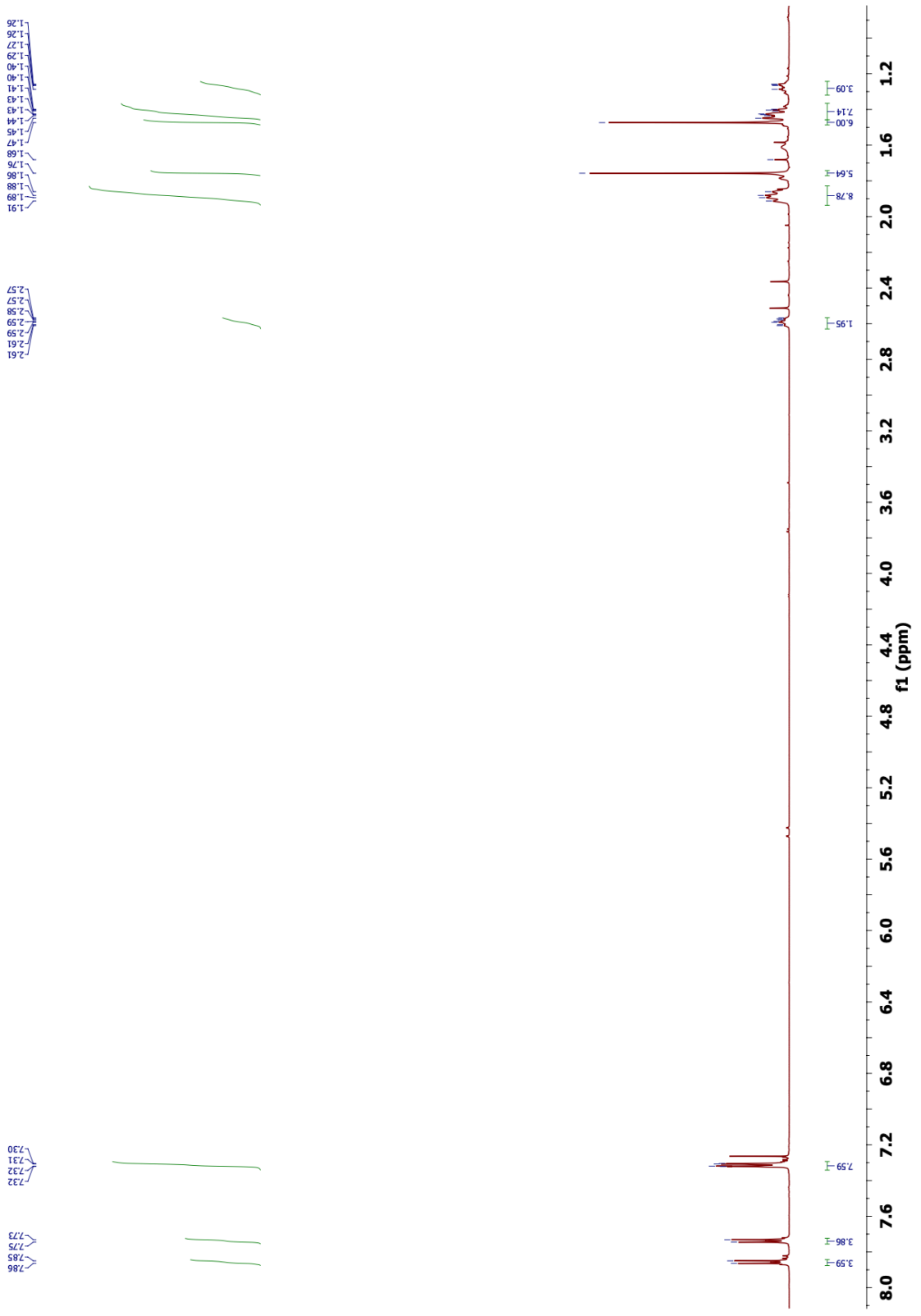

Figure 3.12 ^{1}H NMR of **3.2** in $CDCl_3$ at 500 MHz

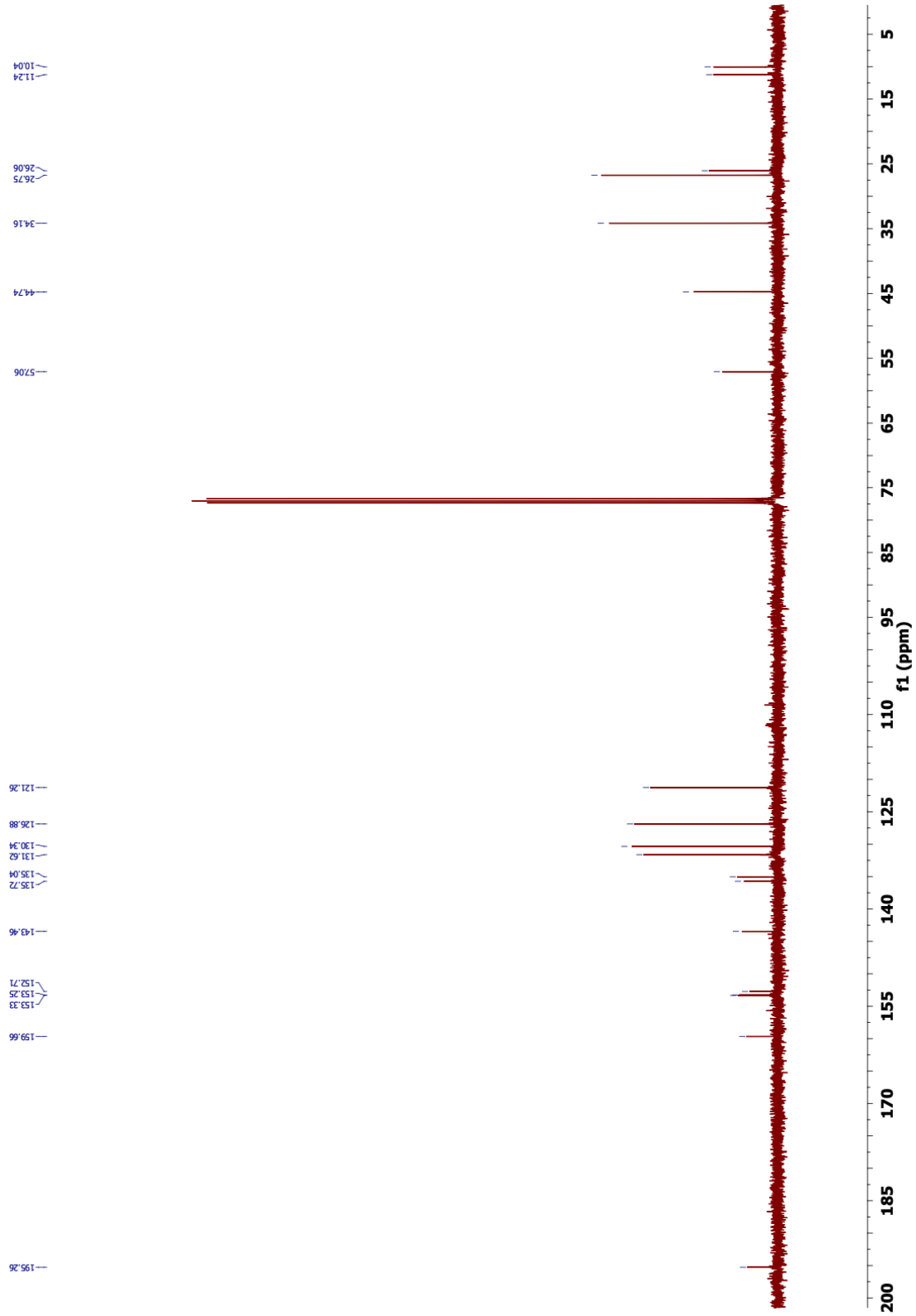

Figure 3.13 $^{13}C\{^{1}H\}$ NMR of **3.2** in $CDCl_3$ at 126 MHz

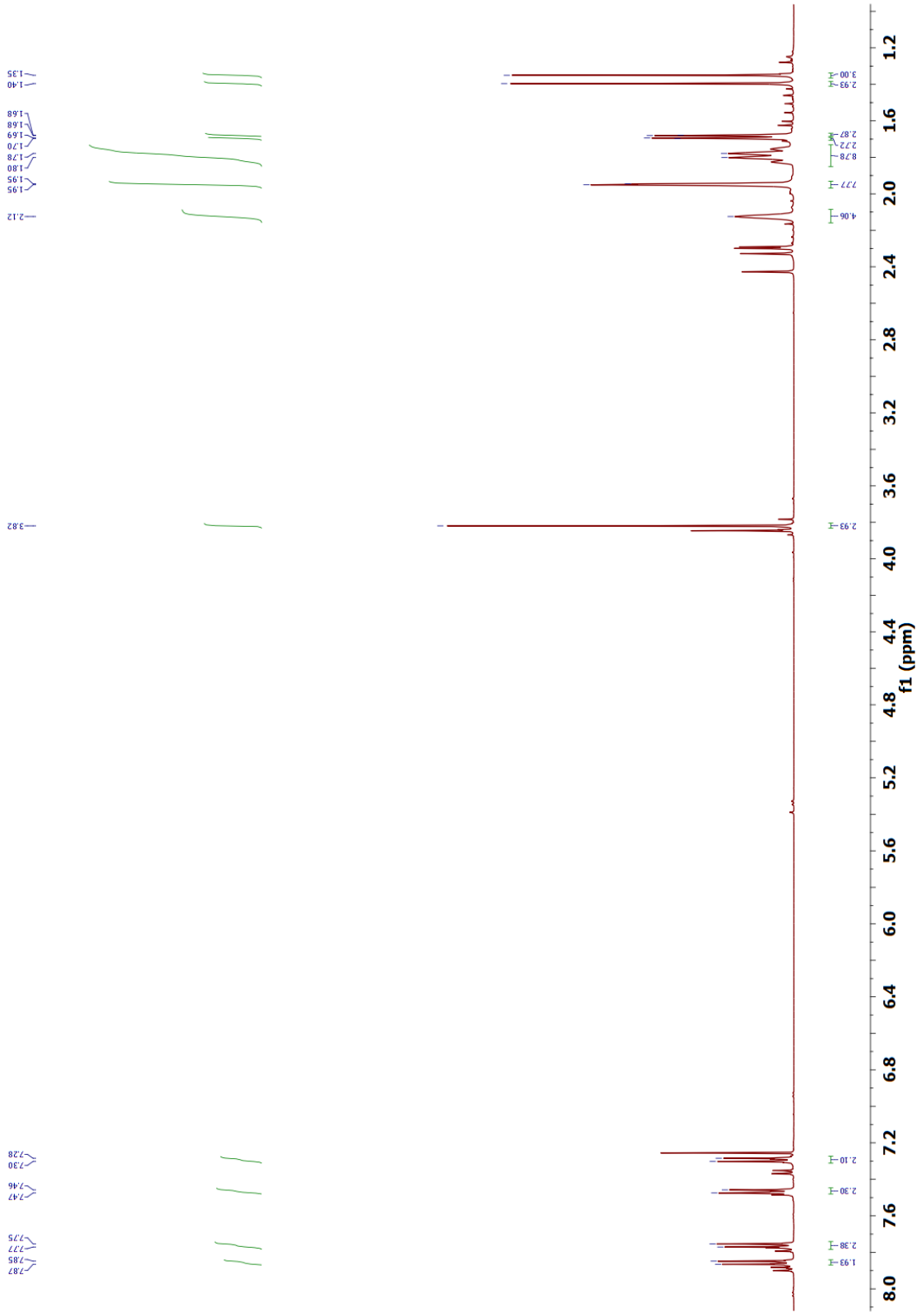

Figure 3.14 ^{1}H NMR of **3.5** in $CDCl_3$ at 500 MHz

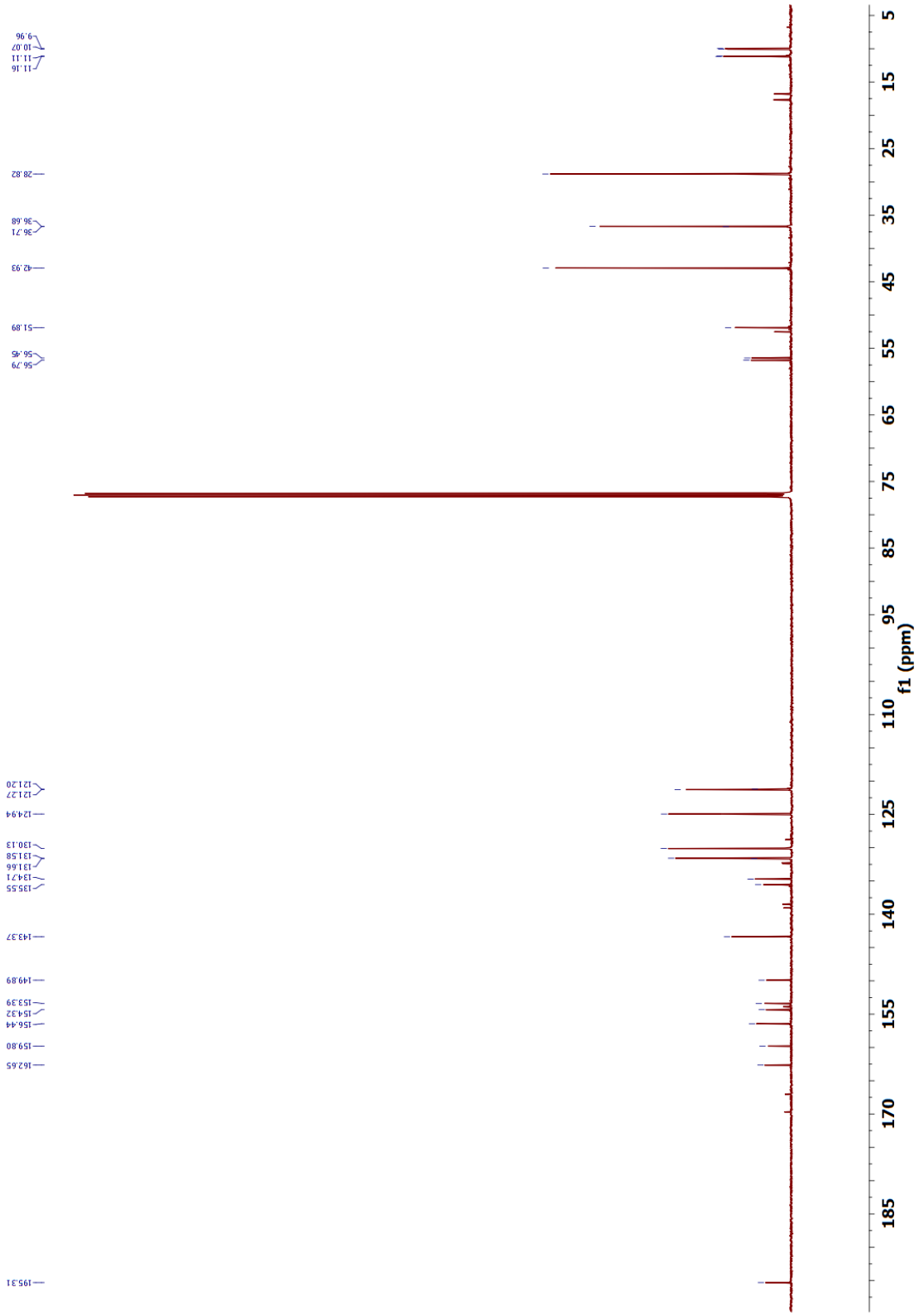

Figure 3.15 $^{13}C\{^{1}H\}$ NMR of **3.5** in $CDCl_3$ at 126 MHz

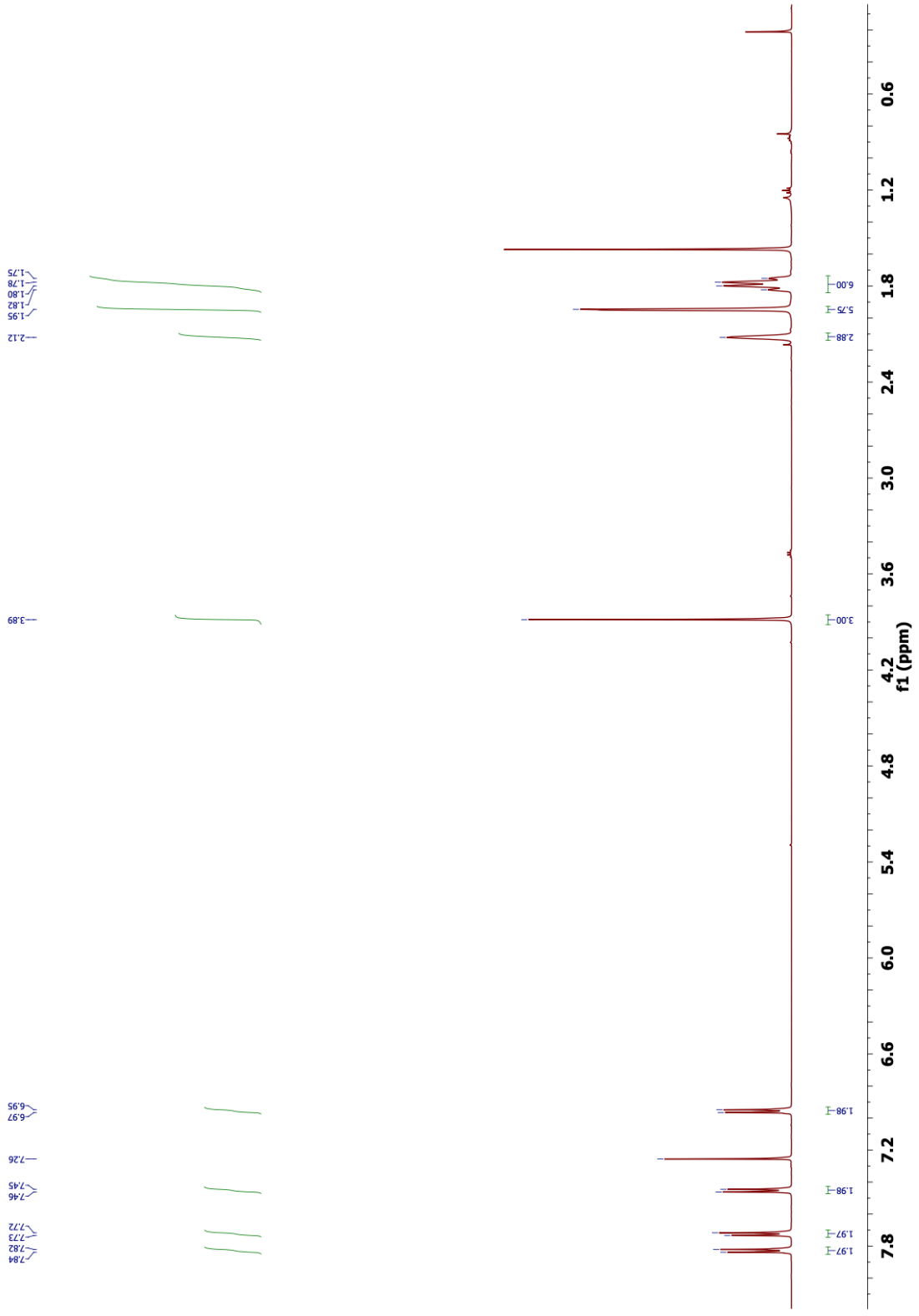

Figure 3.16 ^{1}H NMR of **3.8** in $CDCl_3$ at 500 MHz

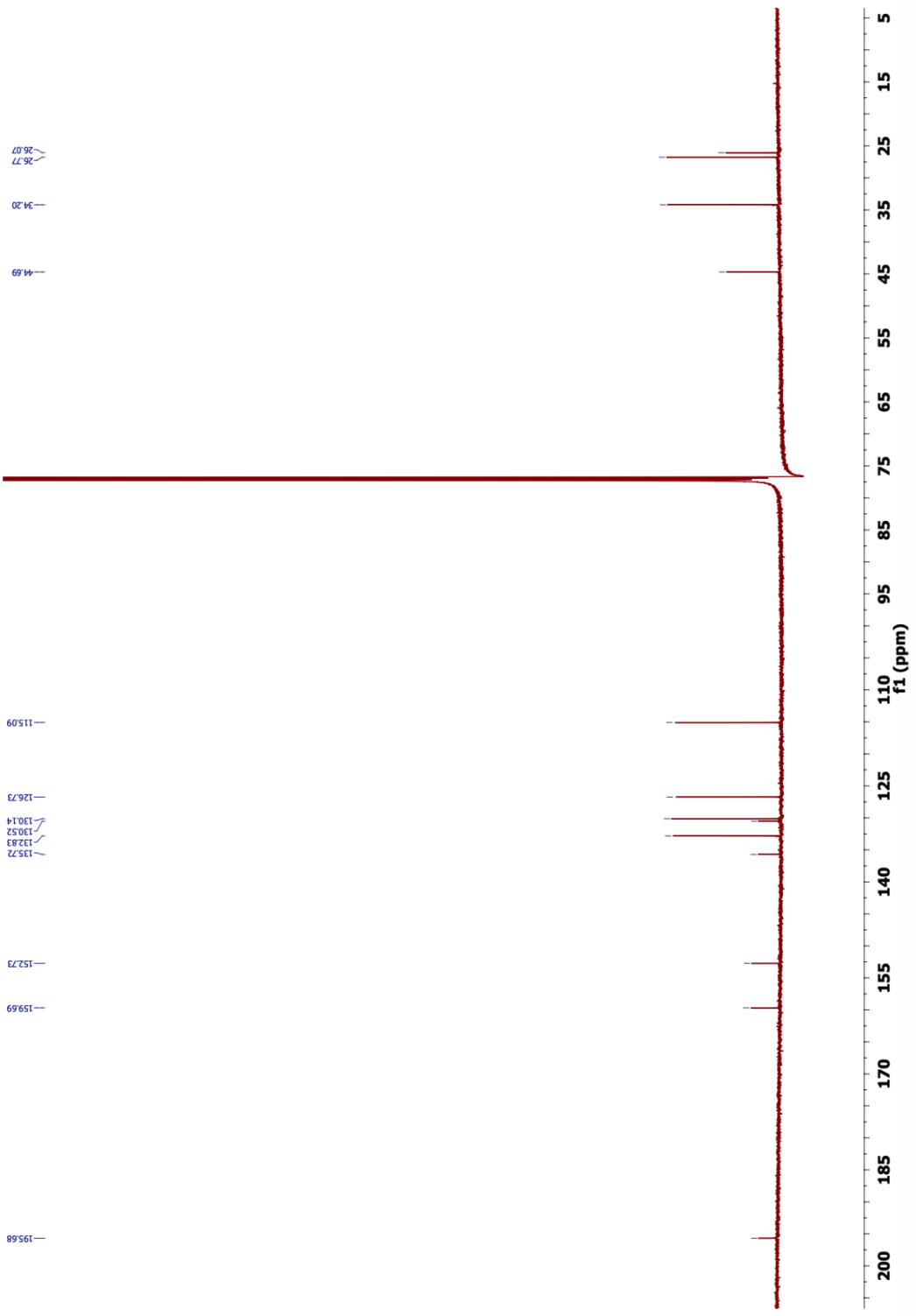

Figure 3.17 $^{13}C\{^{1}H\}$ NMR of **3.8** in $CDCl_3$ at 126 MHz

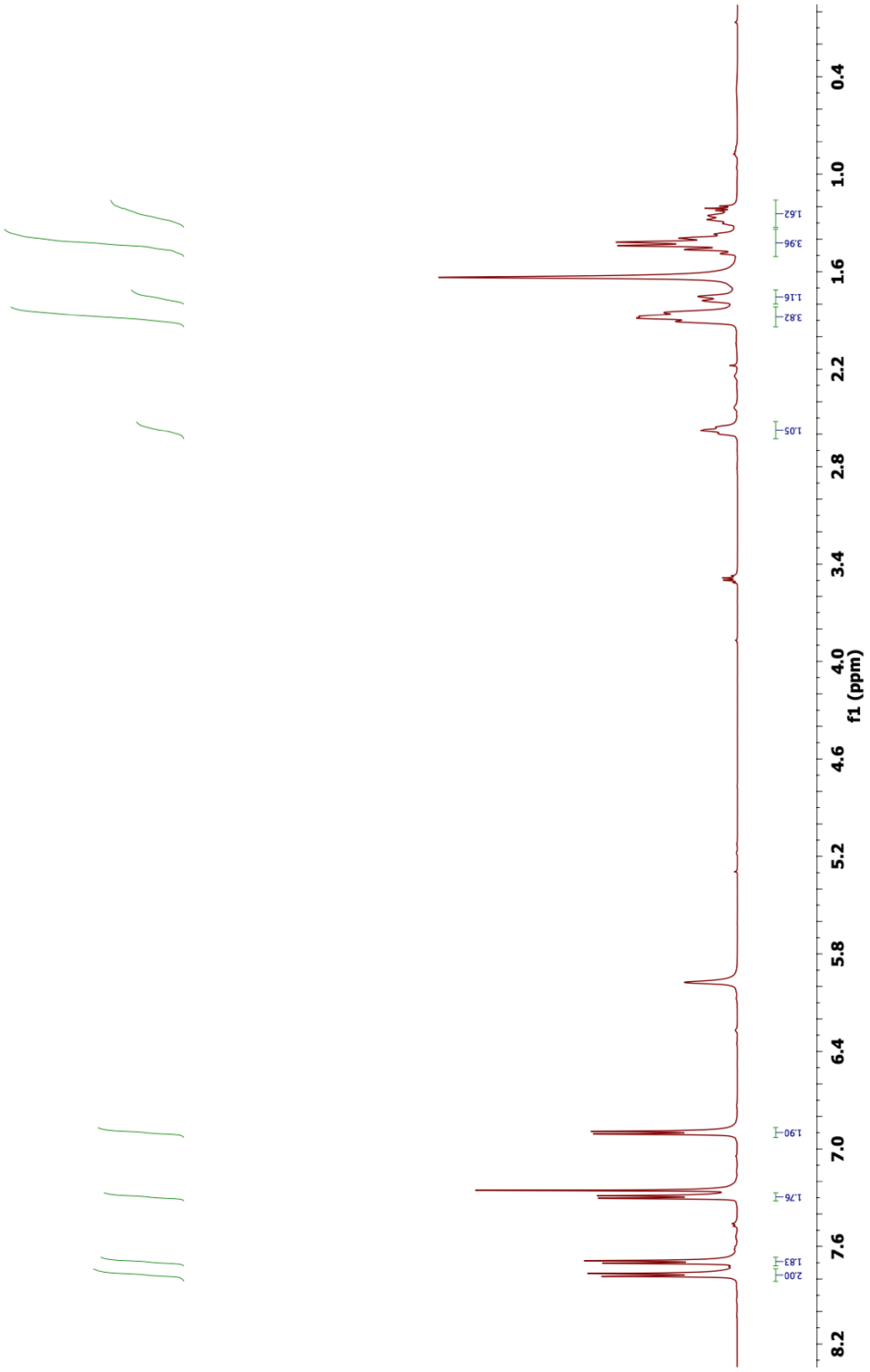

Figure 3.18 ^{1}H NMR of **3.9** in $CDCl_3$ at 500 MHz

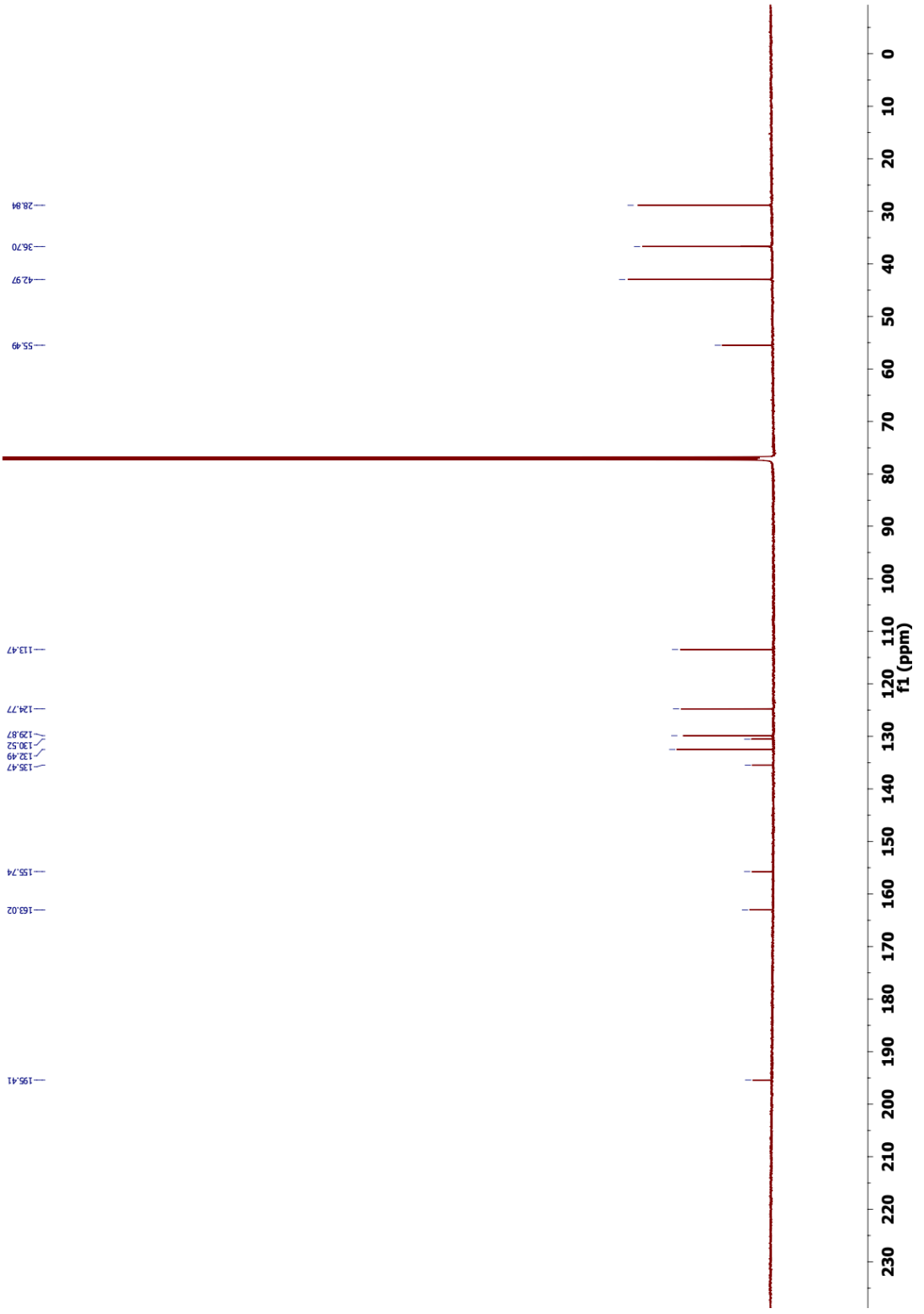

Figure 3.19 $^{13}C\{^{1}H\}$ NMR of **3.9** in $CDCl_3$ at 126 MHz

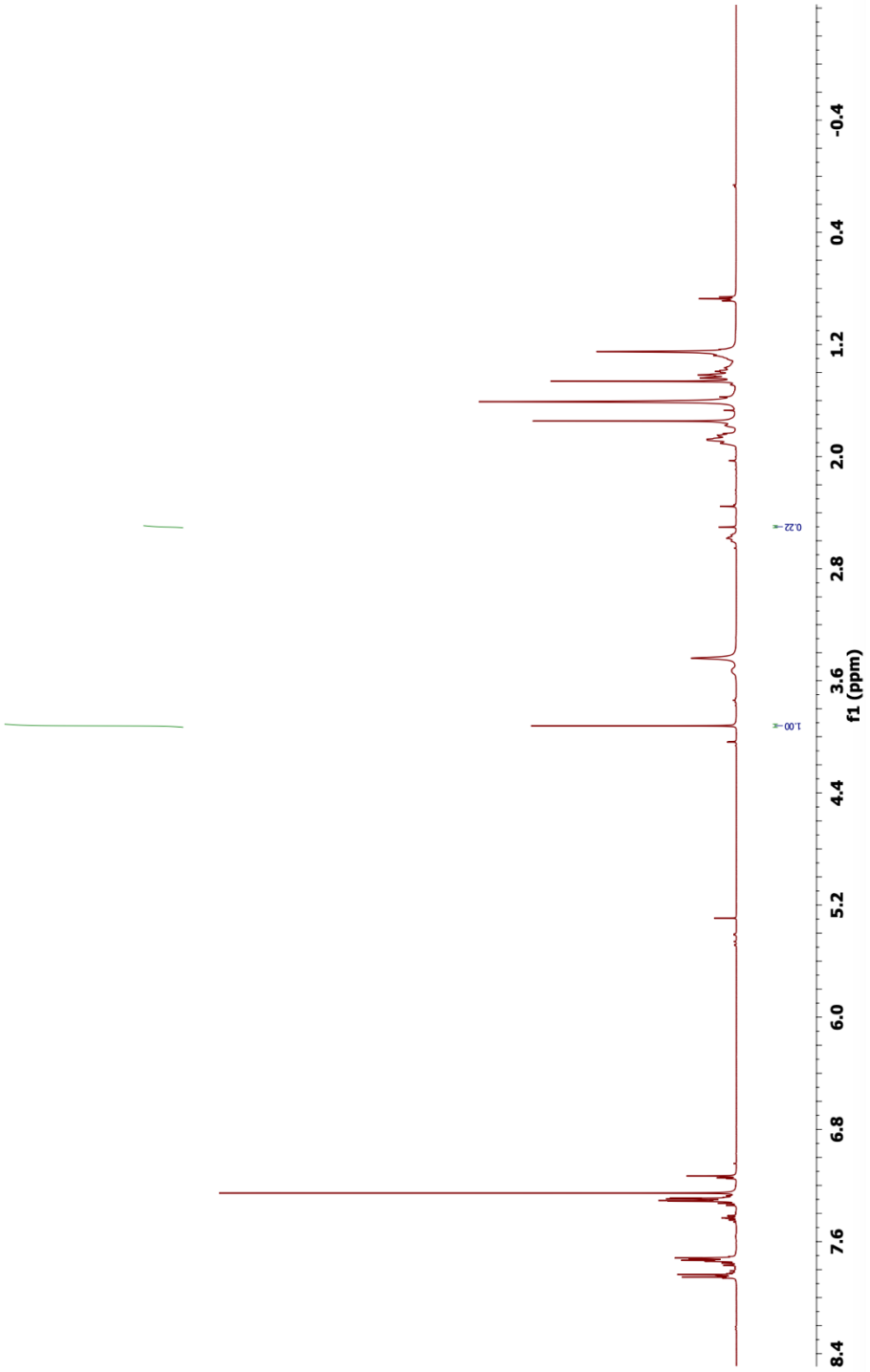

Figure 3.20 ^{1}H NMR of 6 second irradiation of **3.2** with 2-methoxynaphthalene in $CDCl_3$ at 500 MHz

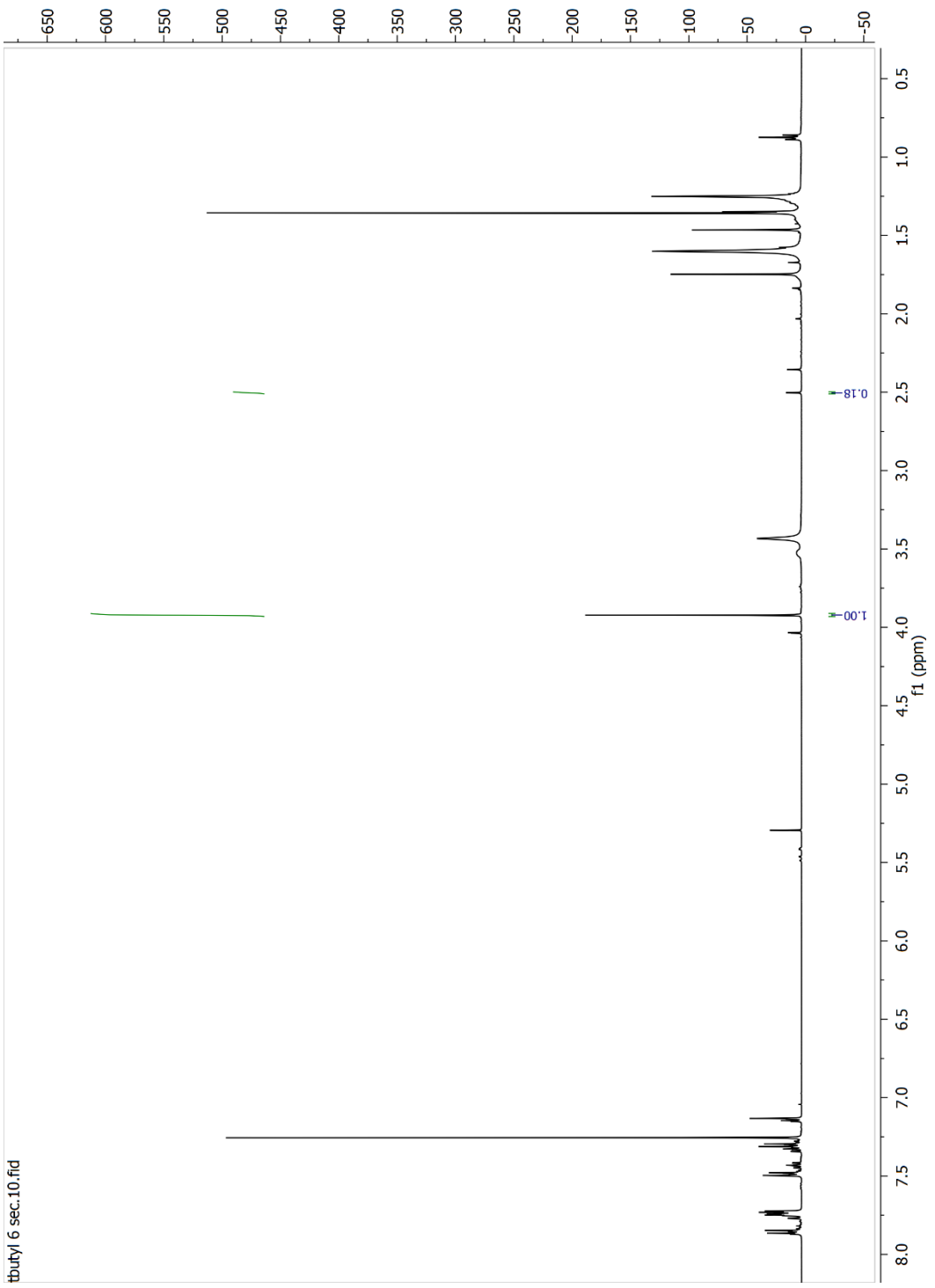

Figure 3.21 ^{1}H NMR of 6 second irradiation of **3.1** with 2-methoxynaphthalene in $CDCl_3$ at 500 MHz

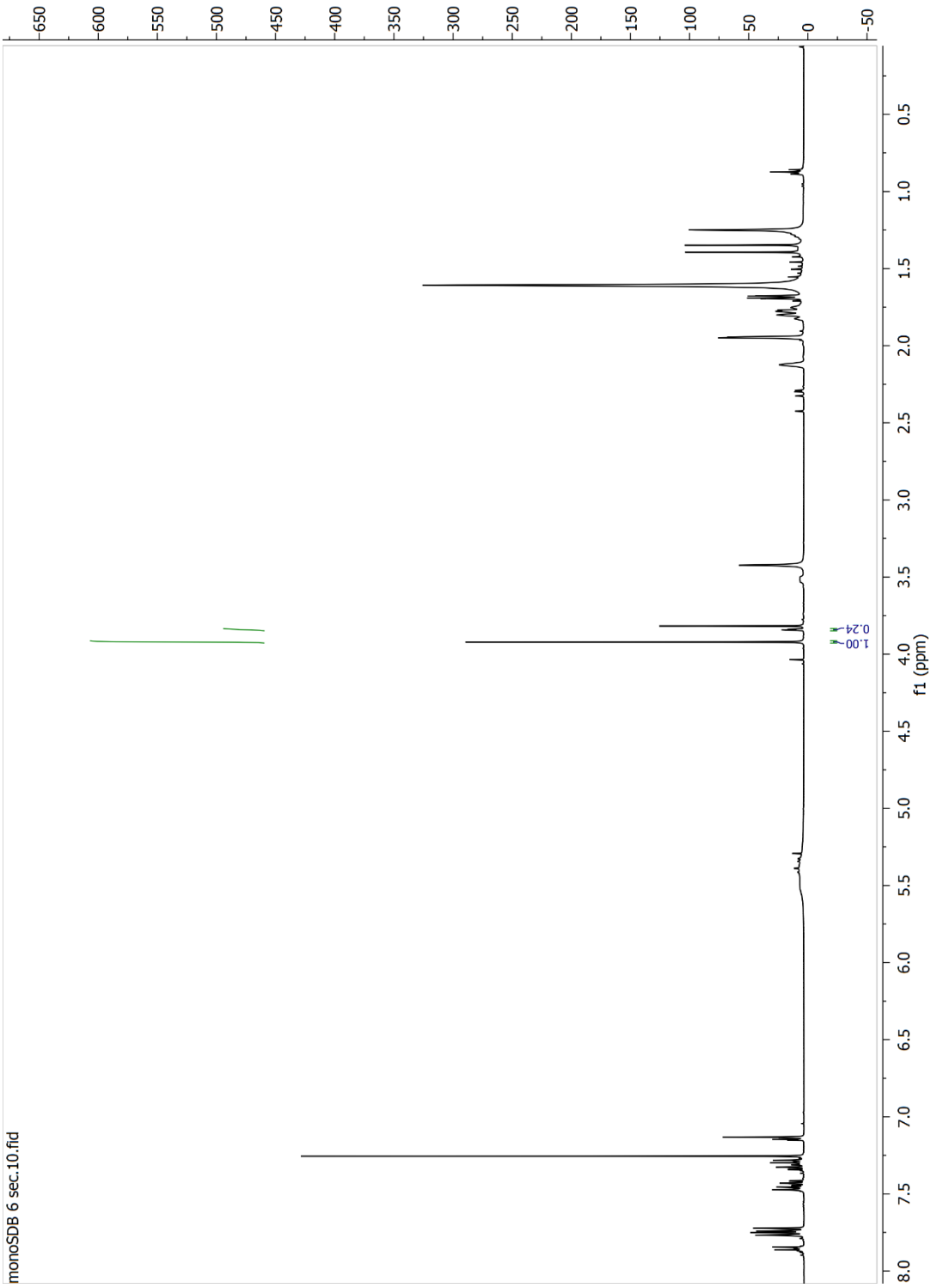

Figure 3.22 ^{1}H NMR of 6 second irradiation of **3.5** with 2-methoxynaphthalene in $CDCl_3$ at 500 MHz

3.7.4 IR Spectra

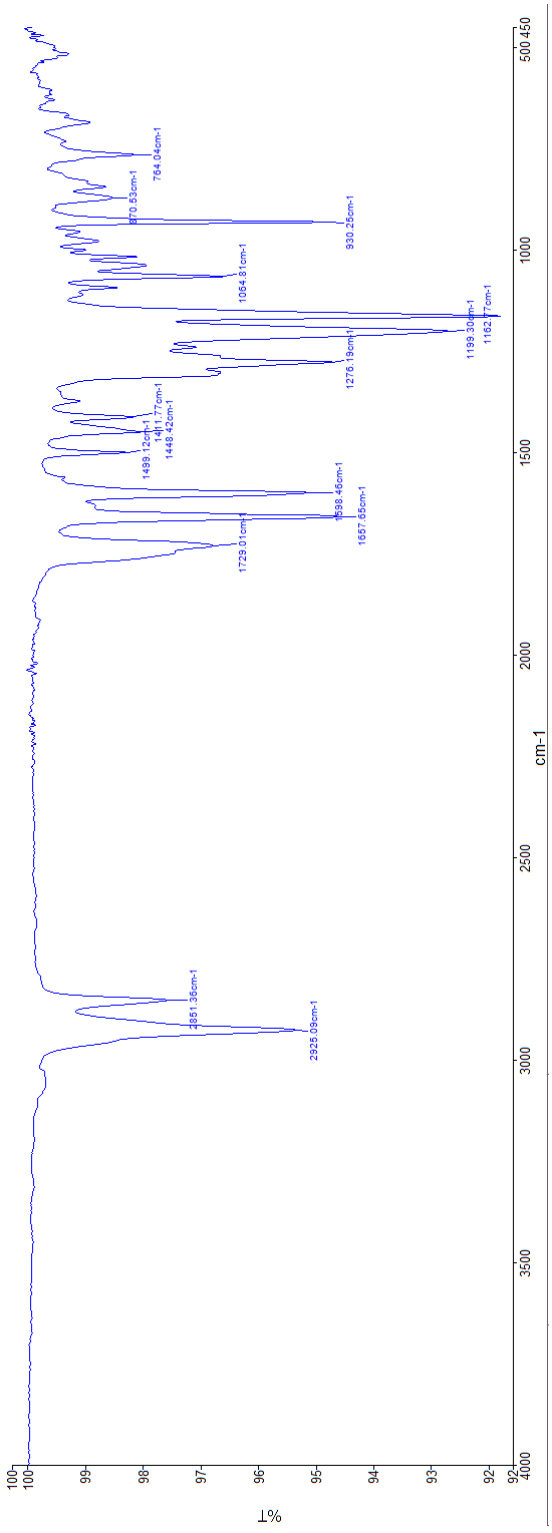

Figure 3.23 FTIR of **3.2**

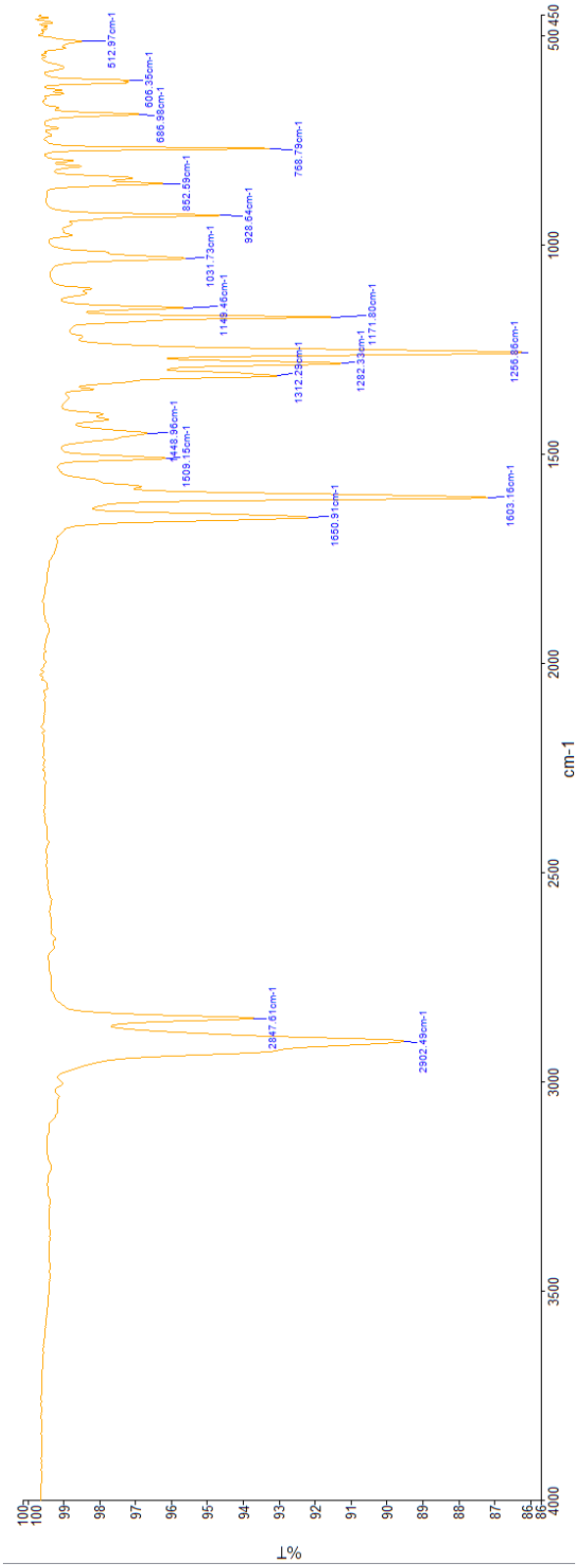

Figure 3.24 FTIR of **3.3**

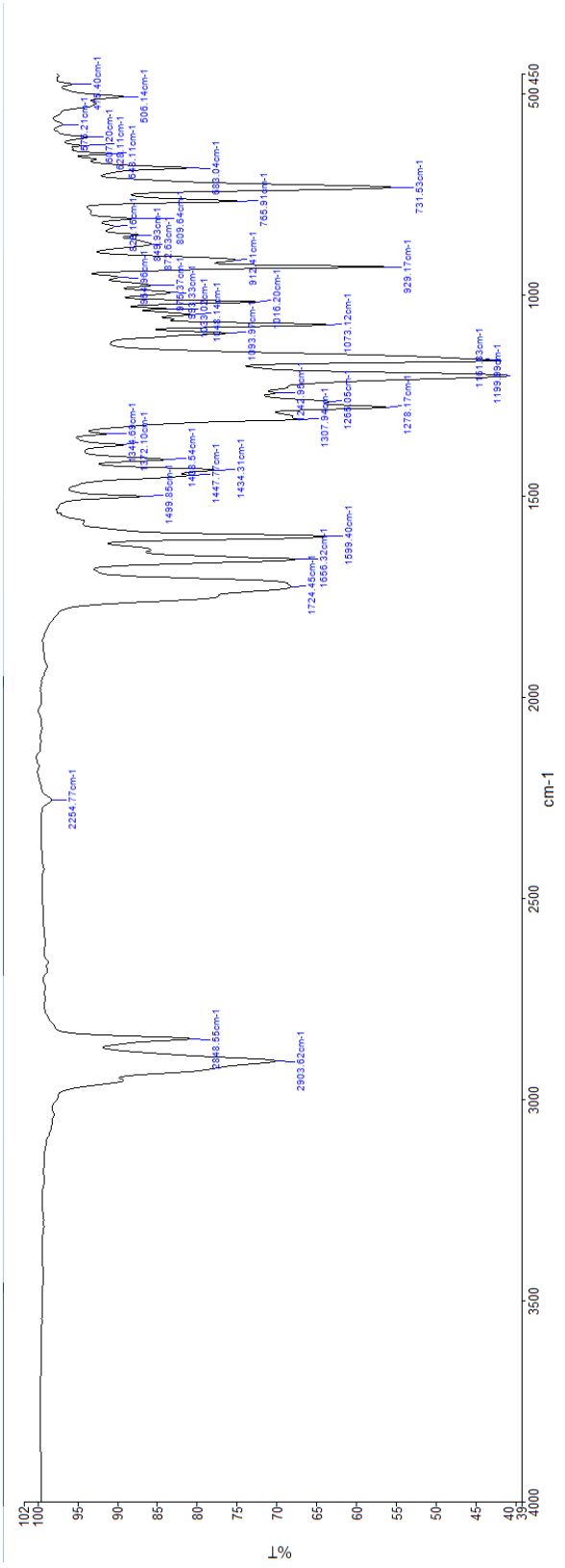

Figure 3.25 FTIR of **3.5**

3.7.5 pXRD

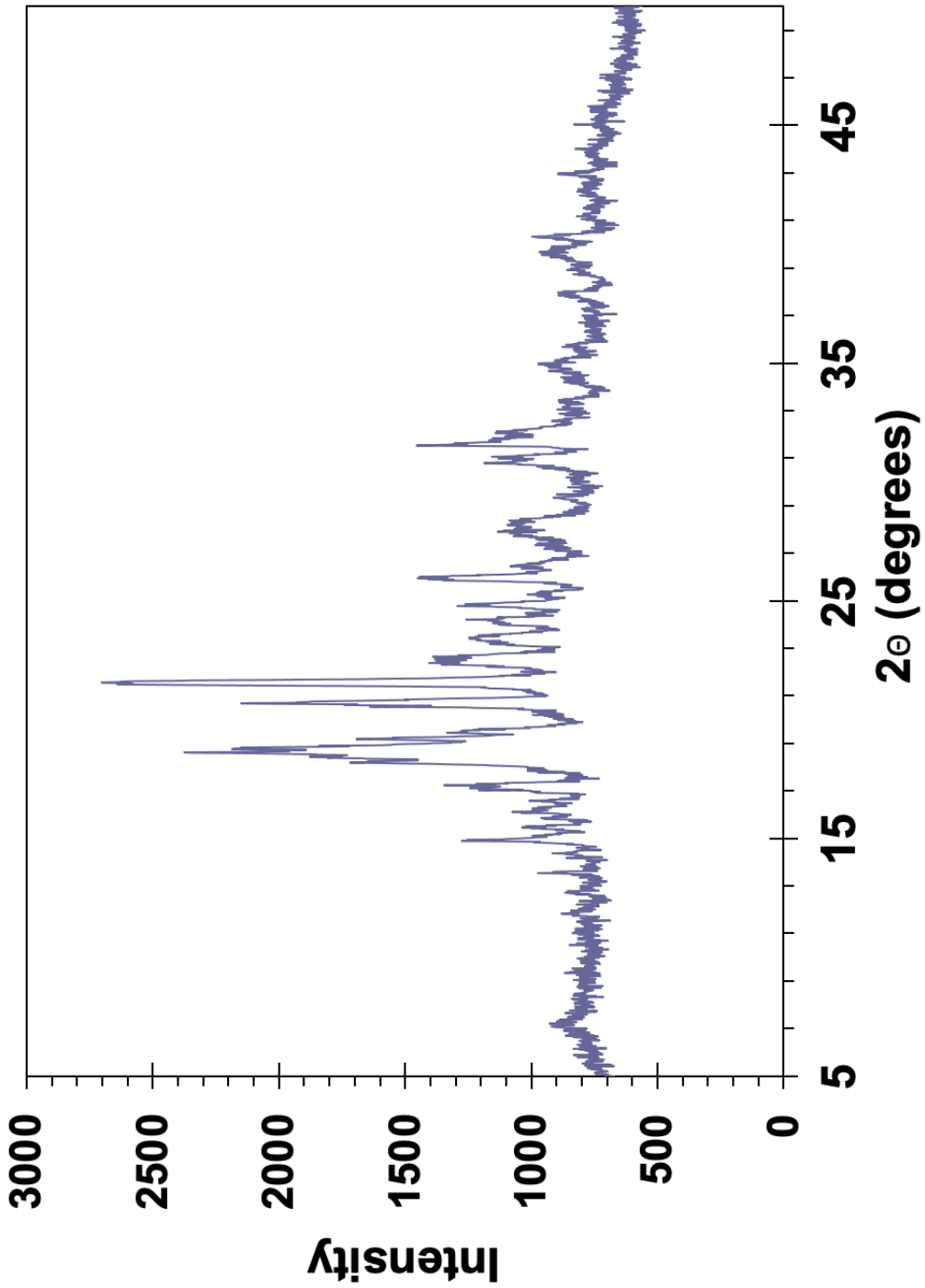

Figure 3.26 pXRD of **3.2**

3.7.6 Quantum Yield Measurements

Quantum yields were measured using the equation below:

Quantum yield: $\Phi_{DB\text{-}OBPh} = (A_{DB\text{-}OBPh}/A_{DCK})(mol_{HB\text{-}OBPh}/mol_{DC})\Phi_{DCK}$

$A_{DB\text{-}OBPh}$: Absorbance of DB-OBPh at given concentration

A_{DCK}: Absorbance of DCK at given concentration

$mol_{HB\text{-}OBPh}$: moles of DB-OBPh photoproduct

mol_{DC}: moles of DC photoproduct

Φ_{DCK}: Quantum yield of DCK (0.19 in nanocrystalline suspension)

Calibration curve details:

Mass IS = 0.0053g

Stock Conc. of IS (M) = (0.0053g/(158.2g/mol))/0.003L = 0.0115 M IS

Mass DC = 0.0056g

Stock Conc. of DC (M) = (0.0056g/(238.37g/mol))/0.003L = 0.00783 M DC

Table 3.1 2-naphthalene-dicumene signal and concentration for calibration curve

Sample #	IS signal	DC signal	ES/DC signal	[DC] M	[ES/DC]
1	9067695	11517613	0.787289432	0.000783096	1.584493458
2	8747473	2626678	3.330241849	0.000195774	6.337973833
3	8842462	619684	14.26930823	4.89435E-05	25.35189533
4	8547186	131272	65.11050338	1.22359E-05	101.4075913
5	8575641	32527	263.6468472	3.05897E-06	405.6303253
6	8292412	4509	1839.080062	7.64742E-07	1622.521301

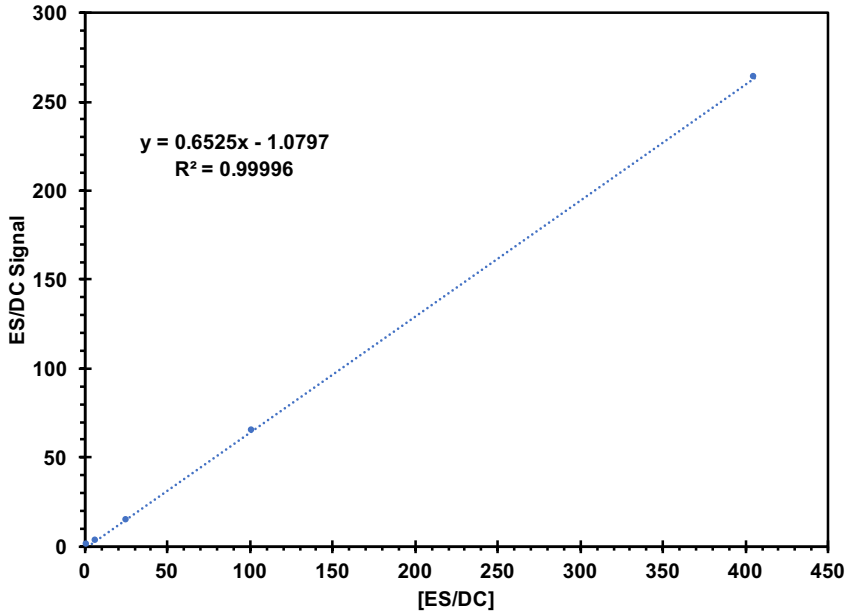

Figure 3.27 Standard curve for measure ES/DC signal as a function of ES/DC concentration

Determining mmol of DC:

ES/DC Signal = Slope*concentration + y-int

Slope = 0.6525

Y-int = -1.0797

In suspension

Suspensions of DB-OBPhs and DCK were made by the reprecipitation method (Kasai, H.; Nalwa, H. S.; Oikawa, H.; Okada, S.; Matsuda, H.; Minami, N.; Kakuta, A.; Ono, K.; Mukoh, A.; Nakanishi, H. *Jpn. J. Appl. Phys. 2,* **1992**, *31*, L1132-L1134.). Stock solutions **3.1** (56mg/mL), **3.2** (62mg/mL), 3.5 (76 mg/mL) and **DCK** (32.5 mg/mL) were made in THF and acetonitrile. A 30 uL aliquot of 3.1, 3.2, and 3.5 stock solution were added to individual 3 mL vortexting 0.50 mM CTAB solution and all samples were optically dense at A = 2.01, 2.07, and 2.08, respectively. A 20 uL aliquot of **DCK** stock solution was added to 3 mL vortexting 4.2 mM SDS solution with A = 2.17. Optically dense suspensions of **DB-OBPh**s and **DCK** were added into separate Pyrex tubes since the conversion rate of **DB-OBPh**s were much greater than that of **DCK**. The conversion rate of **DB-OBPh**s in suspension was so fast that **DB-OBPh** suspension samples were irradiated behind a 5x5 cm neutral density filter (2 OD, 1% T). Suspensions were irradiated within the black box setup (shown below) in the Rayonet photochemical reactor containing four 12 inch 8W (BLE-8T312) 312 nm bulbs. Samples were irradiated for 4, 5, and 6 seconds in triplicate.

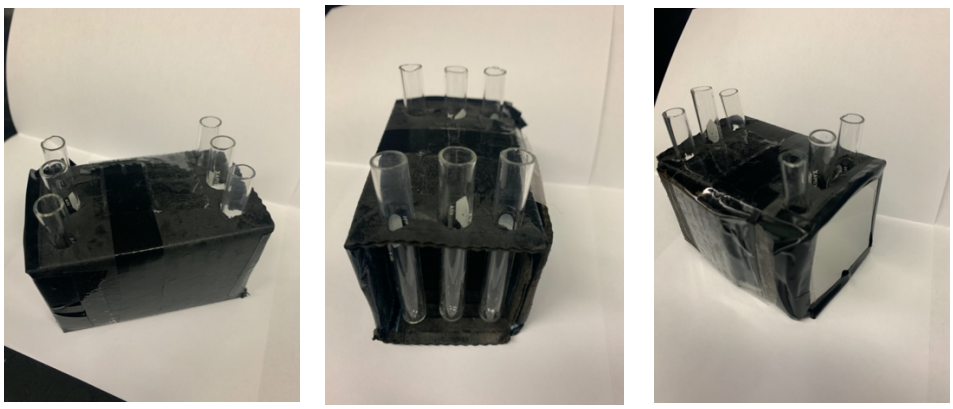

Figure 3.28 Suspension setup for irradiation. There Is a divider in the middle of the black box that does not allow light to travel through from either side.

Quantum yields for suspensions were calculated similarly to the solution protocol described above. Below is an example calculation for samples 3.1, 3.2, 3.5, and DCK suspensions based on ^{1}H NMR and GC-MS integrations

Table 3.2 Quantum yields for **3.1**

Time (sec)	4	5	6
NMR Integration	0.14	0.16	0.20
% Conversion	13	15	22
ES Integration	1	1	1
ES Protons	3	3	3
DB-OBPh tbutyl Protons	6	6	6
rA/ES	0.070	0.080	0.100
nES (mmol)	2.09×10^{-3}	2.09×10^{-3}	2.09×10^{-3}
nES*(rA/ES)	1.46×10^{-4}	1.67×10^{-4}	2.09×10^{-4}
Quantum Yields	~192	~220	~275

Table 3.3 Quantum yields for **3.2**

Time (sec)	4	5	6
NMR Integration	0.15	0.18	0.22
% Conversion	13	15	22
ES Integration	1	1	1
ES Protons	3	3	3
DB-OBPh Cyclohexyl Protons	6	6	6
rA/ES	0.075	0.090	0.110
nES (mmol)	2.09×10^{-3}	2.09×10^{-3}	2.09×10^{-3}
nES*(rA/ES)	1.56×10^{-4}	1.88×10^{-4}	1.24×10^{-4}
Quantum Yields	~234	~281	~343

Table 3.4 Quantum yield of **3.5**

Time (sec)	4	5	6
NMR Integration	0.20	0.19	0.24
% Conversion	27	28	34
ES Integration	1	1	1
ES Protons	3	3	3
monoDB-OBPh Adamantyl Protons	3	3	3
rA/ES	0.20	0.19	0.24
nES (mmol)	2.09×10^{-3}	2.09×10^{-3}	2.09×10^{-3}
nES*(rA/ES)	4.17×10^{-4}	3.96×10^{-4}	5.00×10^{-4}
Quantum Yields	~479	~455	~575

Integrations and product moles for 32.5mg/mL loading of DCK

ES mass = 0.011g

Stock conc (M) = (0.011g/(158.2g/mol))/0.003L = 2.32×10^{-2} mol/L

Conc in GC vial (M) = (2.32×10^{-2} mol/L)*($90 \times 10^{-6}/2 \times 10^{-3}$) = 1.04×10^{-3} mol/L

ES mass in GC vial = (1.04×10^{-3} mol/L)*0.002L*158.2g/mol = 3.3×10^{-4} g

Table 3.5 Calculating mmol of DCK photoproduct dicumene (DC)

Time (sec)	ES Integration	DC Integration	mmol DC
4	1.95×10^{7}	2.04×10^{5}	1.41×10^{-5}
5	2.30×10^{7}	2.17×10^{5}	1.27×10^{-5}
5	1.76×10^{7}	2.19×10^{5}	1.67×10^{-5}

3.8 References

1) Hyndman, H.L.; Monroe, B.M.; Hammond, G.S. "Mechanisms of photochemical reactions in solution. LX. Photochemical isomerization of 2,4-hexadiene via a quantum-chain mechanism", *J. Am. Chem. Soc.*, **1969**, *91*, 2852-2859.

2) Saltiel, J.; Townsend, D. E.; Sykes, A. Quantum chain process in the sensitized cis-trans photoisomerization of 1,3 dienes *J. Am. Chem. Soc*. **1973**, *95*, 5968-5973.

3) Saltiel, J.; D'Agostino, J.; Megarity, E. D.; Metts, L.; Neuberger, K. R.; Wrighton, M.; Zafiriou, O. C. The cis-trans photoisomerization of olefins, Org. Photochem. **1973**, *3*, 1-113.

4) Yee, W. A.; Hug, S.J.; Kliger, D.S. Direct and sensitized photoisomerization of 1,4-diphenylbutadienes *J. Am. Chem. Soc*. **1988**, *110*, 2164-2169.

5) Ganapathy, S.; Liu, R.S.H. Photoisomerization of polyenes. 30. Quantum chain processes in photoisomerization of the all-trans, 7-cis, and 11-cis isomers of retinal *J. Am. Chem. Soc.* **1992**, *114*, 3459-3464.

6) Sundahl, M.; Wennerstrom, O. Catalysis of a photochemical reaction; a cis-trans isomerization proceeding by a quantum chain process *J. Photochem. and Photobio. A.* **1996**, 98, 117-120.

7) Brink, M.; Jonson, H.; Sundahl, M. Catalysis of triplet state cis-trans isomerizations making a quantum chain process more efficient *J. Photochem and Photobio. A.* **1998**, 112, 149-153.

8) Whitten, D. G.; Mercer-Smith, J. A. Photosensitization o Stilbene Isomeriation by Palladium and Platinum Porphyrins, an Intermolecular Quantum Chain Process *J. Am. Chem. Soc.* **1978**, *110*, 2620-2625.

9) Gopal, V. R.; Reddy, M.A.; Rao, V. J. Wavelength Dependent Trans to Cis and Quantum Chain Isomerizations of Anthrylethylene Derivatives *J. Org. Chem.* **1995**, *60*, 7966-7973.

10) Saltiel, J.; Wang, S.; Ko, D.; Gormin, D. A. Cis-Trans Photoisomerization of the 1,6-Diphenyl-1,3,5-hexatrienes in the Triplet State. The Quantum Chain Mechanism and the Structure of the Triplet State *J. Phys. Chem. A.* **1998**, *102*, 5383-5392.

11) Crandall, J. K.; Mayer, C. F. Benzene-photosensitized transformations of the four geometrical isomers of 1,5,9-cyclododecatriene *J. Am. Chem. Soc.*, **1967**, *89*, 4374-4380.

12) Kazakov, V. P.; Voloshin, A. I.; Shavaleev. Chemiluminescence in visible and infrared spectral regions and quantum chain reactions upon thermal and photochemical decomposition of adamantylideneadamantane-1,2-dioxetane in the presence of chelates $Pr(dpm)_3$ and $Pr(fod)_3$ *J. Photochem and Photobio*. **1998**, *11*, 177-186.

13) Lechtken, P.; Yekta, A.; Turro, N. J. Tetramethyl-1,2-dioxetane. Mechanism for an autocatalytic decomposition. Evidence for a quantum chain reaction. *J. Am. Chem. Soc.* **1973**, *95*, 3027-3028.

14) Turro, N. J.; Schore, N. E.; Yekta. Quantum chain processes. Novel procedure for measurement of quenching parameters. Evidence that exothermic triplet-triplet energy

transfer is not diffusion limited and an estimation of the efficiency of exothermic quenching in a solvent cage *J. Am. Chem. Soc*. **1974**, *96*, 1936-1938.

15) Turro, N.J.; Waddell, W. H. Quantum chain processes. Direct observation of high quantum yields in the direct and photosensitized excitation of tetramethyl-1,2-dioxetane *Tetrahedron Letters.* **1975**, *25*, 2069-2072.

16) Schuster, G. B.; Turro, N. J.; Steinmetzer, H.; Schaap, A. P.; Faler, G.; Adam, W.; Liu, J. C. Adamantylideneadamantane-1,2-dioxetane. Chemiluminescence and decomposition kinetics of an unusually stable 1,2-dioxetane *J. Am. Chem. Soc.* **1975**, *97*, 7110-7117.

17) Wilson, T.; Schaap, A. P. Chemiluminescence from cis-diethoxy-1,2-dioxetane. Unexpected effect of oxygen *J. Am. Chem. Soc.* **1971**, *93*, 4126-4136.

18) Turro, N. J.; Lechtken, P.; Schore, N. E.; Schuster, G.; Steinmetzer, H.; Yekta, A. Tetramethyl-1,2-dioxetane. Experiments in chemiexcitation, chemiluminescence, photochemistry, chemical dynamics, and spectroscopy *Acc. Chem. Res.* **1974**, *7*, 97-105.

19) Turro, N. J.; Ramamurthy, V.; Katz, T. J. Energy storage and release. Direct and sensitized photoreactions of Dewar benzene and prismane *Nouveau Journal de Chimie* **1978**, *1*, 363–365.

20) Merkel, P. B.; Roh, Y.; Dinnocenzo, J. P.; Robello, D. R.; Farid, S. Highly Efficient Triplet Chain Isomerization of Dewar Benzenes: Adiabatic rate Constants from Cage Kinetics *J. Phys. Chem. A* **2007**, *111*, 1188–1199.

21) Ferrar, L.; Mis, M.; Dinnocenzo, J. P.; Farid, S.; Merkel, P. B.; Robello, D. R. *J. Org. Chem.* **2008**, *73*, 5683–5692.

22) Hochstrasser R. M. Transfer of Triplet Excitation Energy in Benzophenone Crystals *J. Chem. Phys.* **1963**, *39*, 3153-3154.

23) Nieman, G. C.; Robinson, G. W. Rapid Triplet Excitation Migration in Organic Crystals *J. Chem. Phys.* **1962**, *37*, 2150-2151.

24) Avakian, P.; Merrifield, R. E. Triplet Excitons in Anthracene Crystals - A Review *Molecular Crystals.* **1968**, *5*, 37-77.

25) Katoh, R.; Tamaki, Y.; Furube, A. Transient absorption microscopic study of triplet excitons in organic crystals *J. Photochem. and Photobio. A* **2006**, *183*, 267-272.

26) Jortner, J.; Rice, S. A.; Katz, J. L. Triplet Excitons in Crystals of Aromatic Molecules *J. Chem. Phys.* **1965**, *42*, 309-323.

27) Kepler, R. G.; Caris, J. C.; Avakian, P. Triplet excitons and Delayed Fluorescence in Anthracene Crystals *Phys. Rev. Lett.*, **1963**, *10*, 400-404.

28) Avakian, P.; Merrifield, R. E. Experimental Determination of the diffusion Length of Triplet Excitons in Anthracene Crystals *Phys. Rev. Lett.* **1964**, *13*, 541-545.

29) Kuzmanich, G.; Natarajan, A.; Chin, K. K.; Veerman, M.; Mortko, C. J.; Garcia-Garibay, M. A. Solid-state photodecar-bonylation of diphenylcyclopropenone: a quantum chain process made possible by ultrafast energy transfer *J. Am. Chem. Soc.* **2008***, 130,* 1140-1141.

30) Kuzmanich, G.; Gard, M. N.; Garcia-Garibay, M. A. Photonic amplification by a singlet-state quantum chain reaction in the photodecarbonylation of crystalline diarylcyclopropenones. *J. Am. Chem. Soc.* **2009***, 131,* 11606–11614.

31) Kuzmanich, G.; Simoncelli, S.; Gard, M. N.; Spanig, F.; Henderson, B. L.; Guldi, D. M.; Garcia-Garibay, M. A. Excited State Kinetics in Crystalline Solids: Self-Quenching in Nanocrystals of 4,4'-Disubstituted Benzophenone Triplets Occurs by a Reductive Quenching Mechanism *J. Am. Chem. Soc.* **2011**, *133*, 17296-17306.

32) Wolf, M. W.; Brown, R. E.; Singer, L. A. Deactivation of Benzophenone Triplets via Exciplex Formation. Evidence for Dual Reaction Pathways *J. Am. Chem. Soc.* **1977**, *99*, 526-531.

33) Favaro, G.; Bufalini, G. Bimolecular Interactions of Triplet Benzophenone in Aqueous Solution Studied by Energy Transfer to Biacetyl *J. Phys. Chem*., **1976**, *80*, 800-804.

34) Carbone, N. D.; Ene, M.; Lancaster, J. R.; Koberstein, J. T. Kinteics and Mechanisms of Radical-Based Branching/Cross-Linking Reactions in Pre formed Polymers Induced by Benzophenone and Bis-Benzophenone Photoinitiators *Macromolecules*, **2013**, *46*, 5434-5444.

35) Bhunia, S. K.; Das, P.; Nandi, S.; Jana, R. Carboxylation of Aryl Triflates with CO_2 Merging Palladium and Visible-Light-Photoredox Catalysts *Org. Lett*. **2019**, *21*, 4632-4637.

36) Gniadecki, R.; Assaf, C.; Bagot, M.; Dummer, R.; Duvic, M.; Knobler, R.; Rank, A.; Schwandt, P.; Whittaker, S. The optimal use of bexarotene in cutaneous T-cell lymphoma. *Br. J. Dermatol.* **2007**, *157*, 433-440.

37) Feuerstein, M.; Berthiol, F.; Doucet, H.; Santelli, M. Palladium-tetraphosphine complex: an efficient catalyst for the coupling of aryl halides with alkynes *Org. Biomol. Chem.*, **2003**, *1*, 2235-2237.

38) De Loera, D.; Sopin, A.; Garvia-Garibay, M. A. Photoinduced and Thermal Denitrogenation of Bulky Triazoline Crystals: Insights into Solid-to-Solid Transformation *J. Am. Chem. Soc.* **2013**, *135*, 6626-6632.

CHAPTER FOUR

Investigating Photochemical Reactivity of Crystalline Dewar benzenes

Adapted from: Edris Rivera and Miguel A. Garcia-Garibay

4.1 ABSTRACT

We have recently demonstrated that quantum amplification can be achieved in sensitizer-linked Dewar benzenes (**DB-OBPh**s) in the crystalline solid state. In this work we have also discovered that the solid state environment effects the potential of the quantum chain using alkyl substituted derivatives, **DB-OBPh-tbutyl** and **DB-OBPh-cyclohexyl** with quantum yields of ca. 274 and 343, respectively. Interestingly, we found that a crystalline mono-sensitizer-linked Dewar benzene exhibits greater potential for extending the quantum chain reaction to ca. 575, nearly 2-fold greater than other **DB-OBPh**s. This has spawned investigation into further studies in Dewar benzene scaffolds with unique electronics, confirming significant intramolecular benzophenone self-quenching. In this work we analyze the electronics of **monoDB-OBPh-adamantyl** using transient absorption spectroscopy to determine optical properties of the excited species, investigate the reactivity of a of Dewar benzene-triplet sensitizer salt pair (containing a single sensitizer), and the reactivity of a crystalline non-sensitizer linked Dewar benzene. Moving forward we aim to utilize this work to lay the foundation to further understand the quantum chain process of crystalline Dewar benzenes and achieving quantum yields at least 10^6.

4.1 Introduction

Quantum chain reactions are a rare class of nonlinear photochemical process in which a single photon leads to the formation of many photoproducts.[1,2] A quantum chain reaction can be identified based on characteristics that involve 1) absorption of a photon from a high energy molecule, generating an excited reactant that undergoes 2) an adiabatic process in which the excited reactant transforms into the excited photoproduct along the same excited manifold, followed by 3) an energy transfer process from the excited photoproduct to a neighboring ground state reactant, and thus, propagating the chain by generating a newly excited reactant.[2] Exploration of this type of process is largely limited to the few molecules that are known to undergo each; however, efforts to expand the quantum chain have been pursued.[3-10] We similarly aim to study and expand the quantum chain reaction in Dewar benzenes which are known to undergo this reactivity in the presence of a triplet sensitizer. Since the initial discovery made by Turro, efforts have been made to expand the quantum chain reaction using various triplet sensitizers/co-sensitizers, unique Dewar benzene scaffolds, and studying such processes within rigid polymeric media.[11] While the previous work has shown the extent of the quantum chain for Dewar benzenes in solution is ca. 120 we were interested in expanding the chain by studying reactivity within the crystalline solid state.[12] We have previously shown the potential for quantum amplification in crystalline diphenylcyclopropenones, showcasing quantum yields of ca. 3.3 in a nanocrystalline suspension compared to a quantum yield of unity in solution.[13-14] We became interested in implementing this quantum amplification in crystalline Dewar benzenes with the potential for achieving quantum yields of 10^6 – 10^9 due to the long-lived triplet intermediate (10^{-6}-10^{-3}), the efficiency of the adiabatic process ($\Phi_{AR} \approx 1$), and ultrafast energy

transfer rates based on triplet excitons generated in the crystalline solid state ($k_{ET}=10^{12}$ s^{-1}). So far, we have demonstrated the expansion of the quantum chain reaction of Dewar benzenes by developing and studying sensitizer-linked Dewar benzenes (**DB-OBPh**) with covalently attached benzophenones. Our previous work demonstrated the potential for a Dewar benzene quantum chain of ca. 90-120 in suspension; however, we reasoned that early chain termination was due to the formation of a semi-crystalline suspension. From that discovery, we projected that crystalline Dewar benzenes with similar reactivity should possess quantum yields ca. 100-300. With that in mind we set out to determine quantum yields of crystalline **DB-OBPh** derivatives with alkyl substituents attached to the 4' position of the sensitizer with the goal to ensure crystallinity and determine potential influence of crystal packing on the quantum chain.[15-17] This work proved that crystalline packing plays a role in the extent of the quantum chain reaction of crystalline Dewar benzenes based on quantum yields of DB-OBPh-tbutyl (ca. 274) and DB-OBPh-cyclohexyl (ca. 343). Interestingly, we discovered that a crystalline, mono-sensitizer-linked Dewar benzene scaffold revealed enhanced reactivity almost twice that of the disubstituted derivatives (ca. 575, **Figure 4.1**).

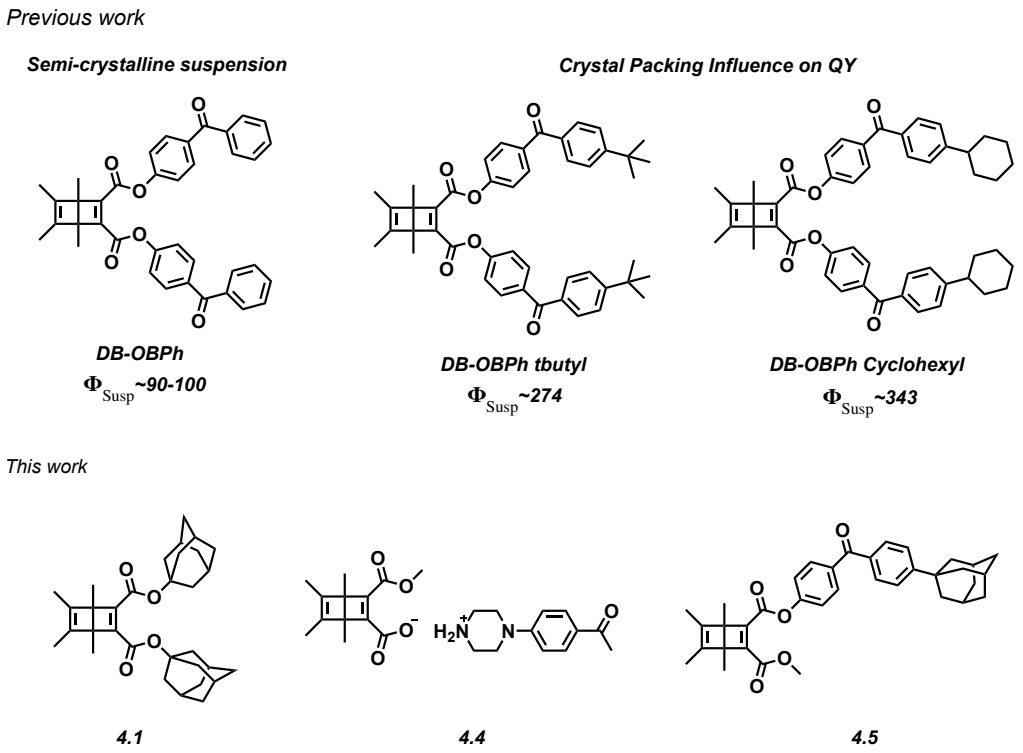

Figure 4.1 Dewar benzene library and reactivity

This reactivity has led to the investigation of **4.5** and its excitation using transient absorption spectroscopy. In this work we not only identify the absorption and lifetime, but also present a culmination of the work that has shown great potential for further investigation, including crystalline Dewar benzene-sensitizer salt pair and crystalline non-sensitizer linked Dewar benzene. We hope this work will aid in our understanding of the Dewar benzene quantum chain process and conjure further investigation into systems that can achieve quantum yields of 10^6.

4.3 Results and Discussion

4.3.1 Synthesis and Characterization

We initially set out to address the possibility of benzophenone quenching the crystalline solid state by synthesizing Dewar benzenes with a single triplet sensitizer covalently attached via ester linkage and compare this reactivity to **DB-OBPh** and a non-sensitizer linked Dewar benzene, DB-OAd, **4.1**. We describe the synthesis for our targets in Figure **4.1**, compound **4.1**, was realized through a Fischer esterification of acetylene dicarboxylate and 1-adamantanol, catalyzed by p-toluenesulfonic acid to give the diadamantyl ester **4.2** (**Scheme 4.1**, top left).[18] This was followed by an $AlCl_3$ catalyzed dimerization of 2-butyne, followed by trimerization onto **4.2** to give desired product in 15% yield (**Scheme 4.1**, top right).[19] Compound **4.3** was achieved based on an EDC-mediated coupling of DB-OOH/Me and 4-hydroxybenzophenone, catalyzed by DMAP (**Scheme 4.1**, bottom right). Due to the lack of crystallinity obtained for **4.3** we developed a Dewar benzene-sensitizer salt pair, **4.4**, by crystallizing DB-OOH/Me and 4-piperazino-aceotphenone in a biphasic liquid-liquid diffusion with a 1:3 solvent ratio of chloroform-n-hexanes (**Scheme 4.1**, bottom left).[20] We also synthesized an adamantyl-sensitizer-mono-substituted Dewar benzene **4.5** to study a covalently attached derivative. The synthesis was similar to synthesis for **4.3**, using 4-hydroxy-4'-adamantylbenzophenone to couple onto DB-OOH/Me, giving the desired product as a white powder.

Scheme 4.1 Synthesis of **4.1**, **4.4**, and **4.5**

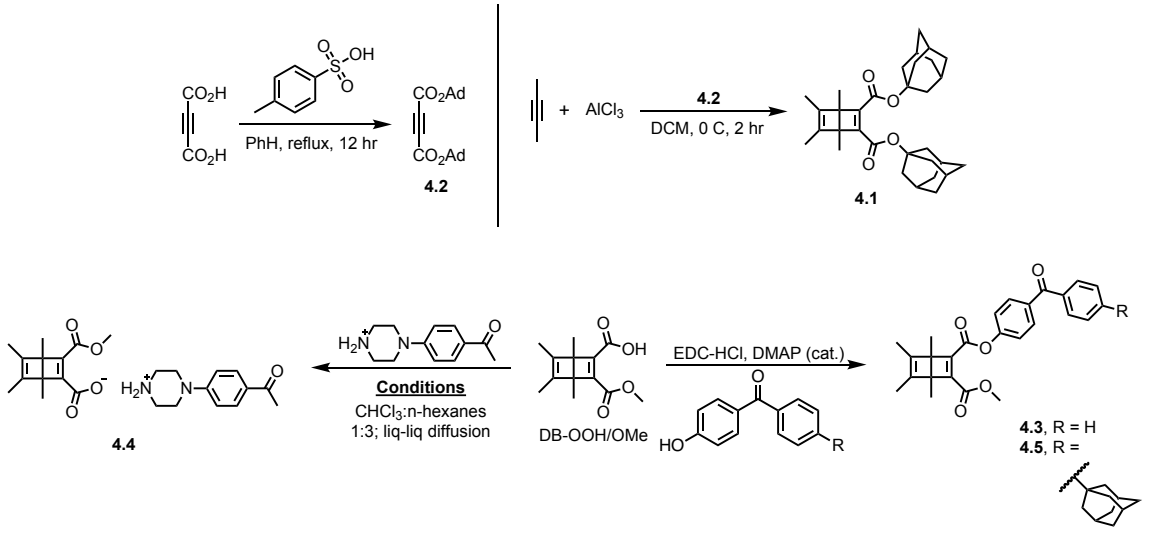

4.3.2 Analysis of Dewar benzene Salt-Pair

To gain insight the potential of enhanced reactivity of Dewar benzenes crystallized with a single triplet sensitizer we first studied the conversion of polycrystalline powders of **DB-OBPh**, **4.1**, and **4.4**. This was performed by irradiating 10 mg of each compound between two glass slides in the Rayonet photochemical reactor with six 8W-312 nm bulbs. The results show promising reactivity for all three compounds (**Table 4.1**).

Table 4.1 Dewar benzene conversions over a 30 minute irradiation (λ=312 nm)

Time (min)	*4.1*	*DB-OBPh*	*4.4*
0	***0%***	***0%***	***0%***
15	***56%***	***75%***	***26%***
30	***83%***	***100%***	***67%***

We found that after the 30 minute irradiation that **DB-OBPh** was fully converted, **4.1** and **4.4** were 83% and 67% converted, respectively. In the case of **DB-OBPh** we have already extensively explored reactivity for this compound both in solution and solid state.

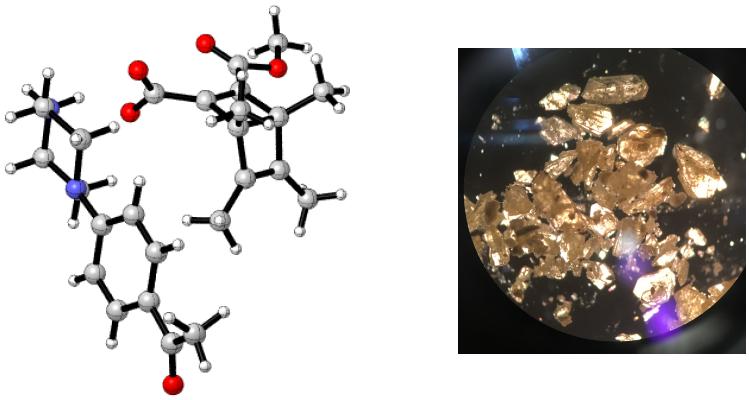

Figure 4.2 Crystal structure of **4.4**

Compound **4.4** takes up a $P2_1/n$ monoclinic space group with four pairs within a unit cell, and unlike other crystalline Dewar benzenes, lacks disorder about the Dewar benzene portion of the molecule (**Figure 4.2**). We reasoned that the low reactivity can be due to the formation of an anhydride side product that competes with absorbing photons. A more reasonable explanation may involve long range distances (5.38Å) between the sensitizer and Dewar benzene pairs. Scheffer reported successful triplet energy transfer in salt pairs containing 4-piperazinoacetophenone but with those made up of short distances (4.11Å), further supporting that the crystal structure may not be optimal for energy transfer. From this work we are eager to study systems that promote the formation of Dewar benzene salt pairs with pyridinyl sensitizers

and mono- and dicarboxylic acid Dewar benzenes that are closer in range. We used fumaric acid as a model system to mimic carboxylic acid Dewar benzenes due to similar pKas. We propose a range of possible sensitizers with high (>63kcal/mol) and low (<63kcal/mol) triplet energy (**Figure 4.3**).[21-26]

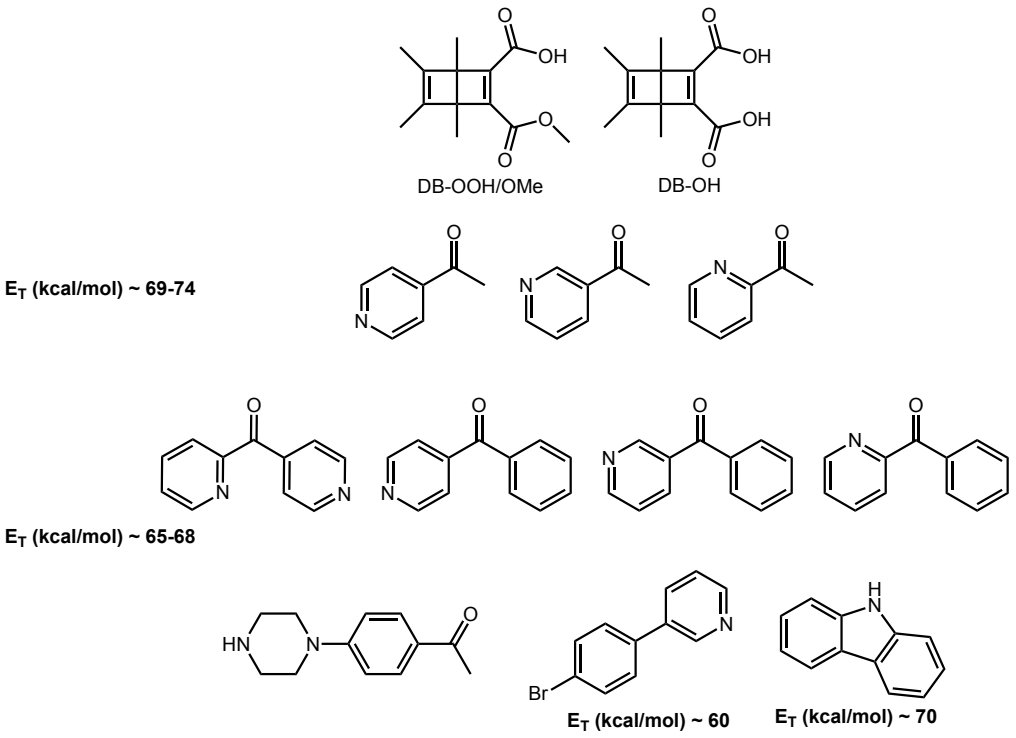

Figure 4.3 Carboxylic acid Dewar benzenes and potential triplet sensitizer salt pair/cocrystal candidates

We hope to gain insight on the efficiency of the energy transfer process based on triplet energy and crystal packing in the bulk crystalline powder.

4.3.3 Diadamantyl Dewar benzene

To compare relative reactivity with a nonsensitizer-linked crystalline Dewar benzene we chose to explore the photochemical isomerization of **4.1**. The crystal structure of **4.1** (**Figure 4.4**) takes up a Pca21 orthorhombic space group with disorder about the Dewar benzene giving either concave or convex forms. A single unit cell has eight Dewar benzene molecules. The most interesting aspect of the irradiation experiment is unexpected reactivity of **4.1** over **4.4**, considering the absence of a triplet sensitizer as demonstrated in Table **4.1**. The efficiency of **4.1** shows evidence of a possible quantum chain reaction of **4.1** in the crystalline solid state.

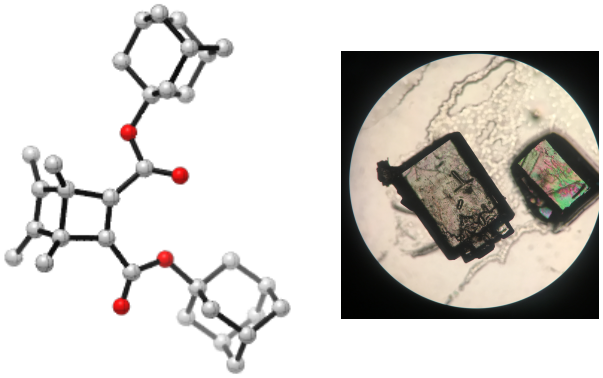

Figure 4.4 Crystal structure of **4.1**

It may be possible that the crystalline environment promotes triplet excitation of the Dewar benzene that allows it to undergo a quantum chain reaction solely in the crystalline solid state.[27,28] Due to its high strain, we were interested to determine if mechanical force could be used to isomerize **4.1**. Although it is known that mechanical force can be utilized to initiate a reaction, its use in the isomerization of Dewar benzenes is currently unknown.[29-31] To explore this

possibility we were able to grind 5.2 mg of the polycrystalline powder of **4.1** using a mortar and pestle and qualitatively demonstrate isomerization occurred as a result of grinding. We have further explored this using an IR press and pulse sonicator and measured the conversion based on ^{1}H NMR (**Table 4.2**). The standard IR pellet press was used to apply pressure to the bulk powder sample between weigh paper at 1,000 bar over time. While there is evidence of isomerization due to the IR press, the conversion is low. We compared this using a probe sonicator on nanocrystalline suspensions of **4.1** and found that conversions were greater over a shorter time period, further supporting the potential for mechanochemical responsiveness.

Table 4.2 Conversion of **4.1** to isomerized product via IR press and probe sonicator

IR Press - Bulk Powder

Time (min)	%Conv
1	*3%*
15	*4%*
20	*9%*

Probe Sonicator - NC suspension

Time (min)	%Conv
0.5	*8%*
1	*13%*
2	*20%*

While this showed very promising evidence for a mechanochemically responsive small molecule we were unable to continue our analysis for **4.1** due to failed attempts to remake the compound. We hope the synthesis can be repeated to give **4.1** and continue analysis for the potential of this compound to undergo a quantum chain reaction and mechanochemically isomerize in the crystalline solid state.

4.3.4 Laser Flash Photolysis of monoDB-OBPh-adamantyl

In order to gain insight on the excited state of the compound **4.5** we performed a pump-probe experiment utilizing nanosecond laser spectroscopy; a Brilliant B Quantel Nd-YAG laser operating at 355 nm with a pulse width of ca. 8 ns for the excitation source. Compound **4.5** was introduced to a mounted 1 cm quartz flow cell through a continuous flow system to ensure fresh material was continuously sampled. Samples were sparged with argon at least an hour prior to beginning the experiment, and remained continuously sparged for the duration of the experiment.

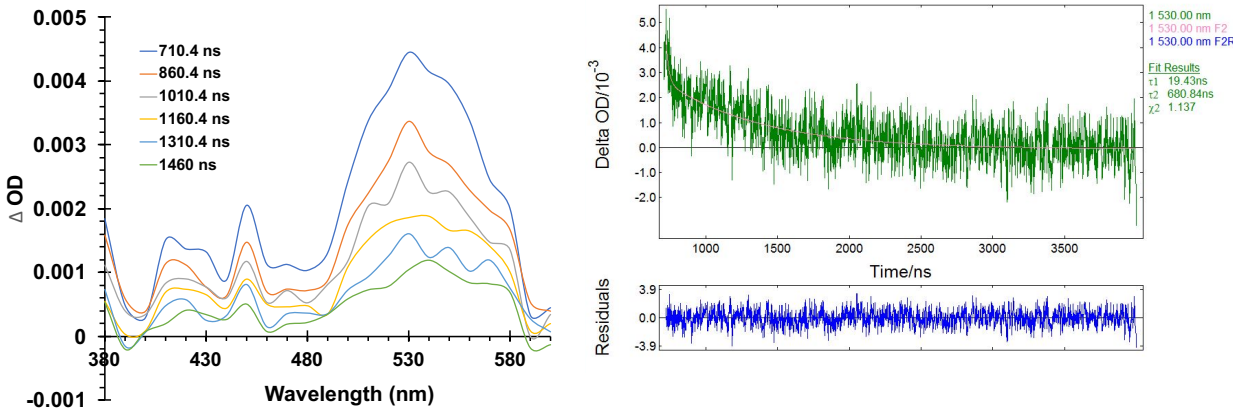

Figure 4.5 Transient absorption of a 0.560 mM **4.5** sample

Figure 4.5 depicts the transient absorption and lifetime of **4.5** in acetonitrile. Like the di-sensitizer linked derivatives, the absorption at 530 nm is attributed to the excitation of the benzophenone. The biexponential decay at 530 nm revealed a lifetimes of 19 and 680 ns, for the short and long-lived components, respectively. This revealed that the long-lived component is almost twice the lifetime of **DB-OBPh**, suggesting significant quenching interactions between intramolecular benzophenones in **DB-OBPh**. We are interested in further exploration of **4.5**

through structural analysis of a crystal structure when a diffraction quality single crystal is obtained.

4.4 Further Investigation into Benzophenone Self-Quenching

To gain further evidence of benzophenone self-quenching and extend the lifetime of the triplet excited photoproduct into the micro- to millisecond regime, we were interested in designing a Dewar benzene with electron-withdrawing groups.[32] Previous work from our group detailed benzophenone self-quenching as a function of benzophenone electronics, suggesting that benzophenones with electron-withdrawing groups avoid benzophenone self-quenching as indicative of long lifetimes in the crystalline solid state. Based on this work we propose Dewar benzenes with electron withdrawing Dewar benzenes covalently attached (**Figure 4.6**).

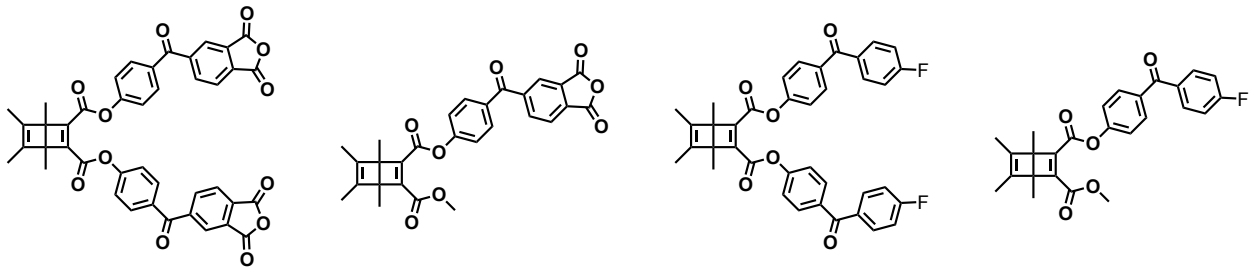

Figure 4.6 Proposed Dewar benzenes equipped with electron-withdrawing groups

While these compounds were not fully realized the proposed synthesis for these derivatives can be used to develop these Dewar benzenes for future investigations (**Scheme 4.2**). We initially proposed that 4.6 and 4.7 can be obtained by first synthesizing a 4-hydroxy-anhydride-benzophenone via oxidation of 4-hydroxy-3,4-dimethylbenzophenone to give the dicarboxylated product **4.10**. The dicarboxylated product can then be cyclized to form the corresponding anhydride using thionyl chloride.

Scheme 4.2 Proposed synthesis of anhydride benzophenone, **4.6**, **4.7**, **4.8**, and **4.9**

Route 1

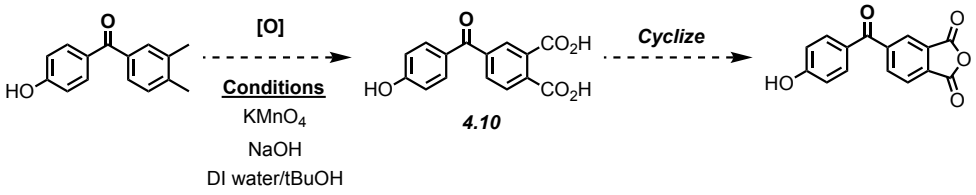

Route 2

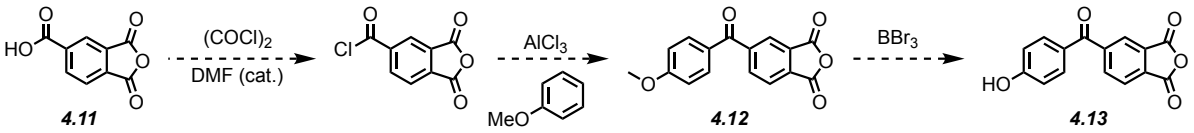

Dewar benzene Synthesis

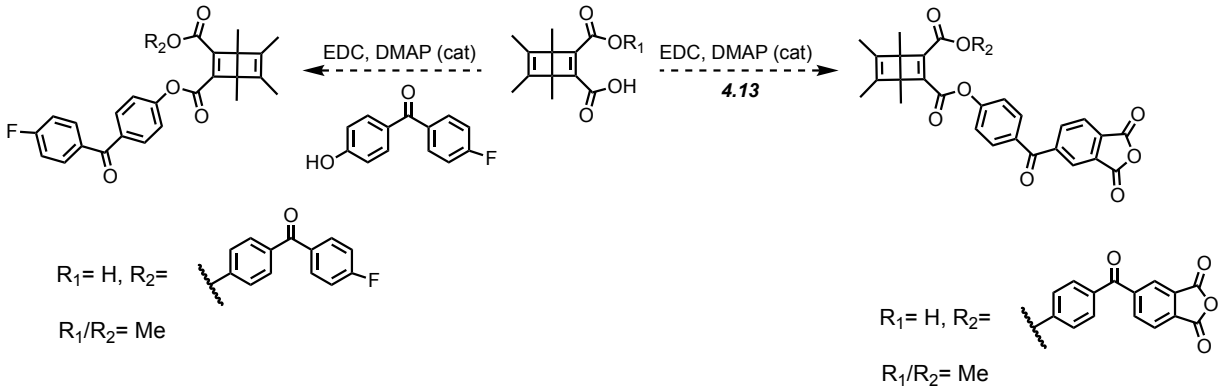

We were unable to proceed with this route due to the lack of selectivity for methyl oxidation over the phenol. An alternative strategy was to synthesize the benzophenone using anisole and trimilletic anhydride, **4.11**. Trimilletic anhydride can be formed as an acid chloride using excess oxalyl chloride and a catalytic amount of anhydrous DMF. The acid chloride can then be subjected to a Friedel Crafts acylation in which $AlCl_3$ catalyzes the reaction with anisole to give the desired benzophenone **4.12**. This compound can then be subjected to deprotection conditions with BBr_3 to give the resulting hydroxybenzophenone **4.13**. This can then be coupled to DB-OH and DB-OOH/OMe using EDC and catalyzed by DMAP to give the corresponding Dewar benzenes 4. Compounds **4.8** and **4.9** can similarly be synthesized coupling commercially available 4-hydroxy-4-fluorobenzophenone, **4.14**, to DB-OH and DB-OOH/Me. With these compounds in hand it may be possible to access long lived lifetimes of the triplet photoproduct (both in solution and the solid state) and measure quantum yields in the crystalline solid state.

4.5 Conclusions

This work has demonstrated unique Dewar benzene reactivity that requires further exploration to understand the extent of photochemical isomerization. While our work has explored limitations of **DB-OBPh** quantum chain reactions such as crystal packing and benzophenone self-quenching we were interested in gaining perspective from a theoretical analysis via computational methods. Our experimental work was supplemented with computational work with former member, Liepuoniute, who determined that another limitation lies along the triplet transition state. Computational methods utilized to calculate transition state energies of **DB-**

OBPh as it transforms to **HB-OBPh** revealed a transition state energy close to the ground state transition state, suggesting that an alternative photophysical mechanism upon triplet excitation. This further supports the necessity for further investigation into optimal crystalline Dewar benzene scaffolds that can efficiently undergo the adiabatic process, reduce triplet self-quenching, and approach triplet lifetimes along 10^{-6}-10^{-3} s.

4.6 Experimental

4.6.1 General Information

All compounds were synthesized under an inert argon atmosphere unless otherwise specified. Nuclear magnetic resonance (NMR) spectra for ^{1}H and ^{13}C were obtained using 500 MHz Bruker NMR spectrometer. All chemical shifts are reported in ppm using natural abundance isotopes of reference solvents. Infrared (IR) spectra was collected using the Perkin-Elmer 1000 Series FT-IR spectrometer.

4.6.2 Synthetic Procedures

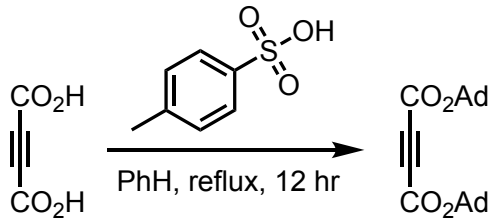

4.2

Synthesis of 4.2: A clean 25 mL round bottom flask was charged with a stir bar, acetylene dicarboxylic acid (0.100 g, 0.877 mmol, 1 equiv), 1-adamantanol (0.334 g, 2.14 mmol, 2.5 equiv), and *p*-toluenesulfonic acid (0.015 g, 0.087 mmol, 0.1 equiv). The compounds were dissolved in benzene (35 mL) and the reaction was set to stir at reflux overnight using a dean stark trap. The yellow solution was allowed to cool to room temperature, followed by a subsequent wash with water and brine. The crude product was extracted in ether. The organic layer was dried over sodium sulfate, filtered, then concentrated under pressure to a yellow oil. Column chromatography was used to purify the desired compound using silica and a gradient of hexanes: ethyl acetate solvent system (50:1, 25:1, 20:1, 10:1). The desired product is a white solid. ^{1}H NMR (500 MHz, CDCl3): δ = 2.18-2.12 (d, 18H), 1.65 (s, 12H). HRMS (DART) calcd for C24H30O4 [M+H]**+** 388.23600, found 388.23012. MP: 180 ^{o}C

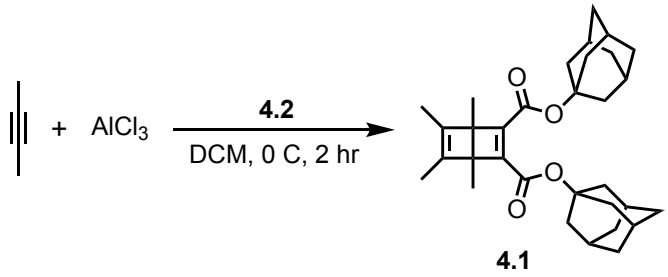

4.1

Synthesis of 4.1: A 25 mL 3-neck flask round bottom flask was flame dried and charged with a stir bar and a $AlCl_3$ (0.090 g, 0.647 mmol, 1 equiv). This was followed by the addition of 4 mL anhydrous dichloromethane (DCM). 2-Butyne was then added dropwise (0.070 g, 101 μL, 1.29 mmol, 2 equiv) and allowed to stir for 10 minutes at 0 ^{o}C. This was followed by the addition of **2** (0.000 g, 0.000 mmol, 0.74 equiv). This was allowed to stir for 60 minutes at room temperature. Dimethylsulfoxide (DMSO) was then added dropwise (1 mL), followed by the addition of anhydrous DCM (4 mL). The reaction was then washed with deionized water, brine, and then extracted in ether. The organic layer was dried over sodium sulfate, filtered, then concentrated under pressure to yield a yellow oil. The crude oil was purified using column chromatography. Utilizing a gradient solvent system composed of hexanes: ethyl acetate (50:1, 25:1, 20:1). The product was recrystallized in DCM:ether mixture to produces white solid. ^{1}H NMR (500 MHz, CDCl3): δ = 2.17 (s, 18H), 1.68 (t, *J* = 9.7 Hz, 11H), 1.63 (s, 6H), 1.29 (s, 6H); ^{13}C NMR (126 MHz, CDCl3) δ = 161.25, 152.32, 143.38, 81.21, 55.84, 41.49, 36.21, 30.86, 11.05, 9.94. HRMS (DART) calcd for C32H42O4 [M+H]**+** 491.31559, found 491.31524. MP: 165 ^{o}C

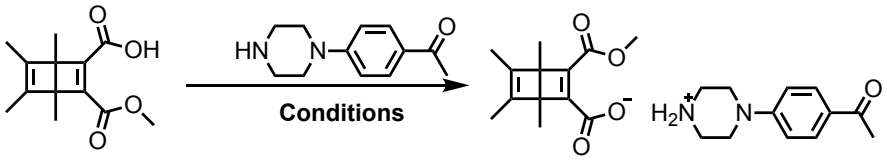

DB-OOH/OMe

4.4

Synthesis of 4.4: An equimolar amount of DB-OOH/OMe and 4-piperazinoacetophenone was weighed and dissolved in a minimal amount of spectral grade chloroform and placed the dissolved compound in a 5 mL scintillation vial. A layer of n-hexanes was carefully layered on top of the chloroform dissolved sample in such a way that it is a 1:3 solvent ratio. The vial was then covered and was allowed to crystallize over several days (3-4 days). The resulting product crystallized to form yellow crystals in quantitative yield. ^{1}H NMR (500 MHz, CDCl3): δ = 1.27 (s 3H), 1.38 (s, 3H), 1.57 (s, 3H), 1.58 (s, 3H), 2.50 (s, 3H), 3.01 (t, 4H), 3.30 (t, 4H), 3.89 (s, 3H) 6.85,6.86 (d, 2H), 7.87,7.88 (d, 2H); ^{13}C NMR (126 MHz, CDCl3) δ = 195.50, 166.36, 159.62, 154.53, 143.67, 142.47, 130.22, 127.44, 113.53, 56.98, 55.35, 53.03, 48.42, 45.85, 26.15, 11.28, 10.87, 9.95, 9.46.

4.6.3 ^{1}H, ^{13}C-NMR Spectra

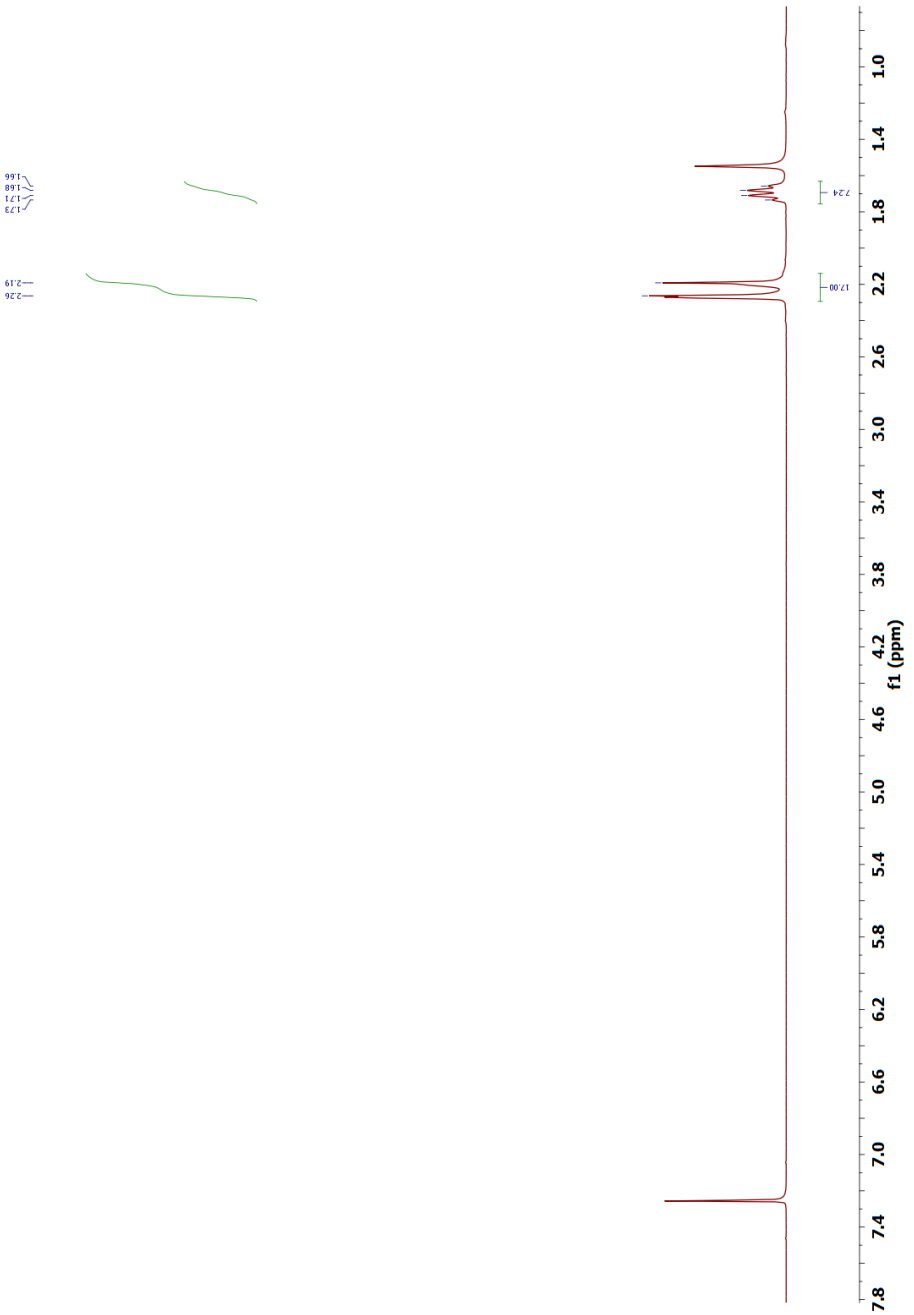

Figure 4.7 ^{1}H NMR of **4.2** in $CDCl_3$ at 500 MHz

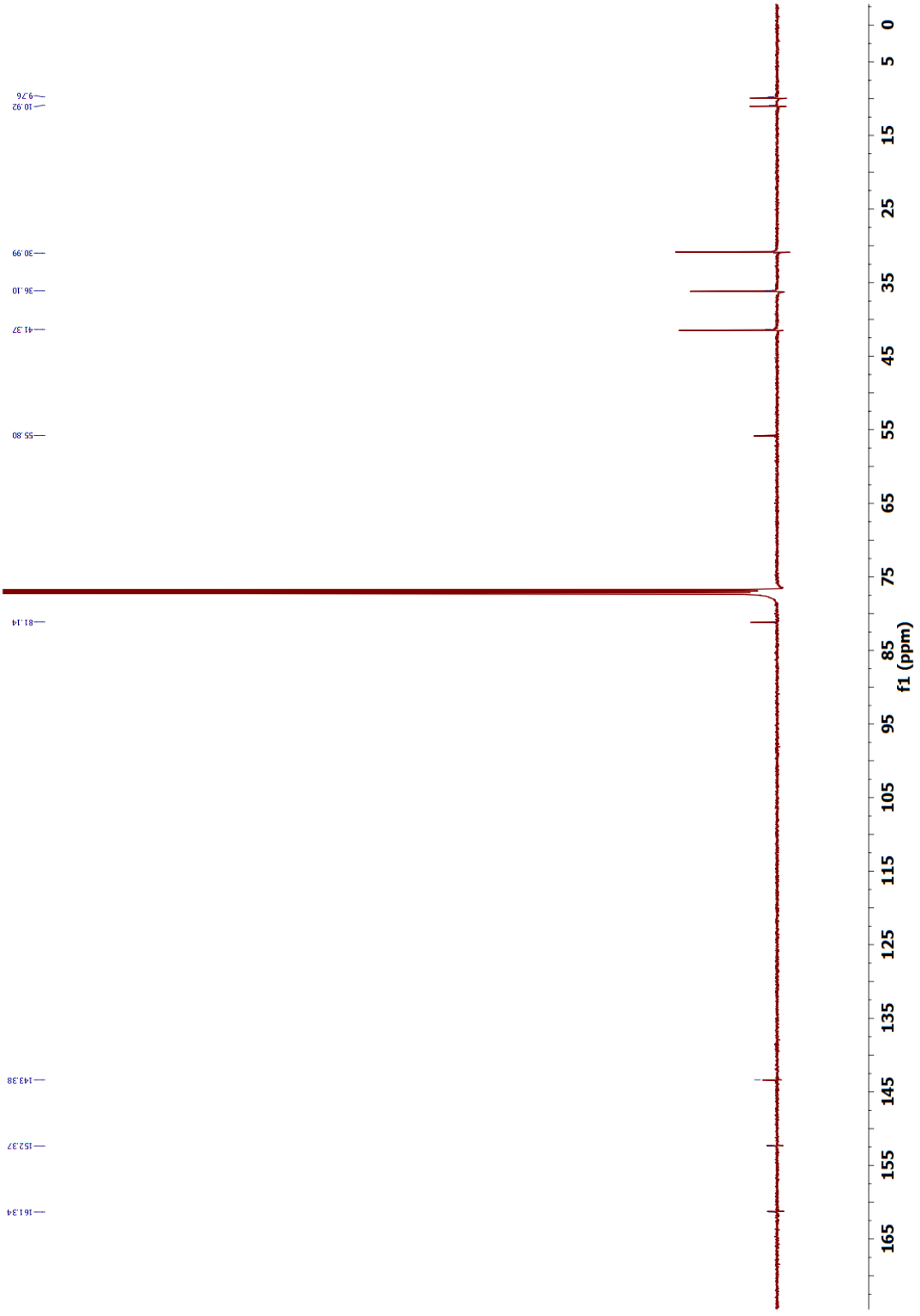

Figure 4.8 $^{13}C\{^{1}H\}$ NMR of **4.2** in $CDCl_3$ at 126 MHz

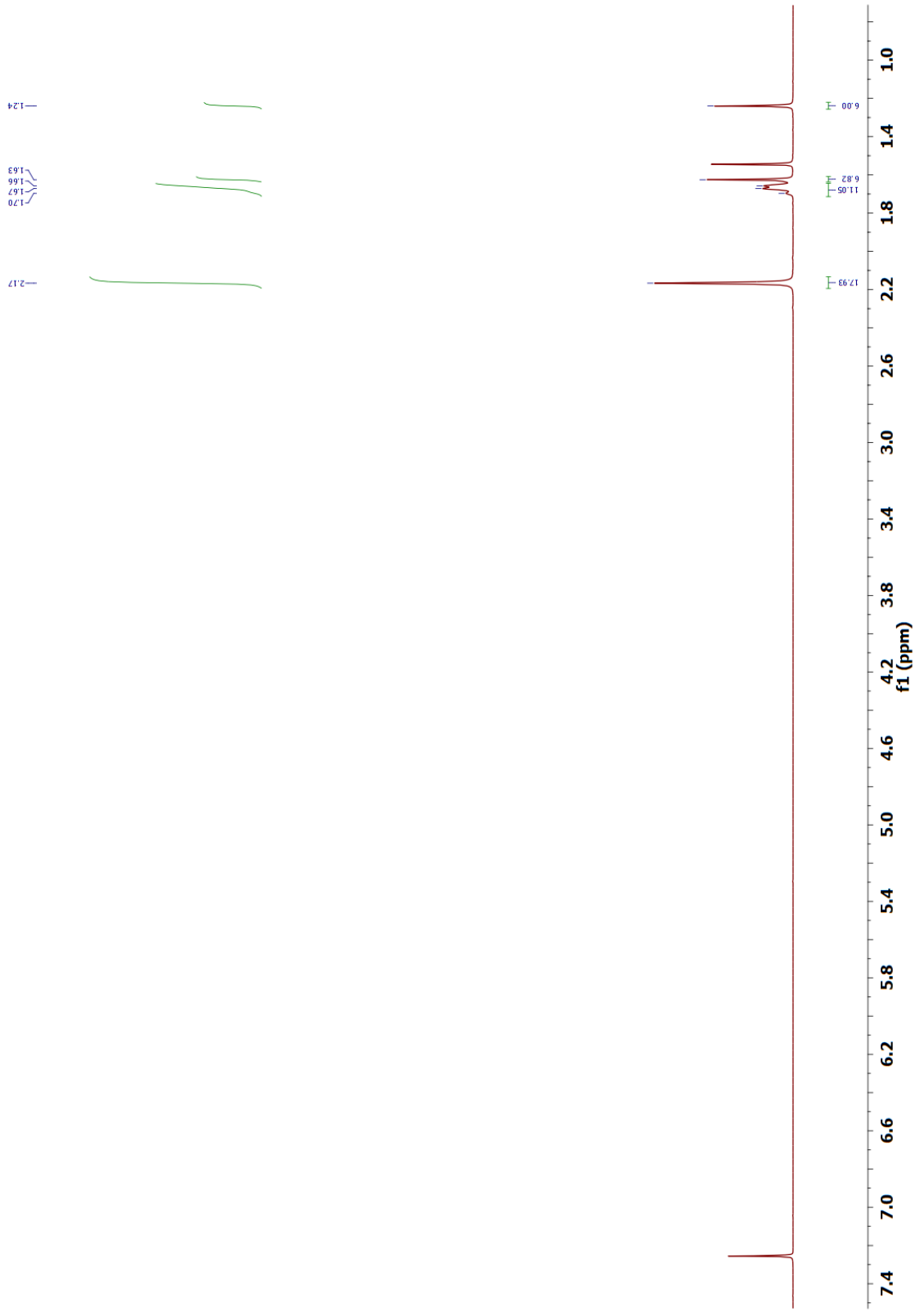

Figure 4.9 ^{1}H NMR of **4.1** in $CDCl_3$ at 500 MHz

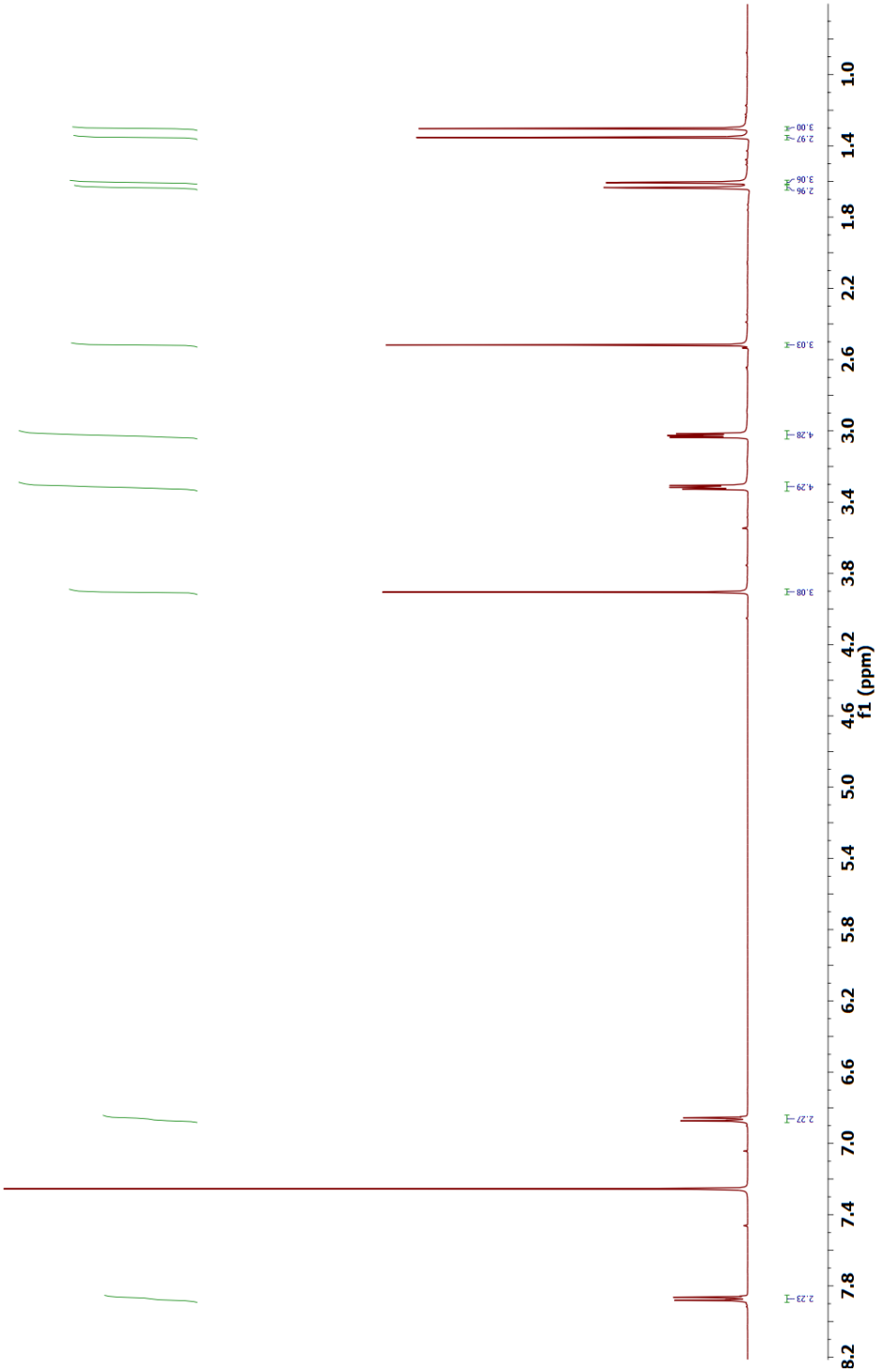

Figure 4.10 ^{1}H NMR of **4.4** in $CDCl_3$ at 500 MHz

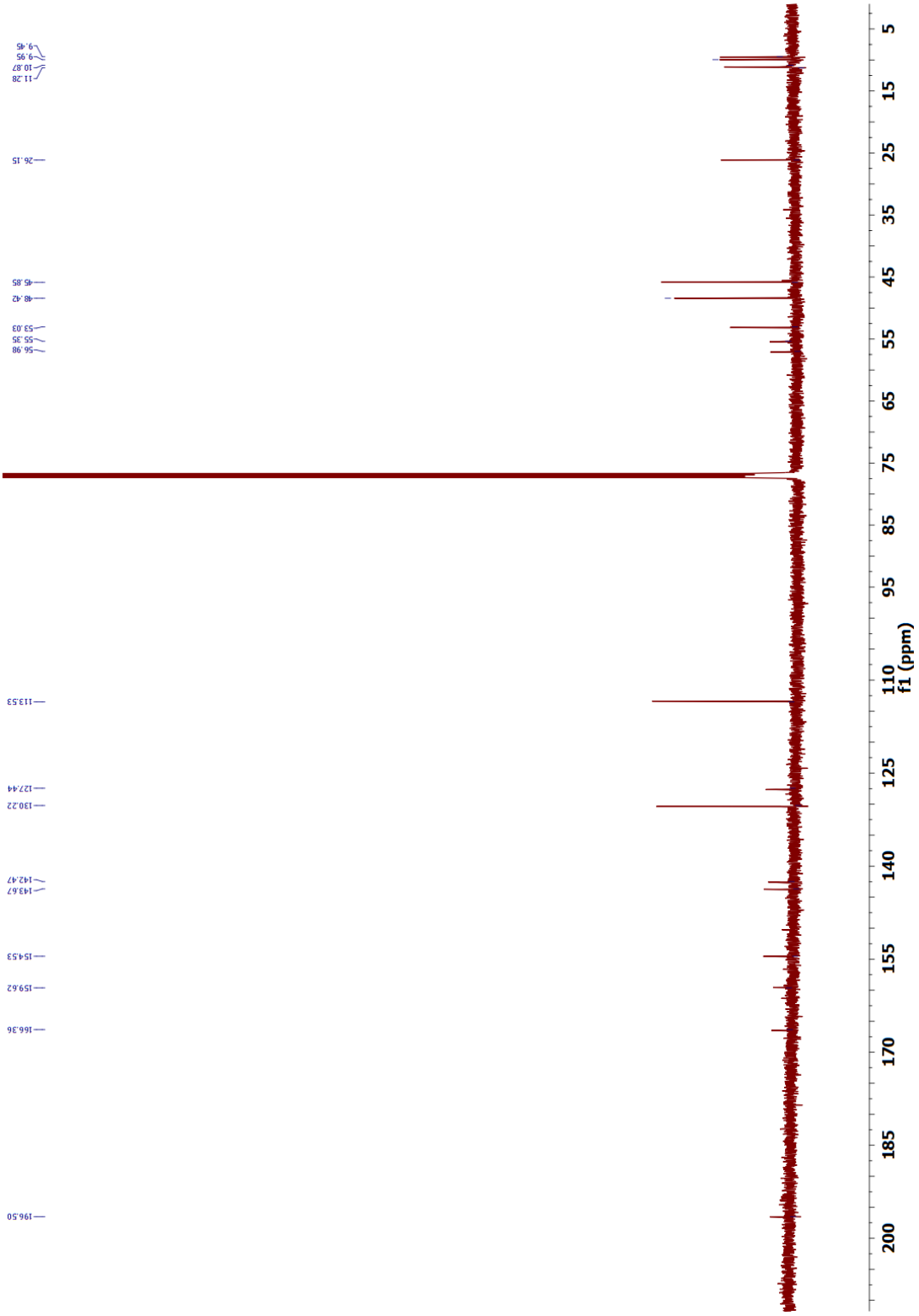

Figure 4.11 $^{13}C\{^{1}H\}$ NMR of **4.4** in $CDCl_3$ at 126 MHz

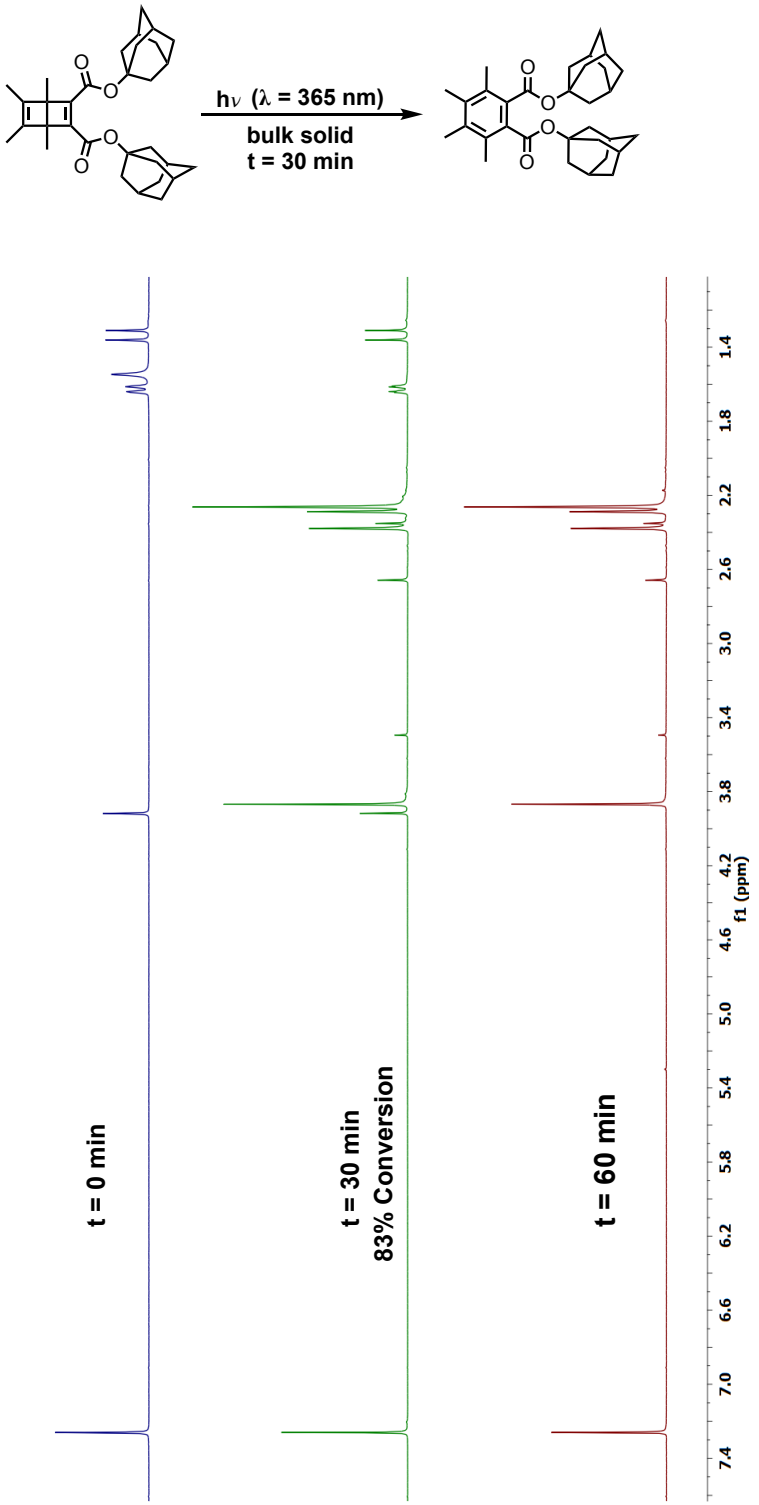

Figure 4.12 Irradiation of **4.1** showing % conversion

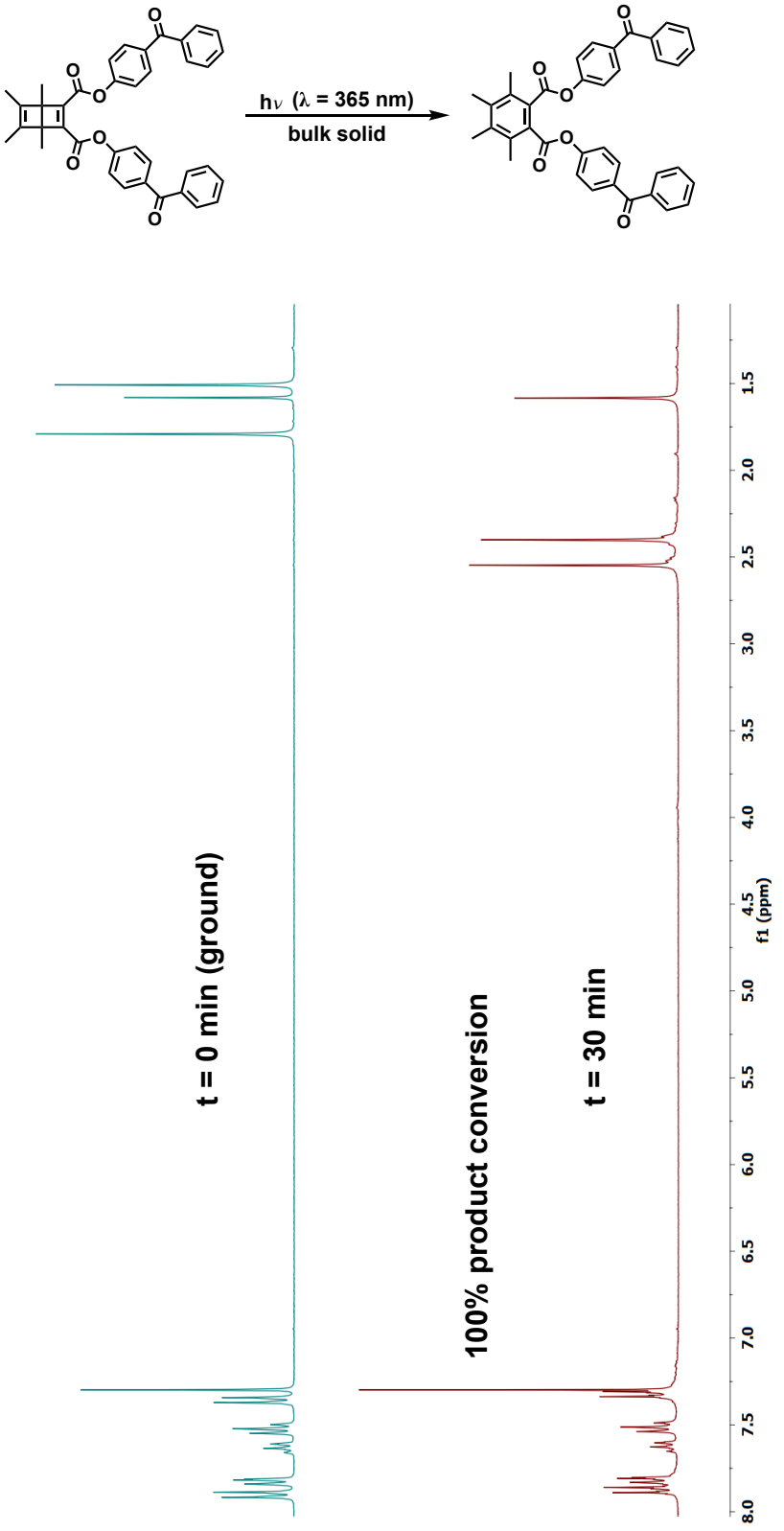

Figure 4.13 Irradiation of **DB-OBPh** showing % conversion

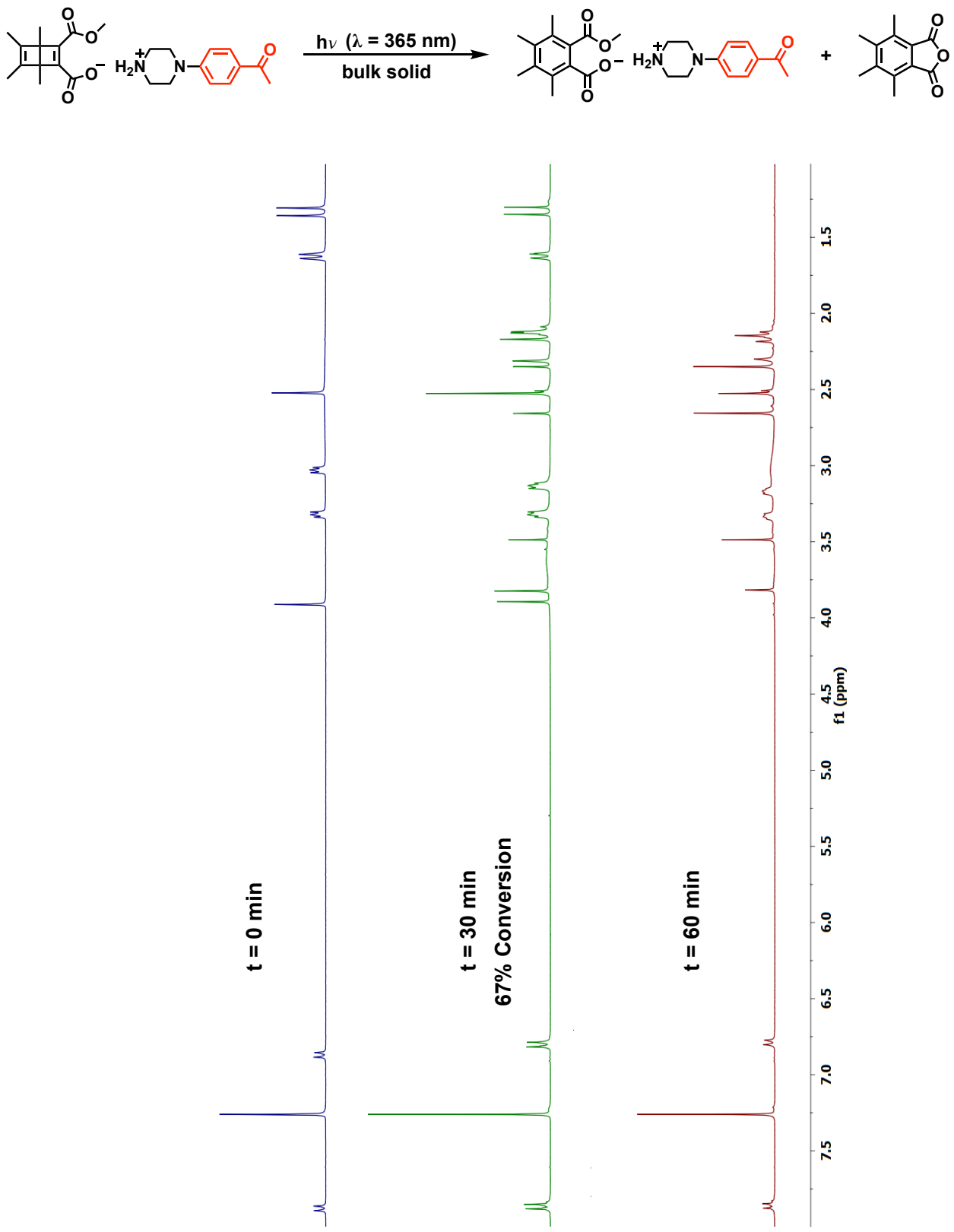

Figure 4.14 Irradiation of **4.4** showing % conversion

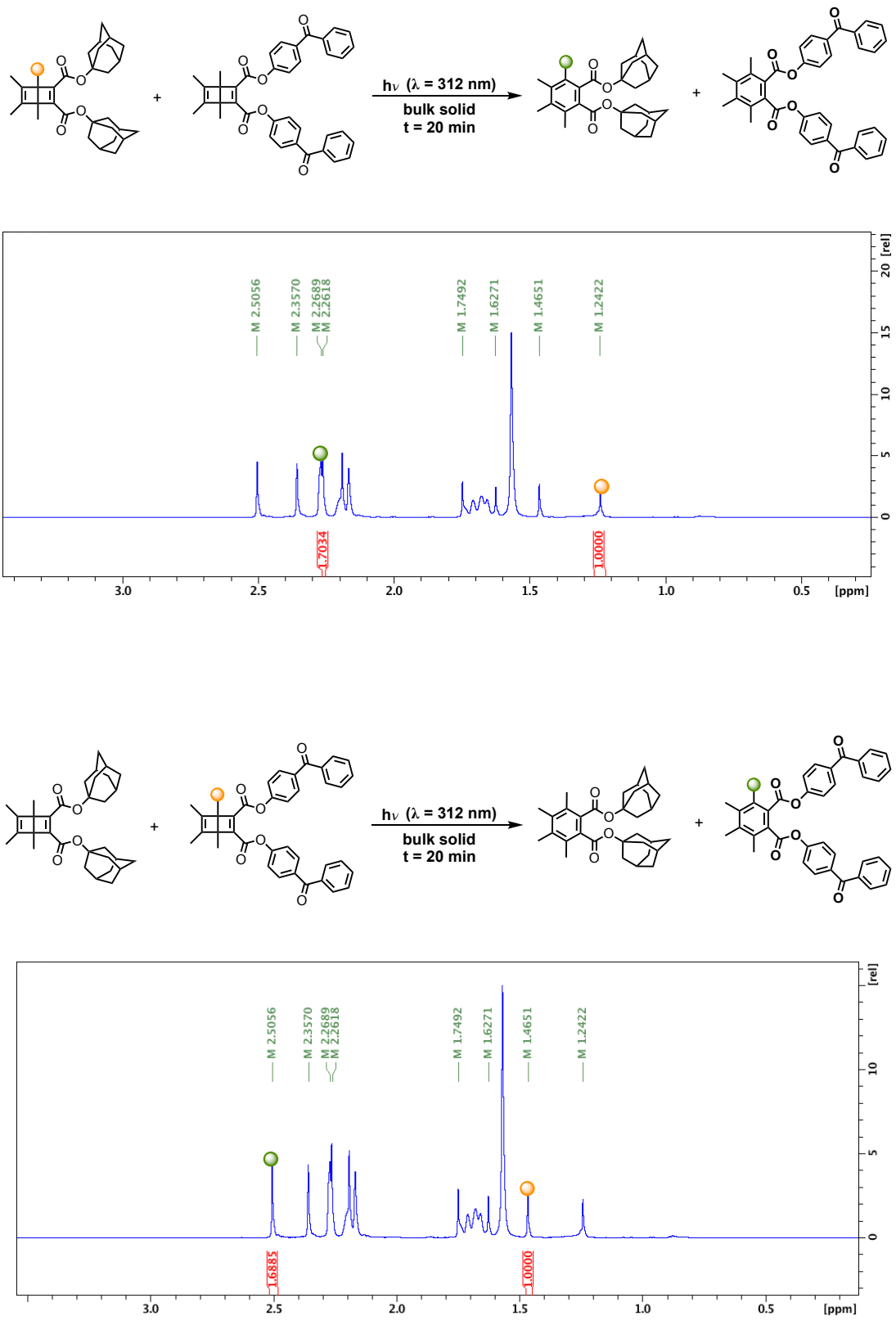

Figure 4.15 Comparative irradiation of mixed **DB-OBPh** and **4.1**

4.6.4 IR Spectra

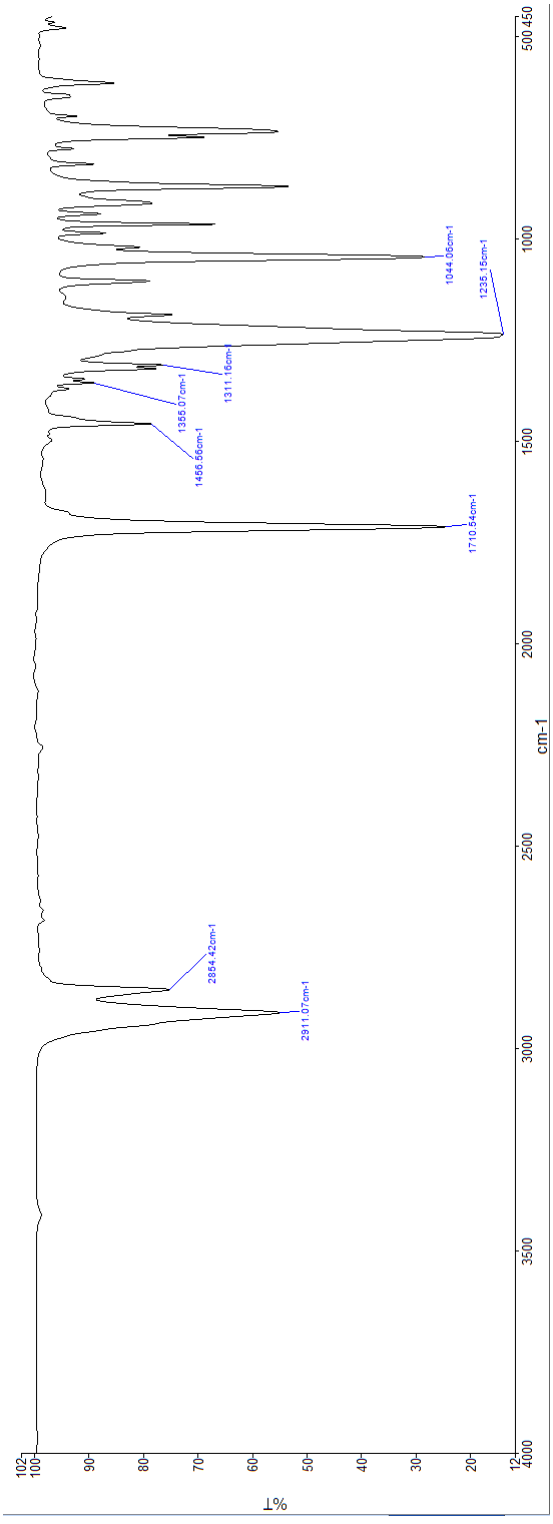

Figure 4.16 FTIR of **4.2**

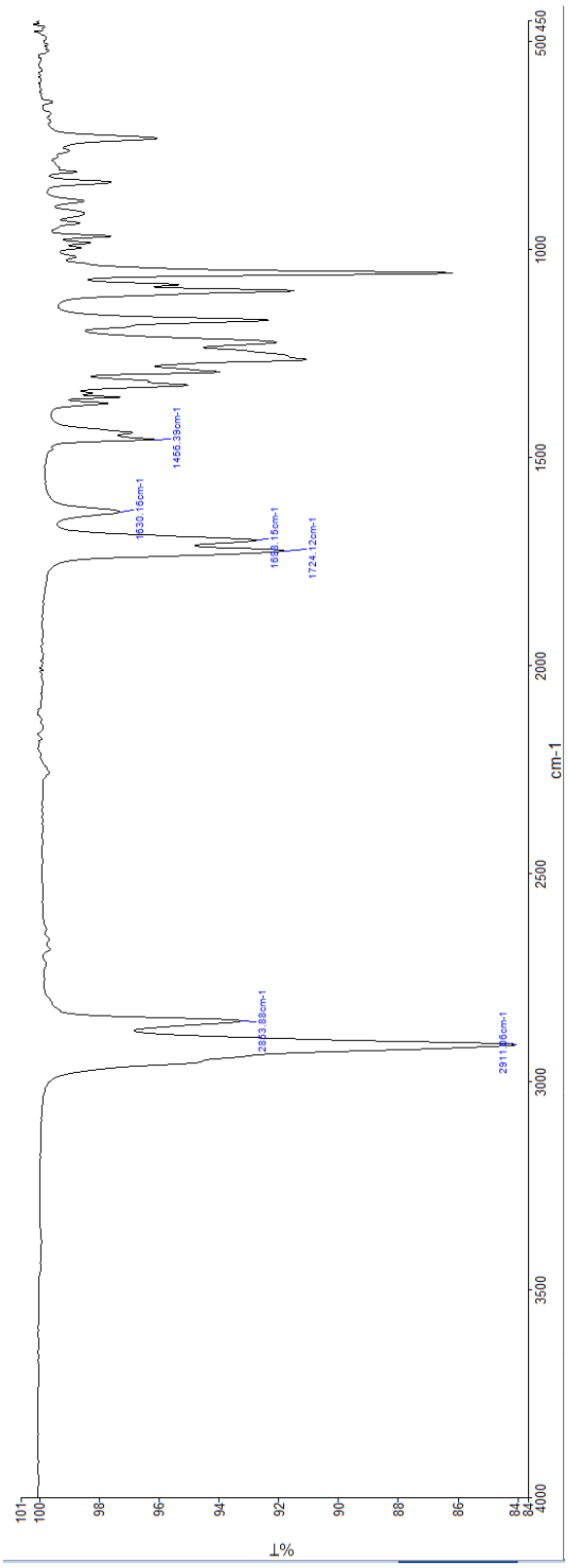

Figure 4.17 FTIR of **4.1**

4.6.5 UV vis Spectra

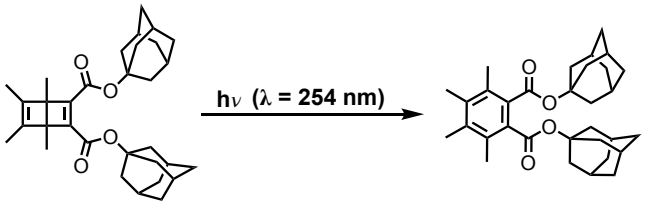

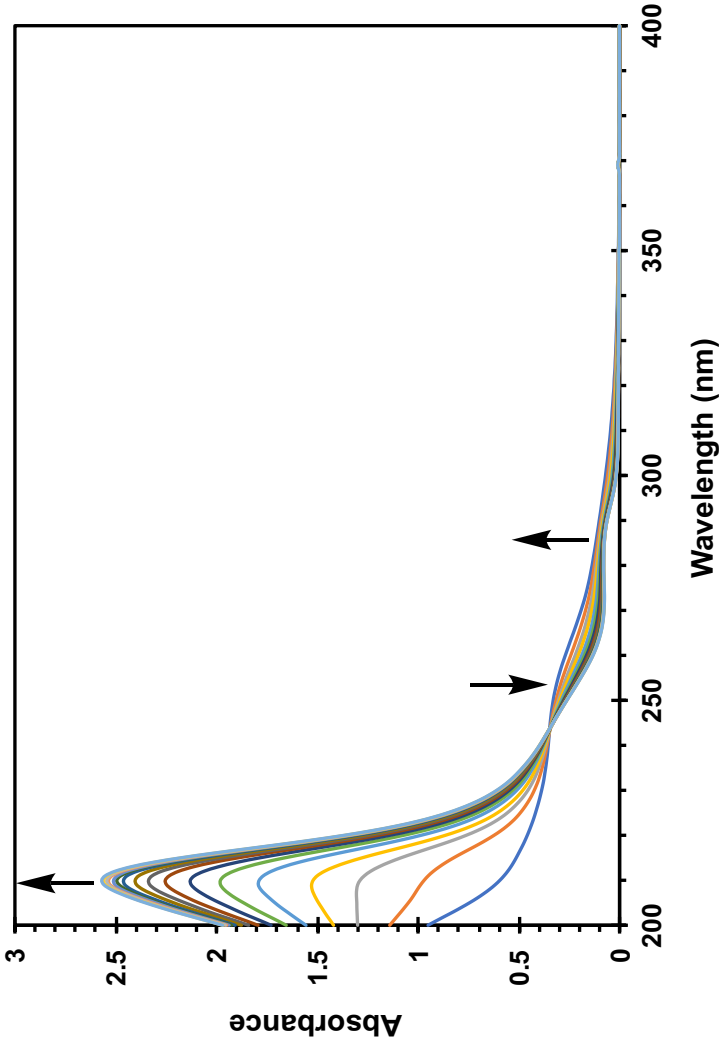

Figure 4.18 UV vis absorption of **4.1** (4.14×10^{-5} M) irradiated at 30 sec time intervals in Air-saturated MeCN

4.7 References

1) Turro, N. J.; Ramamurthy, V.; Katz, T. J. Energy Storage and Release. Direct and sensitized photoreactions of dewar benzene and prismane. *Nouveau Journal de Chimie* **1978**, *1*, 363–365.
2) Turro, N. J.; McVey, j.; Ramamurthy, V.; Lechtken, P. Adiabatic Photoreactions of Organic Molecules *Angew. Chem. Int. Ed. Eng.* **1979**, *18*, 572-586.
3) Crandall, J. K.; Mayer, C. F. Benzene-photosensitized transformations of the four geometrical isomers of 1,5,9-cyclododecatriene J. Am. Chem. Soc., 1967, 89, 4374-4380.
4) Kazakov, V. P.; Voloshin, A. I.; Shavaleev. Chemiluminescence in visible and infrared spectral regions and quantum chain reactions upon thermal and photochemical decomposition of adamantylideneadamantane-1,2-dioxetane in the presence of chelates Pr(dpm)3 and Pr(fod)3 J. Photochem and Photobio. 1998, 11, 177-186.
5) Lechtken, P.; Yekta, A.; Turro, N. J. Tetramethyl-1,2-dioxetane. Mechanism for an autocatalytic decomposition. Evidence for a quantum chain reaction. J. Am. Chem. Soc. 1973, 95, 3027-3028.
6) Turro, N. J.; Schore, N. E.; Yekta. Quantum chain processes. Novel procedure for measurement of quenching parameters. Evidence that exothermic triplet-triplet energy transfer is not diffusion limited and an estimation of the efficiency of exothermic quenching in a solvent cage J. Am. Chem. Soc. 1974, 96, 1936-1938.
7) Turro, N.J.; Waddell, W. H. Quantum chain processes. Direct observation of high quantum yields in the direct and photosensitized excitation of tetramethyl-1,2-dioxetane Tetrahedron Letters. 1975, 25, 2069-2072.

8) Schuster, G. B.; Turro, N. J.; Steinmetzer, H.; Schaap, A. P.; Faler, G.; Adam, W.; Liu, J. C. Adamantylideneadamantane-1,2-dioxetane. Chemiluminescence and decomposition kinetics of an unusually stable 1,2-dioxetane J. Am. Chem. Soc. 1975, 97, 7110-7117.

9) Wilson, T.; Schaap, A. P. Chemiluminescence from cis-diethoxy-1,2-dioxetane. Unexpected effect of oxygen J. Am. Chem. Soc. 1971, 93, 4126-4136.

10) Turro, N. J.; Lechtken, P.; Schore, N. E.; Schuster, G.; Steinmetzer, H.; Yekta, A. Tetramethyl-1,2-dioxetane. Experiments in chemiexcitation, chemiluminescence, photochemistry, chemical dynamics, and spectroscopy Acc. Chem. Res. 1974, 7, 97-105.

11) Kiau, S.; Liu, G.; Shukla, D.; Dinnocenzo, J. P.; Young, R. H.; Farid, S. Kinetics of Isomerization via Photoinduced Electron Transfer. I. Spectral Analysis and Structural Reorganization of Hexamethyl Dewar Benzene Exciplexes *J. Phys. Chem. A* **2003**, *107*, 3625-3632.

12) Ferrar, L.; Mis, M.; Dinnocenzo, J. P.; Farid, S.; Merkel, P. B.; Robello, D. R. Quantum Amplified Isomerization in Polymers Based on Triplet Chain Reactions *J. Org. Chem.* **2008**, *73*, 5683-5692.

13) Kuzmanich, G.; Natarajan, A.; Chin, K. K.; Veerman, M.; Mortko, C. J.; Garcia-Garibay, M. A. Solid-state photodecarbonylation of diphenylcyclopropenone: a quantum chain process made possible by ultrafast energy transfer J. Am. Chem. Soc. 2008, 130, 1140-1141.

14) Kuzmanich, G.; Gard, M. N.; Garcia-Garibay, M. A. Photonic amplification by a singlet-state quantum chain reaction in the photodecarbonylation of crystalline diarylcyclopropenones. J. Am. Chem. Soc. 2009, 131, 11606–11614.

15) Dou, J. H.; Zheng, Y. Q.; Yao, Z. F.; Yu, Z. A.; Lei, T.; Shen, X.; Luo, X.Y.; Sun, J.; Zhang, S.D.; Ding, Y.F.; Han, G.; Yi, Y.; Wang, J.Y.; Pei, J. Fine-Tuning of Crystal Packing and Charge Transport Properties of BDOPV Derivatives through Fluorine Substitution *J. Am. Chem. Soc.* **2015**, *50*, 15947-15956.

16) Kolaric, B.; Baert, K.; Van der Auweraer, M.; Vallee, R.; Clays, K Controlling the Fluoresence Resonant Energy Transfer by Photonic Crystal Band Gap Engineering *Chem. Mater.* **2007**, *23*, 5547-5552.

17) Zhao, W.; Cheung, T. S.; Jiang, N.; Huang, W.; Lam, J. W. Y.; Zhang, X.; He, Z.; Tang, B. H. Boosting the efficiency of organic persistent room-temperature phosphorescence by intramolecular triplet-triplet energy transfer Nat. Comm. **2019**, *10*, 1-11.

18) Shi, H.; Wang, Y.; Hua, R. Acid-catalyzed carboxylic acid esterification and ester hydrolysis mechanism: acylium ion as a sharing active intermediate via a spontaneous trimolecular reaction based on density functional theory calculation and supported by electrospray ionization-mass spectrometry *Phys. Chem. Chem. Phys.* **2015**, *17*, 30279-30291.

19) Koster, J. B.; Timmermans, G. J.; Bekkum, H. V. Reaction of the Tetramethylcyclobutadiene-Aluminum Chloride Complex with Dienophilic Esters *Synthesis,* **1971**, *19*, 139–140.

20) Gamlin, J. N.; Olovsson, G.; Pitchumani, K.; Ramamurthy, V.; Scheffer, J. R.; Trotter, J. Cation to Anion triplet-triplet energy transfer in crystalline organic salts *Tetrahedron Letters*, **1996**, *37*, 6037-604.

21) Mohamed, S.; Tocher, D. A.; Vickers, M.; Karamertzanis, P. G.; Price, S. L. Salt or Cocrystal? A New Series of Crystal Structures Formed from Simple Pyridines and Carboxylic Acids **2009**, *9*, 2881-2889.

22) Tong, W. Q.; Whitesell, G. *Pharm. Dev. Technol.* **1998**, *3*, 215-233.

23) Bowker, M. J. A Procedure for Salt Selection and Optimization. In *Handbook of Pharmaceutical Salts*; Stahl, P.H.; Wermuth, C. G.; Eds.; VHCA and Wiley-VCH: New York, 2002.

24) Johnson, S. L.; Rumon, K. A. Infrared Spectra of Solid 1:1 Pyridine-Benzoic Acid Complexes; the Nature of the Hydrogen Bond as a function of the Acid-Base Levels in the Complex *J. Phys. Chem*. **2008**, *69*, 74-86.

25) Childs, S. L.; Stahly, G. P.; Park, A. The Salt-Cocrystal Continuum: The Influence of Crystal Structure on Ionization State *Mol. Pharmaceutics* **2007**, *4*, 323-338.

26) Bhogala, B. R.; Basavoju, S.; Nangia, A. Tape and layer structures in cocrystals of some di- and tricarboxylic acids with 4,4'-bipyridines and isonicotinamide. From binary to ternary cocrystals *CrystEngComm* **2005**, *7*, 551-562.

27) Folie, B. D.; Haber, J. B.; Refaely-Abarmson, S.; Neaton, J. B.; Ginsber, N. S. Long-Lived Correlated Triplet Pairs in a pi-Stacked Crystalline Pentacene Derivative *J. Am. Chem. Soc.* **2018**, *6*, 2326-2335.

28) Avakian, P.; Merrifield, R. E. Triplet Excitons in Anthracene Crystals – A Review *Molecular Crystals*, **2007**, *5*, 37-77.

29) Miyasaka, A.; Mawatari, Y.; Sone, T.; Tabata, M. Mechanochemical-induced cis-to-trans isomerization of poly(2-ethynyl-3-n-octylthiophene) prepared with a Rh complex catalyst *Polymer Degradation and Stability*, **2007**, *2*, 254-259.

30) Nau, E.; Campagna, D.; Baumann, C.; Gostl, R. Polymer mechanochemistry-enabled pericyclic reactions *Polym. Chem*., **2020**, *11*, 2274-2299.

31) Black, A. L.; Lenhardt, J. M.; Craig, S. L. From molecular mechanochemistry to stress-responsive materials *J. Mater. Chem.*, **2011**, *21*, 1655-1663.

32) Kuzmanich, G.; Simoncelli, S.; Gard, M. N.; Spanig, F.; Henderson, B. L.; Guldi, D. M.; Garcia-Garibay, M. A. Excited State Kinetics in Crystalline Solids: Self-Quenching in Nanocrystals of 4,4'-Disubstituted Benzophenone Triplets Occurs by a Reductive Quenching Mechanism J. Am. Chem. Soc. **2011**, *43*, 17296-17306.